Reply to the comments from referee # 1

(In red our replies, in green the text added.)

We first kindly thank the referee for his time, useful comments, and constructive criticism. We used his suggestions to prepare a new version of the manuscript.

This paper discusses the air quality measurement campaign, AROMAT, and puts it into the context of if/how these measurements can assist in future validation efforts for satellites, such as Sentinel 5P TROPOMI. The significance of this work is within the scope of AMT and is key as the air quality community works toward validating satellites that measure urban air quality (e.g., TROPOMI) and there are some novel 'take-home' messages from this work that are worthy for publishing. From what is shared in the paper, the quality of the work appears valid however there is clarity needed in some areas. This paper also needs restructuring to improve the clarity of the take-home conclusions. For example: The paper lacks details about the campaign and information about the measurements are scattered throughout the paper.

We have added two sections to describe the campaign deployment and mention more intensively the supplement when appropriate, the supplement contains more details and measurements. We also added a schematic for the overall deployment.

Specific comments/questions:

• The title of this paper does not clearly reflect the contents of the paper. The current title would attract readers as an overview paper for the measurements during AROMAT, but this is not the purpose of this paper nor is there a detailed overview of the entire campaigns. If agreed by the authors, I suggest changing to title to something that reflects that AROMAT could be a concept model for validation campaigns of satellite retrievals.

This paper aimed to be an overview paper but we agreed we had put too much information in the supplement so we added section 2.4 and 2.5 which describe the campaign deployments, they were previously in the Supplement. We prefer to keep our title.

• Are conclusions made about validation only valid over Romania? Or can these lessons be extended beyond Romania? Please be clear in the paper which conclusions can be extended beyond the AROMAT region.

About NO2, since Bucharest is a relatively small source compared to other cities, many other urban areas could be used as target for satellite validation using airborne measurements, we have performed other airborne measurements in Berlin and in Belgium in the AROMAPEX and BUMBA campaign which are already in the references.

About SO2 and H2CO, our conclusions are valid for Romania only since there are larger sources in other parts of the world. We have already mentioned Serbia in the conclusions.

We added a sentence to extend the scope of the conclusions for NO2:

These conclusions for NO2 above Bucharest apply to other large polluted urban areas.

• It seems that the model for the conclusions is based on TROPOMI requirements. Please comment on if/how this extends to the requirements of the other planned missions or make the specific message in the paper that the conclusions that are made are specific to TROPOMI.

The qualitative part of the conclusion is also valid for future satellites which are in Table 1 but the quantitative accuracy we give is indeed based on TROPOMI characteristics. We rephrased

Our simulations, which are based on our measurements and TROPOMI characteristics, indicate that we can constrain the accuracy of the satellite NO2 VCDs within 37 or 28%, with and without information on the aerosol and NO2 profile, respectively.

• A weakness in the general analysis is the lack of discussion on temporal variation and the time of the airborne and ground based measurements and how this relates to the time of the satellite overpass, emissions inventories, etc. The authors should keep this in mind to address through revisions.

We do not fully agree with the comment. When the time difference could explain an observed discrepancy we have mentioned it, e.g for the AirMAP to MPIC Mobile-DOAS comparisons in Bucharest

Note that the systematic differences between AirMAP and the MPIC Mobile-DOAS at the eastern part of the ring road on 31 August 2015 were due to the time differences between both measurements.

About the satellite validation, we have assessed the temporal error (in Section 4.1.2) for the comparison between an airborne and a satellite instrument. This is anyway more visible in this new version of the manuscript since we have included in the main manuscript the figure from the supplement which illustrates how we quantified the temporal error.

About the emissions section, we have added a sentence in the new paragraph presenting this section to emphasize the fact that we compare instantaneous emissions with yearly emission inventories:

The comparisons with reported emissions should not be overintrepreted since we compare campaign-based flux measurements performed during a few days in daytime with reported emissions which represent yearly averages. Nevertheless, they give interesting indications about the operations of the FGD units of the power plants and possible biases in emission inventories.

• Section 2 should start by painting a picture of AROMAT 1 and 2 deployments and measurements that used in this analysis. While much of this information is in the supplement and scattered throughout the paper, the general reader enters Section 3

without the proper background to assess what is being discussed. Currently, it does not effectively communicate the needed details about the AROMAT campaign before moving into the results sections. To fix this, the authors could reorganize the section by moving 2.3 to before 2.1 and 2.2. Then there needs to be discussion (and maybe a Table) that summarizes each campaign. This table and/or discussion must include time periods of each deployment, location of each deployment, payloads for the aircraft and relevant details about ground measurements (in line with Tables 4-6) and could extend into partners and other details from 2.3 as seen fit.

We thank the referee for his suggestion but we do not want to move Section 2.3 before Section 2.1 and 2.2 because we think it is clearer to present the sites before the campaign deployment on these sites. About the tables for the campaign, we also prefer to let them in the supplement since they are quite large and include ancillary measurements (ground-based in-situ, ACSM…) that we do not use later on in the main manuscript. So we think it would be distracting to put them in the main article.

But for clarity, we have moved the sections which present the practical deployments in 2014 and 2015 from the supplement to the main manuscript. We have also added a schematic for the campaign. We present this new schematics in Sect 2.3.

Figure 4 illustrates the typical instrumental deployment during the campaigns. The set-up combined airborne and ground-based measurements to sample the 3-D chemical state of the lower troposphere above polluted areas.

Table 3 does not add substantial information to this paper and that space would be more effectively be used to summarize the campaigns themselves.

We agree with the comment and moved Table 3 to the Supplement.

Section 3 and 4 are hard to follow as its jumps between regions and different trace gas measurements. A suggestion would be to reorganize into sections focuses on specific trace gases. For example: Section 3 could just be about NO2. With the following sections.
3.1: similar for 3.1.3 with summarizing Bucharest observations
3.2: similar for 3.2.1 with summarizing The Jiu Valley observations
3.3: Relevant discussion from Section 4 about lessons about validation

We thank the referee for his advices but we prefer to keep our structure because it follows in Sect. 3 a geographical order with the two sites which corresponds to the geographical presentation of Sect.2. This is interesting for a reader interested in pollution sources in Romania. In Sect. 4 we draw conclusions for each molecule, which is more interesting for a reader coming from the AQ satellite validation community. We have written a new introduction for Sect. 4.4 which presents our flux estimates.

• Section 3.1.1 and 3.1.2 and their associate figures do not fit within the scope of the paper as separate sections. Any relevant discussion could fit in within the other trace gas sections, in the supplement, or omitted.

We agree with this comment. We have moved the figure to the Supplement.

The below of the comments are organized by trace gas.

• **NO2:**

Line 209: The statement about the datasets in Figure 7 appearing consistent is not valid, which is alluded to later in the paragraph. Please reword or omit that statement in the discussion.

We meant that the measurements were consistent for each given day, not in general. We have removed this statement which was indeed misleading.

Line 221: what is the difference in time between the two measurements?

The AirMAP/Cessna VCDs correspond to several flight lines recorded between 12:00 and 13:30 UTC. We have added this info to the text, which already included the CAPS/BN-2 time.

between 12:00 and 13:30 UTC

The statement about NO2 vmr at 300m being a proxy for NO2 VCD is not valid. It may be for that specific case but not overall. The results over the Jiu Valley even refute this statement.

Although we had written at the beginning of the sentence “along this portion of the flight, which was inside the plume but outside the city,” we agree that the scope of validity of this statement was not clear enough. We rephrased this paragraph for clarity:

This suggests that along this portion of the flight, which was inside the plume but outside the city, the NO2 VMR measured at 300 m a.s.l. may be used as a proxy for the NO2 VCD. Indeed, the BLH was about 1500m (Fig.S9 in the Supplement) during these observations. Assuming a constant NO2 250 VMR of 3.5 ppb in the boundary layer leads to a NO2 VCD of 1.4 x 1016 molec cm2. This estimate is close to the AirMAP NO2 VCD observed in the plume (Fig. 6). When measured at 300 m a.s.l., the NO2 VMR thus seems a good estimate of its average within the boundary layer. Note that this finding is specific to the configuration in Bucharest where we flew at 10 km from the city center and does not apply to our measurements in the exhaust plume of the Turceni power plant (Fig. 9). Future campaigns should include vertical soundings inside the Bucharest plume to further investigate its NO2 vertical distribution.

Line 229: Is the Avantes spectrometer the Bremen Nadir instrument from Table 7? Please make descriptions consistent.

Indeed, we rephrased:

from the IUP-Bremen nadir instrument

Not required but Figure S3 seems like a good candidate to move to the actual manuscript for comparing/contrasting with SO2. It could also be helpful to see how Figure 7 and other airborne figures translate to the TROPOMI pixels. When talking about the validation context.

We agree with these comments which improve the manuscript. We have moved Figure S3 to the main manuscript, merging it with the SO2 map. The figure S10 of the previous version of the Supplement, which illustrated the temporal variation, also shows how airborne measurements translate to hypothetical TROPOMI pixels. We have also moved it to the main manuscript.

Line 334: It seems that temporal variation could also lead to overestimation in the slope depending on how the NO2 is varying through time.

A systematic variation of the NO2 VCD through time would lead to a bias between reference (x) and satellite measurements (y) if the NO2 VCD, this bias could be either positive or negative.

But considering only a random variation added to the reference measurement as a noise, the dynamic range of this 'noisy' reference measurements is likely to increase, which could lead to an underestimation of the slope between x and y without this temporal noise. We have actually made some simulations to emphasize this effect and added a figure (Fig.12). Here is its legend:

Effect of an underestimation of the random error in a regression analysis simulating TROPOMI validation using airborne mapping as reference measurements of NO2 VCDs. The dynamic range (blue line) of the reference measurements increases with the applied random error. For the considered a priori random error (dashed vertical line, 1x10^15 molec.cm-2), this leads to an underestimation of the regression slope (red line). These simulations use the AirMAP data of 31 August 2015 (afternoon flight).

And the added text

Finally, it should be noted that these regression simulations assume a correct estimation of the temporal random error. Underestimating this error propagates in the fit of the regression slope. Figure 12 presents the possible effect of such an underestimation when the a priori random error of the reference measurements is set at 1x1015 molec cm-2, using again the AirMAP observations of Fig. 5 (right panel) as input data. As the dynamic range of the reference measurements increases with the applied error, the fitted slope decreases. For a true error of 4x1015, this leads for instance to an underestimation of the slope of about 5%. This effect is small but other sources of random error (e.g undersampling the satellite pixels) would add up in a real-world experiment. Wang (2017) observed such a systematic decrease of the regression slope when averaging MAX-DOAS measurements within larger time windows around the satellite overpass.

It should be noted that the temporal variation uncertainty quantified in this paper was specific to that area during that particular morning and more data would have to be analyzed to see if this is a typical value or not. These temporal variations are also

likely much different during the time TROPOMI overpasses (not in the early morning) and on different days. Though the technique for quantifying temporal variation using the airborne data is novel and would be interesting to extend to other datasets.

We agree with the comment. We had already emphasized that writing *Clearly, the NO2 VCD temporal variation depends on characteristics of a given validation experiments, such as the source locations and the wind conditions during the measurements* in Section 4.1.2 and in the conclusion *it varies with local conditions for a given experiment*.

We have further emphasized that it also depends on the time of the day and that our measurements were not at the TROPOMI overpass time.

The temporal variation also depends on the time of the day and we base our estimate here on measurements around 11:00 LT while TROPOMI overpass is at 13:30 LT.

It would also be helpful to add some more details in the writing or references about the exercise done in the first paragraph of section 4.1.3 so it can be recreated by others with similar datasets.

It seems to us that the important steps of our method are already described but we have added a reference to the section 4.1.1 describing the input data, to improve the clarity.

We simulated TROPOMI Cal/Val exercises with the spatially averaged AirMAP observations described in Sect. 4.1.1

Moreover, we have moved to the main manuscript the figure from the supplement which illustrates the quantification on the temporal error as it also shows the average of the airborne measurements at the resolution of TROPOMI so we think it improves the overall clarity of this section. This figure is described in the previous section :

Figure 11 illustrates our estimation of the temporal variation of the NO2 VCDs comparing consecutive AirMAP overpasses above Bucharest from the morning flight of 31 August 2015.

• H2CO and SO2

Line 239-240: Are there H2CO direct emissions in Bucharest? That seems to be the implication with the statement in line 239.

We do not know that. We clearly measured an enhancement of H2CO above Bucharest but we can not conclude on its origin. To investigate that, we would need 1) more measurements, in particular of the VOCs which are the main H2CO precursors, and 2) modelingstudies. Such work was done in particular by Johansson et al. (2014)

Johansson, J. K. E., Mellqvist, J., Samuelsson, J., Offerle, B., Moldanova, J., Rappenglück, B., … Flynn, J. (2014). Quantitative measurements and modeling of industrial formaldehyde emissions in the Greater Houston area during campaigns in 2009 and 2011. *Journal of Geophysical Research: Atmospheres*, *119*(7), 4303–4322. https://doi.org/10.1002/2013JD020159

But it is outside the scope of our study. We agree that our word 'source' is misleading as it can be understood as direct source. So we have rephrased:

The difference between NO2 and H2CO spatial patterns may be explained by the different origins of NOx compared to H2CO.

This is relevant to both SO2 and H2CO since they both have the conclusion that validation of satellite H2CO and SO2 is better suited with ground-based measurements.

Is this a recommendation only for Romania?

As replied above, this is valid for Romania. There are larger SO2 sources such as volcanoes or oil industry in the Persian Gulf which may be interesting for airborne validation. For large power plants outside Romania without FGDs, one should study the satellite data to verify that their signal-to-noise ratio enables their validation with airborne measurements in practice (e.g. considering the costs). Note that the signal-to-noise may improve with geostationary platforms.

Are there ground based measurements from AROMAT that can be discussed in terms of validation like the airborne data is? If so, add this to the discussion. If not, the conclusion that ground-based measurements would be better suited than airborne may not be valid.

We have discussed the interest of our Mobile Max-DOAS (Ground based) for H2CO in Section 4.2, and the interest of the temporary SO2 cameras (Ground based) for SO2 in Section 4.3. These findings motivate the installation of automatic and static instruments since 1) MAX-DOAS are already demonstrated for H2CO VCD validation 2) TROPOMI-derived fluxes are already demonstrated and their volcanic part is already used for SO2 validation. So we consider our conclusions valid. But we agree we missed a reference for H2CO. We added a reference to Desmedt (2015) in the H2CO section, and modified a sentence:

Indeed, long-term ground-based measurements at two sites would be useful to investigate seasonal variations of H2CO, as already demonstrated in other sites (De Smedt, 2015).

Its mentioned that the individual flights cannot always help in validation, which is true. But systematic measurements may help as discussed in the conclusions. Please say something about this within the sections themselves.

We modified a sentence in sect 4.2:

This limits the relevance of individual mapping flights for the validation of H2CO, yet systematic airborne measurements would improve the statistics.

And added one in sect 4.3

As for H2CO, systematic airborne measurements would improve the statistics.

Emissions section (section 4.4):

• This section lacks sufficient background on the methodology for computing fluxes and lacks the context on how this fits with the scope of the paper. Fluxes are not mentioned in the abstract, intro, nor is emission estimate validation within the requirements for validation of satellite products. Though emission estimations put into the context of satellite applications is important and evaluating that is very important scientifically from that perspective.

Options:
§ Omit this section.
§ Add sufficient details or references for emission flux calculations and put this into the context on how this helps with satellite product evaluation as alluded to in the latter part of section 4.3. (Though, this section with all details could potentially be a stand-alone manuscript).
• If kept, when comparing the emissions to inventories, be sure to consider variations in emissions from hourly/daily/seasonal timescales and the AROMAT measurements were only a small subset in time.

We agree that this section was not introduced enough in the abstract and introduction and we have modified both to mention this part of the study. We added in the abstract:

We also quantify the emissions of NOx and SO2 at the two sites.

We added a sentence in the introduction:

Eventually, we use the AROMAT measurements to derive NOx and SO2 fluxes from the two sites.

Several studies already present in detail the traverse method used to quantify the fluxes with the DOAS method.e.g:

Ibrahim, O., Shaiganfar, R., Sinreich, R., Stein, T., Platt, U., and Wagner, T.: Car MAX-DOAS measurements around entire cities: quantification of NO_x emissions from the cities of Mannheim and Ludwigshafen (Germany), Atmos. Meas. Tech., 3, 709–721, https://doi.org/10.5194/amt-3-709-2010, 2010.

Johansson, J. K. E., Mellqvist, J., Samuelsson, J., Offerle, B., Moldanova, J., Rappenglück, B., Lefer, B., and Flynn, J. (2014), Quantitative measurements and modeling of industrial formaldehyde emissions in the Greater Houston area during

campaigns in 2009 and 2011, *J. Geophys. Res. Atmos.*, 119, 4303– 4322, doi:10.1002/2013JD020159.

From AirMAP, this is also explained in the AROMAT AirMAP study

Meier, A. C., Schönhardt, A., Bösch, T., Richter, A., Seyler, A., Ruhtz, T., Constantin, D.-E., Shaiganfar, R., Wagner, T., Merlaud, A., Van Roozendael, M., Belegante, L., Nicolae, D., Georgescu, L., and Burrows, J. P.: High-resolution airborne imaging DOAS measurements of NO_2 above Bucharest during AROMAT, Atmos. Meas. Tech., 10, 1831–1857, https://doi.org/10.5194/amt-10-1831-2017, 2017.

We added an introduction with these references at the beginning of the section :

This section presents our estimates of the NOx and SO2 fluxes from Bucharest and the power plants in the Jiu Valley, combining our different 2014 and 2015 measurements. Campaign-based estimates of NOx emissions from large sources are relevant in a context of satellite validation since the high resolution of TROPOMI enables to derive such emissions on a daily basis Lorente(2019). Regarding SO2, as discussed in the previous section, the low signal-to-noise ratio of the satellite measurements implies averaging for several months to derive a SO2 flux (Fioletov-2019), yet campaign measurements are useful to select an interesting site and test the ground-based apparatus and algorithms.

The comparisons with reported emissions should not be overintrepreted since we compare campaign-based flux measurements performed during a few days in daytime with reported emissions which represent yearly averages. Nevertheless, they give interesting indications about the operations of the FGD units of the power plants and possible biases in emission inventories.

Our flux estimates are all based on optical remote sensing measurements. They involve integrating a transect of the plume along its spatial extent and multiplying the outcome by the plume speed, which may correspond to the stack exit velocity (camera pointing to the stack) or to the wind speed (Mobile-DOAS and imaging-DOAS). We refer the reader to previous studies for the practical implementations. Ibrahim (2010) presented the method we used for Bucharest, where we encircled the city with the Mobile-DOAS. Meier (2017) presented the AirMAP-derived flux estimations, while Johansson (2014) derived industrial emissions from a car-based Mobile-DOAS instrument as we did for the Turceni power plant. Constantin (2017) presented the fluxes based on the ULM-DOAS measurements. Regarding the SO2 Camera, we present hereafter the method and previous related works.

Other comments within the text:

• Line 27-28: Veefkind et al., 2012 doesn't reference the 3.5x5.5km resolution. Refer to the switch through the Readme file or another reference that talks about it: http://www.tropomi.eu/sites/default/files/files/publicSentinel-5P-Nitrogen-Dioxide-Level-2-Product-Readme-File.pdf

We agree with the comment, nevertheless Veefkind (2012) is a more complete reference for TROPOMI. So we kept it and added the readme in the references and a note after the reference to Veefkind:

the original TROPOMI resolution of 7x5.5 km2 was increased on 6 August 2019 MPC (2019))

• Line 45: Can it be made clear what small signals mean? Does this mean the small signal:noise ratios or more a reference to clean areas that don't have a lot of signal?

There are several aspects of the small signals, as Richter et al. (2013) point out:

An additional challenge is the small signal often obtained for tropospheric species,either because their abundances are small or because it is difficult to separate the tropospheric from the stratospheric signals. In many cases, the validation measurements themselves are also not as accurate and precise for these small signals as one would like, adding the uncertainty of the validation data to that of the satellite measurement.

We mention this paper from Richter et al. just before, L.42.:

Richter et al. (2014) have discussed the challenges associated with the validation of tropospheric reactive gases.

So we consider we have given the reader the useful reference to have more information on this aspect.

• Line 114: what are the European thresholds? Add a reference and values.
The reference (EEA,2019) is already given in the sentence right after, which also gives the typical value for yearly NO2 in the center of Bucharest, we added the EU limit value for yearly NO2 to compare with.

"For instance, the annual mean concentration of NO2 at the traffic stations was about 57 ug.m-3 in 2017 (EEA,2019), when the EU limit is 40 ug.m-3. "

• Table 1: change GEMS to launched instead of planned.
Corrected.

• Throughout the paper: Spatial resolution is in km and not km2. For example, 7 x 7km2 is not the same as 7km x 7km.

We do not agree with this comment, we think width x height in km2 is clear enough and shorter, thus better. This way of writing is largely used in other publications including by the TROPOMI science team. e.g. recently:

van Geffen, J., Boersma, K. F., Eskes, H., Sneep, M., ter Linden, M., Zara, M., and Veefkind, J. P.: S5P TROPOMI NO_2 slant column retrieval: method, stability, uncertainties and comparisons with OMI, Atmos. Meas. Tech., 13, 1315–1335, https://doi.org/10.5194/amt-13-1315-2020, 2020.

• Line 261: delete the word ‘those’

Here we think our sentence is clearer as it is since we do not show all the sonde measurements, neither a random selection of them, but only the ones which detected the plume. Grammatically, we think it is also fine to use “those” … “which” since the Nobel prize in literature Bertrand Russell used this structure in his essay ‘Our knowledge of the external world’ (1914)

Things are those series of aspects which obey the laws of physics.

• Line 396: change ‘As for’ to ‘Similar to’
Corrected.

• Line 399: Start a new paragraph with the sentence starting with ‘On the other hand’

Corrected.

Reply to the comments from referee # 2

(In red our replies, in italic the text already written, in green the added text.)

We first kindly thank the referee for his time, useful comments, and constructive criticism. We used his suggestions to prepare a new version of the manuscript.

The manuscript titled The Air borne Romanian Measurements of Aerosols and Trace gases(AROMAT) campaigns at two areas provides relevance of each instrument for validation of air quality satellite (e.g., TROPOMI) products. The paper identifies a significant source of comparison error (measurement time difference), which is a useful information for the satellite validation. It summaries DL, BIAS, measurement range of several trace gas species for each instrument. However, the paper misses detailed description of instrument characteristics and measurement geometry, data used for each instrument AMF and their effects of the retrieved products. There has been no analysis about horizontal and vertical representativeness of each instrument although the campaign is to aim for validation of TROPOMI. The manuscript needs to be improved considering those major issues.

There were already two published studies (Meier et al., 2017, Merlaud et al., 2018) dedicated to the AROMAT airborne measurements, these studies include the AMF description and vertical sensitivities (box-AMF) of the airborne DOAS instruments. The Supplement already gives technical description of each instrument, giving the published references.

We agree that these two papers and the Supplement were not visible enough in the manuscript so we added several references to it (see below). We also rephrased the end of the introduction:

Two aforementioned publications focused on the AirMAP and SWING operations during the 2014 AROMAT campaign (Meier et al., 2017; Merlaud et al., 2018). In this work, we present the overall instrumental deployment during the two campaigns and analyze the relevance of these measurements for the validation of several air quality satellite products: tropospheric NO2, SO2 and H2CO VCDs.
[…]
The paper is structured as follows: Section 2 describes the two target areas and the deployment strategy. Section 3 characterizes the investigated trace gases fields in the sampled areas. Section 4 presents a critical analysis of the strengths and limitations of the campaign results while elaborating on recommendations for future validation campaigns in Romania. Eventually, we use the AROMAT measurements to derive NOx and SO2 fluxes from the two sites. The Supplement presents technical details on the instruments operated during the campaigns and presents additional information and measurements.

We also added a schematic for the geometry of the measurements.

About the horizontal representativeness, we emphasized in the conclusions that one main advantage of continuous airborne mapping is that the horizontal representativeness error cancels.

Abstract and Introduction: The objectives of this present study and campaign needs to be clearly distinguished. The objectives of the campaign are described in Abstract as “Their main objectives were to test recently developed air borne observation systems dedicated to air quality studies and to verify the concept of such campaigns in support of the validation of space borne atmospheric missions such as the TROPOspheric Monitoring Instrument (TROPOMI)/Sentinel-5 Precursor (S5P).” However, there are differences between the objectives of the campaign and those of this present work. Please address the objectives of this present study in Abstract.

We agree with the comment and we have added the objectives of this paper in the abstract

We present the AROMAT campaigns, focusing on the findings related to the validation of tropospheric NO2, SO2, and H2CO. We also quantify the emissions of NOx and SO2 at the two sites.

The objectives were already described in the introduction, but we rephrased it to better define the scope of the study (see above).

Line 218: “.The comparison reveals a good agreement when averaging the forward and backward-looking Mobile-DOAS NO2 VCDs, with a MPIC/AirMAP slope of 0.93 and a correlation coefficient of 0.94.” One of the campaign objectives is to identify relevance and capability of each measurement type on ground or air borne platforms for validation of TROPOMI products. There are missing of both qualitative and quantitative causes for “slope (between ground based MPIC mobile DOAS and AirMAP) of 0.93 and a correlation coefficient of 0.94”.

We are comparing collocated and almost time coincident measurements of NO2 VCDs. If everything would be perfect, the slope and correlation coefficient would both be 1. The remaining difference is small and may have several causes: instrumental bias, the small time difference of the measurements, errors of AMFs, different horizontal sensitivity. We have added this in the text as:

The remaining discrepancy may be explained by AMFs errors and differences in time and horizontal sensitivity.

Line 224: I do not understand how “the NO2 vmr measured at 300 m a.s.l. can be used as a proxy for the NO2 VCD”. Please describe how it can be used used as a proxy for the NO2 VCD. Please also use capital letter for VMR rather than vmr.

We had tried to give the explanation in the next sentences, which compared the NO2 VCD derived from the proxy with the AirMAP NO2 VCD measurement but we agree it was not clear enough. We have rephrased for clarity and changed vmr to VMR here and across the document

This suggests that along this portion of the flight, which was inside the plume but outside the city, the NO2 VMR measured at 300 m a.s.l. may be used as a proxy for the NO2 VCD. Indeed, the BLH was about 1500m (Fig.S9 in the Supplement) during these observations. Assuming a constant NO2 250 VMR of 3.5 ppb in the boundary layer leads to a NO2 VCD of 1.4 x 1016 molec cm2. This estimate is close to the

AirMAP NO2 VCD observed in the plume (Fig. 6). When measured at 300 m a.s.l., the NO2 VMR thus seems a good estimate of its average within the boundary layer. Note that this finding is specific to the configuration in Bucharest where we flew at 10 km from the city center and does not apply to our measurements in the exhaust plume of the Turceni power plant (Fig. 9). Future campaigns should include vertical soundings inside the Bucharest plume to further investigate its NO2 vertical distribution.

Line255-260: In comparisons between data of airborne AIRMAP, SWING, and ground based Mobile DOAS, it is important to explain if they measure the same target in terms of horizontal and vertical coverage. -If each instrument measures a target (in particular plume) at different geometry and location, there should be large differences between the retrieved NO2 VCDs. Authors need to explain reasons that cause such differences in terms of the algorithms, measurement geometries, effect of platforms, etc., in detail.

The instruments aim at the same target at the same time but from different locations and geometry, the ground for the Mobile-DOAS (zenith-looking) and from 3 km altitude for the airborne-DOAS (nadir-looking).

We had explained the main reasons for these differences, to our understanding, at the end of the paragraph, which also refers to our previous study which already compared airborne and mobile-DOAS measurements:

This is partly related to air mass factor uncertainties, but probably also to 3-D effects as the plume is very thin and heterogeneous close the power plants, as discussed in Merlaud et al. (2018).

We have to invoke another reason (3-D effects) in addition to the AMF only, since the latter can not explain the discrepancy between Mobile and airborne measurements. At the time of writing our manuscript this was still a conjectural but colleagues from another team are studying that with a 3D RT code, and their results seem consistent with what we wrote. See e.g. this presentation at ATMOS 2018

Implementation Of Three-Dimensional Box-Air-Mass-Factors In The LibRadtran Radiative Transfer Model

Schwaerzel, Marc; Emde, Claudia; Kuhlmann, Gerrit; Brunner, Dominik; Buchmann, Brigitte; Berne, Alexis

http://atmos2018.esa.int/page_session11.php

We rephrased and added a sentence to strengthen our initial explanation.

This is partly related to air mass factor uncertainties, but they can not explain alone such a discrepancy. Close to the power plant, the plume is very thin and heterogeneous which leads to 3-D effects in the radiative transfer, as suggested in Merlaud et al. (2018). In these conditions, the 1-D atmosphere of the radiative transfer models used to calculate the airborne AMFs may not be realistic enough and bias the VCDs measured from the aircraft.

-In the paper, a difference between mobile DOAS and those of airborne is partly related to air mass uncertainties. There is absence of description of NO2 AMFs for mobile DOAS and those for AirMAP and SWING. What are the input data used to calculate each AMF?

We agree it was not clear enough. For the airborne instruments, the NO2 profile is a box of 500 m as used in the reference we give in Meier et al. 2017 for Bucharest during AROMAT-1. We agree it was not clear enough that it was the same so we added the Phd of Andreas Meier as a reference in the AirMAP section of the supplement. This PhD includes AirMAP operation during AROMAT-2.

Note that a PhD thesis Meier (2018) describes in detail the AirMAP operations and the algorithms used to analyze the AROMAT data.

For the Mobile-DOAS, it was a zenith-only measurements and- we simply used the geometric approximation i.e. 1, as mentioned as a typical AMF value in the AMF NO2 table of the supplement. Here the AMF does not correspond to the reference (Constantin et al., 2013) since this previous work used a Chimere profile, which is not representative of the plume so close to the power plant.

We mentioned in the text and the legend of the figure that the Mobile-DOAS were zenith-only

Both AMFs actually correspond to the typical values given in the NO2 AMF table of the supplement, which we further emphasized:

Table S2 in the Supplement gives the typical AMFs used for this analysis for airborne and zenith-only Mobile-DOAS.

-please add schematic graph which shows instrument setup and measurement geometry (including measurement azimuth angles for target locations such as location of plume) of each instrument

We added a schematic (Fig.4) to explain the main campaign set-up. We did not add the azimuth however since as most of the measurements were mobile, it varied between 0 and 360°.

We have added a sentence presenting the figure in Sect 2.2

Figure 2 illustrates the typical instrumental deployment during the campaigns, which combined airborne and ground-based measurements.

This is the legend of this new figure 2 :

Geometry of the main measurements performed during the AROMAT campaigns. The Imaging-DOAS instruments map the NO2 and SO2 VCDs at 3 km altitude above

the target area while the in-situ samplers measure profiles of trace gases and aerosols. Ancillary ground measurements include Mobile-DOAS to quantify trace gases VCDs and lidars to measure the aerosol optical properties.

Line 300: There are many sentences which mention “reference measurements”. Please define “reference measurements”

Following Richter et al. (2013), we mean “independent data with known and documented uncertainties” that we can meaningfully compare with satellite products. We have expanded the sentence in the introduction which first use this expression:

Validation involves a statistical analysis of the differences between measurements to be validated and reference measurements, which are independent data with known uncertainties (Von Clarmann, 2006, Richter 2013).

Line 304: What are “typical air mass factors (AMF) used here for each species and what are the references for each AMF value for each species for each instrument?

The sentence just after (line 305) already indicates the typical AMF: *“Table S1 in the Supplement presents these typical AMFs and detection limits”*. The references for each AMF comes from their different reference paper. We have added that in the legend of the three AMF tables.

See the references in Sect. 2 for details on the AMF calculations of the airborne instruments. We used geometric approximations for the ground-based DOAS instruments, pointing to zenith (AMF = 1), and 22° above the hrozon (AMF = 2.7).

Line 394: Please address the definition of “combined uncertainty” including how “combined uncertainty” has been calculated.

We had already explained this definition at the beginning of the sentence*: Adding in quadrature the biases of the SO2 VCDs for airborne measurements (40%, Table 6) and for TROPOMI (30%, Table 2) already leads to a combined uncertainty of …’ It seems already clear to us.*

Throughout the figures tables, there no quantitative comparisons between various measurement data which were carried out at the same or similar time in the same site. Please consider adding the plots with analysis or address the reasons for not doing that.

We had put the quantitative comparisons in the Supplement, where there are SWING vs AirMAP comparisons for NO2 and SO2 (Fig. S1 and S2) and AirMAP vs Mobile-DOAS measurements (S6), with correlation coefficients, slopes, intercepts, and number of points. We also show a CAPS versus NO2 sonde intercomparison (Fig. S5) but here it did not make sense to quantify the slope as the sonde was calibrated with the CAPS data. So we think we have already the quantitative intercomparisons needed to support the conclusions of our study. But we agree it was not visible enough in the main article so we added references to these figures in

the section 3.2.2 and 4.1.2 where these corresponding measurements are discussed and used:

In Sect. 3.2.2, we had already written that the SWING and AirMAP VCDs agree within 10%, we have added:

Figure S4 in the Supplement shows the corresponding time series of SWING and AirMAP SO2 DSCDs.

In Sect. 4.1.2

Figure S3 in the Supplement presents the corresponding AirMAP and SWING NO2 DSCDs.

Moroever, we added a quantitative description in the conclusion for the comparisons between airborne and mobile-DOAS in Bucharest.

These measurements agree within 7\% *with ground-based measurements*

The Airborne ROmanian Measurements of Aerosols and Trace gases (AROMAT) campaigns

Alexis Merlaud[1], Livio Belegante[2], Daniel-Eduard Constantin[3], Mirjam Den Hoed[4], Andreas Carlos Meier[5], Marc Allaart[4], Magdalena Ardelean[6], Maxim Arseni[3], Tim Bösch[5], Hugues Brenot[1], Andreea Calcan[6], Emmanuel Dekemper[1], Sebastian Donner[8], Steffen Dörner[8], Mariana Carmelia Balanica Dragomir[3], Lucian Georgescu[3], Anca Nemuc[2], Doina Nicolae[2], Gaia Pinardi[1], Andreas Richter[5], Adrian Rosu[3], Thomas Ruhtz[7], Anja Schönhardt[5], Dirk Schuettemeyer[10], Reza Shaiganfar[8], Kerstin Stebel[9], Frederik Tack[1], Sorin Nicolae Vâjâiac[6], Jeni Vasilescu[2], Jurgen Vanhamel[1], Thomas Wagner[8], and Michel Van Roozendael[1]

[1]Royal Belgian Institute for Space Aeronomie (BIRA-IASB), Avenue Circulaire 3, 1180 Brussels, Belgium
[2]National Institute of R&D for Optoelectronics (INOE), Magurele, Street Atomistilor 409, Magurele 77125, Romania
[3]"Dunarea de Jos" University of Galati, Faculty of Sciences and Environment, Str. Domneasca, Nr. 111, Galati 800008, Romania
[4]Royal Netherlands Meteorological Institute (KNMI), De Bilt, The Netherlands
[5]Institute of Environmental Physics, University of Bremen (IUP-Bremen), Otto-Hahn-Allee 1, 28359 Bremen, Germany
[6]National Institute for Aerospace Research "Elie Carafoli" (INCAS), Bd. Iuliu Maniu no. 220, Bucharest, Romania
[7]Institute for Space Sciences, Free University of Berlin (FUB), Carl-Heinrich-Becker-Weg 6-10, 12165 Berlin, Germany
[8]Max-Planck-Institute for Chemistry (MPIC), Hahn-Meitner-Weg 1, 55128 Mainz, Germany
[9]Norwegian Institute for Air Research (NILU), Instituttveien 18, 2007 Kjeller, Norway
[10]European Space Agency (ESA-ESTEC), Keplerlaan 1, 2201 AZ Noordwijk, The Netherlands

Correspondence: A.Merlaud (alexism@oma.be)

Abstract.

The Airborne ROmanian Measurements of Aerosols and Trace gases (AROMAT) campaigns took place in Romania in September 2014 and August 2015. They focused on two sites: the Bucharest urban area and the power plants in the Jiu Valley. Their main objectives were to test recently developed airborne observation systems dedicated to air quality studies and to verify the concept of such campaigns in support of the validation of spaceborne atmospheric missions such as the TROPOspheric Monitoring Instrument (TROPOMI)/Sentinel-5 Precursor (S5P). We present the AROMAT campaigns, focusing on the findings related to the validation of tropospheric NO_2, SO_2, and H_2CO. We also quantify the emissions of NO_x and SO_2 at the two sites.

We show that tropospheric NO_2 vertical column density (VCD) measurements using airborne mapping instruments are in principle valuable for satellite validation. The signal to noise ratio of the airborne NO_2 measurements is one order of magnitude higher than its spaceborne counterpart when the airborne measurements are averaged at the TROPOMI pixel scale. A significant source of comparison error appears to be the time variation of the NO_2 VCDs during a flight, which we estimated at about 4x10^{15} molec cm^{-2} in the AROMAT conditions. Considering the random error of the TROPOMI tropospheric NO_2 VCD (σ), the dynamic range of the NO_2 VCDs field extends from detection limit up to 37 σ (2.6x10^{16} molec cm^{-2}) or 29 σ (2x10^{16} molec cm^{-2}) for Bucharest and the Jiu Valley, respectively. For the two areas, we simulate validation exercises of the

TROPOMI tropospheric NO_2 product using airborne measurements. These simulations indicate that we can closely approach the TROPOMI optimal target accuracy of 25% by adding NO_2 and aerosol profile information to the airborne mapping observations, which constrains the investigated accuracy to within 28%. In addition to NO_2, we also measured significant amounts of SO_2 in the Jiu Valley, as well as a hotspot of H_2CO in the center of Bucharest. For these two species, we conclude that the best validation strategy would consist in deploying ground-based measurement systems at key locations which the AROMAT observations help identify.

1 Introduction

Since the launch of the Global Ozone Monitoring Experiment (GOME, Burrows et al. (1999)) in 1995, spaceborne observations of reactive gases in the UV-visible range have tremendously improved our understanding of tropospheric chemistry. GOME mapped the large urban sources of NO_2 in North America and Europe, the SO_2 emissions from volcanoes and coal-fired power plants (Eisinger and Burrows, 1998), and the global distribution of H_2CO with its maxima above East Asia and the tropical forests (De Smedt et al., 2008). Subsequent air-quality satellite missions expanded on the observation capabilities of GOME. Table 1 lists the past, present, and near-future nadir-looking satellite instruments dedicated to ozone and air quality monitoring with their sampling characteristics in space and time. The pixel size at nadir has shrunk from 320x40 km^2 (GOME) to 3.5x5.5 km^2 (TROPOMI, Veefkind et al. (2012), the original TROPOMI resolution of 7x5.5 km^2 was increased on 6 August 2019, MPC (2019)). This high horizontal resolution enables for instance to disentangle contradictory trends in ship and continental emissions of NO_2 in Europe (Boersma et al., 2015) or to distinguish the different NO_2 sources in oil sand mines in Canada (Griffin et al., 2019). The satellite-derived air quality products are now reliable enough to improve the bottom-up emission inventories (e.g. Kim et al. (2009), Fioletov et al. (2017), Bauwens et al. (2016)) and to be used in operational services, for instance to assist air traffic control with the near-real time detection of volcanic eruptions (Brenot et al., 2014). The bottom lines of Table 1 presents the near-future perspective in spaceborne observation of the troposphere: a constellation of geostationary satellites will provide hourly observations of the troposphere above east Asia (GEMS, (Kim, 2012)), North America (TEMPO, Chance et al. (2013)), and Europe (Sentinel-4, Ingmann et al. (2012)). These new developments will open-up new perspectives for atmospheric research and air quality policies (Judd et al., 2018).

Validation is a key aspect of any spaceborne Earth observation mission. This aspect becomes even more important as the science matures and leads to more operational and quantitative applications. Validation involves a statistical analysis of the differences between measurements to be validated and reference measurements, which are independent data with known uncertainties (von Clarmann, 2006; Richter et al., 2014). The aim of validation is to verify that the satellite data products meet their requirements in terms of accuracy and precision. Table 2 presents such requirements for the TROPOMI-derived tropospheric vertical column densities (VCDs) of NO_2, SO_2, and H_2CO (ESA, 2014). Richter et al. (2014) have discussed the challenges associated with the validation of tropospheric reactive gases. These challenges arise from the large variability in space and time of short-lived reactive gases, the dependency of the satellite products on different geophysical parameters (surface albedo, profile of trace gases and aerosols), the differences in vertical sensitivity between satellite and reference (ground-based or

airborne) measurements, and the small signals. An ideal validation study would involve a reference dataset of VCDs whose well-characterized uncertainties would be small compared to those required for the investigated products. This reference dataset would cover a large amount of satellite pixels with adequate spatial and temporal representativeness at different seasons, places, and pollution levels. Beside the VCDs, the ideal validation exercise would also quantify the geophysical parameters that impact the retrieval of the investigated satellite products. In the real world however, Richter et al. points out that "the typical validation measurement falls short in one or even many of these aspects".

The first validations of the tropospheric NO_2 and H_2CO VCD products of GOME involved in-situ samplings from aircraft (Heland et al., 2002; Martin et al., 2004). Such measurements may cover good fractions of satellite pixels but they miss the lower part of the boundary layer, where the trace gas concentrations often peak. Schaub et al. (2006) and Boersma et al. (2011) summarize other early validation studies for the tropospheric NO_2 VCDs retrieved from GOME, SCIAMACHY, and OMI. Several of these studies make use of the NO_2 surface concentration datasets from air quality monitoring networks. Compared to campaign-based data acquisition, operational in-situ networks provide long-term measurements, but their comparison with satellite products relies upon assumptions on the NO_2 profile. Other validation studies use remote-sensing from the ground and aircraft, in particular based on the Differential Optical Absorption Spectroscopy (DOAS) technique (Platt and Stutz, 2008), which is also the basis for the retrieval algorithms of the satellite-derived products. In comparison with in-situ measurements, DOAS has the benefit of being directly sensitive to the column density of a trace gas, i.e. the same geophysical quantity which is retrieved from space. Heue et al. (2005) conducted the first comparison between a satellite-derived product (SCIAMACHY tropospheric NO_2) and airborne DOAS data. Many validation studies also use ground-based DOAS measurements, in particular since the development of the Multi-AXis DOAS (MAX-DOAS) technique (Hönninger et al., 2004). MAX-DOAS measurements are valuable for validation due to their ability to measure integrated columns at spatial scales comparable to the satellite ground pixel size. Moreover, they broaden the scope of validation activities since they also provide limited profile information on both trace gases and aerosols (Irie et al., 2008; Brinksma et al., 2008; Ma et al., 2013; Kanaya et al., 2014; Wang et al., 2017; Drosoglou et al., 2018). The limitations of using the MAX-DOAS technique for validation arise from their still imperfect spatial representativeness compared to typical satellite footprints and to some extent from their limited sensitivity in the free troposphere. Spatial representativeness has often been invoked to explain the apparent low bias of the OMI tropospheric NO_2 VCDs in urban conditions (Boersma et al., 2018).

The unprecedented horizontal resolution enabled by the last generation of air-quality space-based instruments motivated preparatory field studies around polluted areas in North America (DISCOVER-AQ, https://discover-aq.larc.nasa.gov), Europe (AROMAT and AROMAPEX, Tack et al.,2019) and Korea (KORUS-AQ, https://www-air.larc.nasa.gov/missions/korus-aq/). These campaign activities quantified key pollutants (NO_2, SO_2, O_3, H_2CO, and aerosols) and assessed practical observation capabilities of future satellite instruments while preparing for their validation. They combined ground-based and airborne measurements. DISCOVER-AQ involved the deployment of the Geostationary Trace gas and Aerosol Sensor Optimization instrument (GEOTASO, Leitch et al.,2014; Nowlan et al.,2016) and of the Geostationary Coastal and Air Pollution Events (GEO-CAPE) Airborne Simulator (GCAS, Kowalewski and Janz,2014;Nowlan et al.,2018). In Europe, the two AROMAT campaigns, which took place in Romania in September 2014 and August 2015, demonstrated a suite of new instruments such

as the Airborne imaging DOAS instrument for Measurements of Atmospheric Pollution (AirMAP, Schönhardt et al.,2015; Meier et al.,2017), the NO_2 sonde (Sluis et al., 2010), and the Small Whiskbroom Imager for atmospheric compositioN monitorinG (SWING, Merlaud et al.,2018). Different airborne imagers were intercompared and further characterized during the AROMAPEX campaign in April 2016 (Tack et al., 2019).

Two aforementioned publications focused on the AirMAP and SWING operations during the 2014 AROMAT campaign (Meier et al., 2017; Merlaud et al., 2018). In this work, we present the overall instrumental deployment during the two campaigns and analyze the relevance of these measurements for the validation of several air quality satellite products: tropospheric NO_2, SO_2 and H_2CO VCDs. The datasets collected during AROMAT fulfill several requirements of the ideal validation study, as described above. We further investigate the strengths and limitations of the acquired data sets.

The paper is structured as follows: Section 2 describes the two target areas and the deployment strategy. Section 3 characterizes the investigated trace gases fields in the sampled areas. Section 4 presents a critical analysis of the strengths and limitations of the campaign results while elaborating on recommendations for future validation campaigns in Romania. Eventually, we use the AROMAT measurements to derive NO_x and SO_2 fluxes from the two sites. The Supplement presents technical details on the instruments operated during the campaigns and presents additional information and measurements.

2 Target areas and deployment strategy

This section presents the two target areas of the AROMAT campaigns, Bucharest and the Jiu Valley. It also lists available studies on air quality at these two sites as well as logistical aspects of relevance.

Figure 1 presents a map of the tropospheric NO_2 vertical column densities (VCDs) above Romania, derived from OMI measurements (Levelt et al., 2006) and averaged between 2012 and 2016. The map also indicates the position of the 8 largest cities of the country. Compared to highly polluted areas in western Europe such as northern Belgium or the Netherlands, Romania appears relatively clean at the spatial resolution of the satellite data. There are however two major NO_2 sources clearly visible from space, which appear to be of similar magnitude with NO_2 columns around 2.5 x 10^{15} molec cm^{-2}: the Bucharest area and the Jiu Valley, northwest of Craiova. For the latter, the NO_2 enhancement is due to a series of large coal-fired thermal power plants.

2.1 Bucharest

Bucharest (44.4° N, 26.1° E) is the capital and largest city (1.9 million inhabitants according to the 2011 census) of Romania. Within its administrative borders, the city covers an area of 228 km^2. Adding the surrounding Ilfov county, the total Bucharest metropolitan area numbers 2.3 million inhabitants in 1.583 km^2. The built-up areas are mainly located within a ring road whose diameter is around 20 km.

Iorga et al. (2015) described in detail the Bucharest Greater Area in the context of an extensive study of the air quality in the city between 2005 and 2010. Bucharest is located in a low-altitude plain, with a maximum altitude of 92 m a.s.l. The geographic configuration of the Carpathian Mountains explains the dominant northeast winds.

The NO_2 VCDs seen from space above Bucharest appear lower than over western European sites at the resolution of OMI (see Fig.S1 in the Supplement). However, this is partly due to the dilution effect for this relatively small and isolated source. Local studies based on the 8 air quality stations inside the city point out that, regarding local PM and NO_x levels, Bucharest is amongst the most polluted cities in Europe (Alpopi and Colesca, 2010; lorga et al., 2015). The city center is the most heavily polluted, with concentrations of pollutants well above the European thresholds. For instance, the annual mean concentration of NO_2 at the traffic stations was about 57 μ g.m^{-3} in 2017 (EEA, 2019), when the EU limit is 40 μ g.m^{-3}. Stefan et al. (2013) have shown the importance of local conditions and anthropogenic factors in air quality analysis in areas close to Bucharest, during two weeks of measurements in 2012. lorga et al. (2015) and Grigoraş et al. (2016) showed that the main NO_x contributions came from traffic and production of electricity, spread over about 10 medium-size thermal power plants within the city.

Figure 2 shows the Bucharest metropolitan area and the flight tracks of the two scientific aircraft used during AROMAT-2 (the FUB Cessna-207 and the INCAS BN-2). Note that the BN-2 tracks are actually a good indication of the Bucharest ring road. We were not allowed to cross the ring road with the BN-2, except in the North of the city. The figure also pinpoints important locations for the AROMAT campaigns. The FUB Cessna took-off and landed at the Baneasa international airport, located 8 km north of Bucharest city center (44.502° N, 26.101° E). The INCAS BN-2 also used Baneasa airport during AROMAT-2, but this plane was mainly based at the Strejnicu airfield (44.924° N, 25.964° E), which lies 60 km north of Bucharest, near Ploiesti. The UAV operations in Bucharest during AROMAT-1 were performed at Clinceni airfield (44.359° N, 25.931 ° E). The latter is located in the southwest of the city, 7 km west of the INOE observatory in Magurele (44.348°N, 26.031°E).

2.2 The Jiu Valley between Targu Jiu and Craiova

The second NO_2 plume in Fig. 1 lies around 250 km west of Bucharest. It corresponds to a series of four thermal power plants located along the Jiu river between the cities of Targu Jiu (82,000 inhabitants, 45.03°N, 23.27°E) and Craiova (269,000 inhabitants, 44.31°N, 23.8°E). These plants were built in this area due to the presence of lignite (brown coal), which is burned to produce electricity.

The altitude of the valley ranges from 268 m a.s.l. in Targu Jiu to 90 m in Craiova. The valley is surrounded by moderately elevated hills (400 m a.s.l.). Due to the orography, the prevailing wind directions is from southwest to southeast.

Beside NO_2, the SO_2 emissions from these plants are also visible from space, as first reported by Eisinger and Burrows (1998) using GOME data. Since 2011, the OMI-derived trends above the area indicate that the emissions of SO_2 have been decreasing, while those of NO_2 are stable (Krotkov et al., 2016). This is related to the installation of flue gas desulfurization (FGD) systems, which was part of environmental regulations imposed on Romania following its entry in the European Union in 2007.

Figure 3 presents a map of the Jiu Valley area with the four power plants. The map also shows the tracks of the two airborne platforms (the FUB Cessna and an ultralight operated by UGAL) operated in this area during AROMAT-2. Table S1 in the

Supplement presents the geographical positions, nominal capacities, and smokestack heights of the four power plants. From north to south, the plants are named according to their locations: Rovinari, Turceni, Isalnita and Craiova II.

During the AROMAT campaigns, we focused in particular on the emissions of the Turceni power plant (44.67°N, 23.41°E). With a nominal capacity of 1650 MW, it is the largest electricity producer in Romania. The Turceni power plant is located in a rural area, 2 km ESE of the village of Turceni. The plant emits aerosols, NOx, and SO_2 from the 280 m high smokestacks.

Scientific studies on air quality inside the Jiu Valley are sparse. Previous measurements performed by INOE during a campaign in Rovinari in 2010 indicated elevated volume mixing ratios of NO_2 (up to 30 ppb) and of SO_2 (up to 213 ppb) (Nisulescu et al., 2011; Marmureanu et al., 2013). The maximum ground concentrations occurred in the morning, before the planetary boundary layer development. Mobile-DOAS observations performed in 2013 revealed columns of NO_2 up to 1 x 10^{17} molec cm^{-2} (Constantin et al., 2015).

2.3 Groups, instruments, and platforms

The AROMAT consortium consisted of research teams from Belgium (BIRA-IASB), Germany (IUP-Bremen, FUB, MPIC), The Netherlands (KNMI), Romania (University "Dunarea de Jos" of Galati, hereafter UGAL, National Institute of R&D for Optoelectronics, hereafter INOE, and National Institute for Aerospace Research "Elie Carafoli", hereafter INCAS), and Norway (NILU). The AROMAT consortium had a common focus on measuring the tropospheric composition using various techniques.

Figure 4 illustrates the typical instrumental deployment during the campaigns. The set-up combined airborne and ground-based measurements to sample the 3-D chemical state of the lower troposphere above polluted areas. The Supplement presents the main atmospheric instruments operated during the two campaigns, classified into airborne, ground-based, remote sensing, and in-situ sensors. The primary target species during AROMAT-1 were NO_2 and aerosols while the observation capacities expanded in AROMAT-2 through the improvements of the AirMAP and SWING sensors for SO_2 measurements and the deployments of other instruments such as SO_2 cameras, DOAS instruments targeted to H_2CO, and a PICARRO instrument to measure water vapor, methane, CO, and CO_2.

We used two small tropospheric aircraft: the Cessna-207 from FUB, and the Britten-Norman Islander (BN-2) from INCAS. The Cessna was dedicated to remote sensing. It mainly performed mapping flights at 3 km a.s.l. for the airborne imagers, while parts of the ascents and descents were used to measure aerosol extinction profiles with the FUBISS-ASA2 instrument. The BN-2, which was only used during AROMAT-2, was dedicated to in-situ measurements around Bucharest between surface and 3000 m a.s.l.. In AROMAT-2, there was also an ultralight aircraft used by UGAL for nadir-DOAS observations in the Jiu Valley. The ultralight aircraft typically flew between 600 and 1800 m a.s.l. Two UAVs, operated by INCAS and UGAL flew during AROMAT-1. These measurements were not repeated during AROMAT-2 since the coverage of the UAVs was too limited, both in horizontal and vertical direction. Finally, we also launched balloons carrying NO_2 sondes from Turceni and performed Mobile-DOAS measurements from several cars during both campaigns. The Supplement provides more details about the practical deployments during the campaigns.

2.4 The 2014 AROMAT campaign

The AROMAT-1 campaign took place between 1 and 13 September 2014. The operations started in Bucharest with the continuous observations from the Romanian Atmospheric 3D Observatory (RADO, Nicolae et al. (2010)) observatory and synchronized car-based Mobile-DOAS observations around the Bucharest ring road and within the city. During the first two days of the campaign, the INCAS UAV flew from the Clinceni airfield with two different aerosol payloads (the TSI Dust Trak DRX and TSI aerosol particle sizer) up to an altitude of 1.2 km a.s.l. The Cessna was not allowed to fly over the city but performed loops above the ring road at a low altitude of 500 m a.s.l. The remote sensing measurements stopped on 4 September due to bad weather. On 5 and 6 September, we collected data only from the ground, and in broken cloud conditions.

On 7 September 2014, part of the campaign crew moved to the Jiu Valley. We installed the INOE mobile laboratory (in-situ monitors, MILI lidar, and ACSM) in Turceni and performed the first UAV flights around the power plant on 8 September 2014 with the NO_2 sonde and SWING. On the same day in Bucharest, the Cessna flew above the city with AirMAP and Mobile-DOAS operated on the ground. On the following day, 9 September 2014, the Cessna did a second mapping of Bucharest and we started to launch balloons from Turceni, carrying the NO_2 sonde. In total, 11 balloons were launched between 8 and 12 September 2014, out of which 10 led to successful measurements. Technical issues with both the UAV and the Cessna interrupted the flights for a couple of days. The UAV operations started again with a SWING flight on 10 September 2014. On 11 September 2014, the AirMAP and SWING flew in coincidence above Turceni, on the Cessna and the UAV respectively, and we performed two more short SWING-UAV flights. On 12 and 13 September, we performed two more Cessna flights above the Jiu Valley but the weather conditions were degrading. During the entire second week of the campaign, Mobile-DOAS measurements were performed in Turceni and around the other power plants of the Jiu Valley.

Table S5 in the Supplement summarizes the main measurement days during AROMAT-1, specifying if the measurements were taken in Bucharest or in the Jiu Valley. The "golden days" of the AROMAT-1 campaigns are 2, 8, and 11 September 2014. These days are particularly interesting due to good weather conditions and coincident measurements. On 2 September 2014, we operated the three Mobile-DOAS together around Bucharest. On 8 September 2014, we flew AirMAP above Bucharest with the UGAL and MPIC Mobile-DOAS on the ground. Finally, on 11 September 2014, SWING and AirMAP were time-coincident above the Turceni power plant, and two balloons sampled the vertical distribution of NO_2.

2.5 The 2015 AROMAT-2 campaign

The AROMAT-2 campaign took place between 17 and 31 August 2015. We started in Bucharest with car-based Mobile-DOAS measurements and observations at RADO. The INOE mobile lab was installed in Turceni on 19 August 2015, followed by an SO_2 camera (instrument described in Kern et al., 2015; Stebel et al., 2015) and NO_2 camera (Dekemper et al., 2016). Poor weather conditions limited the relevance of the measurements during the first days of the campaign. Two Mobile-DOAS teams in Bucharest moved from Bucharest to the Jiu Valley on 23 August 2015. From then, the weather was fine until the end of the campaigns, and valuable data were collected during all days between 24 and 31 August 2015.

In the Jiu Valley, the crew was based in Turceni and most of the static instruments were installed at a soccer field. Beside the INOE mobile lab with in-situ samplers, the scanning lidar, SO_2 cameras and the NO_2 camera pointed to the power plant plume. The NO_2 camera acquired images until 25 August 2015. The car-based Mobile-DOAS operated in the Valley between the different power plants. From 24 August, the SO_2 cameras were splitted: one of them stayed in the soccer field, the two others were installed at several points around Turceni. Also on 24 August, the UGAL ultralight took off from Craiova and flew to the Jiu Valley until Rovinari, carrying a nadir-looking spectrometer. This experiment was repeated on 25, 26, and 27 August. On 28 August 2015, the Cessna flew above Turceni with AirMAP and SWING.

In Bucharest, the BN-2 flew first on 25 August 2015. It took off from Strejnicu and carried various in-situ instruments: the TSI nephelometer and Aerosol Particle Sizer, the NO_2 CAPS, the PICARRO, and the KNMI NO_2 sonde, and flew in a loop pattern at 500 m a.s.l. around the city ring road. After this test flight, the aircraft performed 6 flights between 27 and 31 August 2015, which included soundings around Baneasa and Magurele, up to 3300 m a.s.l. On 30 and 31 August 2015, the Cessna mapped the city of Bucharest, performing two flights per day. It also performed soundings to measure AOD profiles with the FUBISS-ASA2 instrument (Zieger et al., 2007).

Table S6 in the Supplement summarizes the measurements of the AROMAT-2 campaign, specifying if the measurements were taken in Bucharest or in the Jiu Valley. Compared to the AROMAT-1 campaign, a larger number of instruments took part and also a larger number of 'golden days' occurred. All the days between 24 and 31 August 2015 led to interesting measurements. Regarding intercomparison exercises for the airborne imagers, the best days are 28 August 2015 (Jiu Valley) and 31 August 2015 (Bucharest).

3 Geophysical results

This section presents selected findings related to tropospheric NO_2, SO_2 and H_2CO in the two target areas. The Supplement gives details about the instruments involved in these observations and presents additional measurements in Bucharest and the Jiu Valley. Tables S7 and S8 of the Supplement summarize the observed ranges of the main geophysical quantities for the two campaigns.

3.1 Bucharest

3.1.1 Horizontal distribution of NO_2

Figure 5 presents two maps of the AROMAT NO_2 measurements performed with the AirMAP, CAPS, and MPIC mobile-DOAS instruments above Bucharest, on 30 (Sunday afternoon, left panel) and 31 (Monday afternoon, right panel) August 2015. AirMAP is a remote sensing instrument that mapped the NO_2 VCDs from the Cessna at 3 km a.s.l. and produced the continuous map. The CAPS is an in-situ instrument, it was operated on the BN-2 and sampled the air at 300 m a.s.l. and performed vertical soundings above Magurele. The MPIC Mobile-DOAS mainly drove along the Bucharest ring road.

The datasets of Fig. 5 reveal large differences of NO_2 amounts on Sunday 30 August 2015 compared to Monday 31 August 2015. On Sunday afternoon, the NO_2 VCDs peak around 1.5 x 10^{16} molec cm^{-2}. On Monday, the NO_2 plume spread from the center to the northeast of the city. The observed NO_2 VCDs were smaller than the detection limit upwind and reach up to 3.5 x 10^{16} molec cm^{-2} inside the plume. The NO_2 VMR measured with the CAPS was close to the detection limit on Sunday while it reached 5 ppb inside the plume on Monday 31 August 2015. Note that the systematic differences between AirMAP and the MPIC Mobile-DOAS at the eastern part of the ring road on 31 August 2015 were due to the time differences between both measurements. Meier (2018) compared the two instruments during the morning flights, which include more simultaneous observations. The comparison reveals a good agreement when averaging the forward and backward-looking Mobile-DOAS NO_2 VCDs, with a MPIC/AirMAP slope of 0.93 and a correlation coefficient of 0.94. The remaining discrepancy may be explained by AMFs errors and differences in time and horizontal sensitivity. Figure S2 in the Supplement presents this quantitative comparison.

Figure 6 presents collocated CAPS and AirMAP NO_2 measurements on 31 August 2015. The BN-2 carrying the CAPS flew from Magurele to the East of Bucharest, remaining outside the city ring at 300 m a.s.l. between 12:30 and 12:55 UTC, while AirMAP onboard the Cessna was mapping the city between 12:00 and 13:30 UTC. We extracted the AirMAP NO_2 VCDs at the position of the CAPS observations. The figure confirms that the two instruments detected the plume at the same place. This suggests that along this portion of the flight, which was inside the plume but outside the city, the NO_2 VMR measured at 300 m a.s.l. may be used as a proxy for the NO_2 VCD. Indeed, the BLH was about 1500m (Fig.S8 in the Supplement and discussion therein) during these observations. Assuming a constant NO_2 VMR of 3.5 ppb in the boundary layer leads to a NO_2 VCD of 1.4 x 10^{16} molec cm^{-2}. This estimate is close to the AirMAP NO_2 VCD observed in the plume (Fig. 6). When measured at 300 m a.s.l., the NO_2 VMR thus seems a good estimate of its average within the boundary layer. Note that this finding is specific to the configuration in Bucharest where we flew at 10 km from the city center and does not apply to our measurements in the exhaust plume of the Turceni power plant (Fig. 9). Future campaigns should include vertical soundings inside the Bucharest plume to further investigate its NO_2 vertical distribution.

3.1.2 Horizontal distribution of H_2CO

Figure 7 shows the H_2CO and NO_2 VCDs measurements from the IUP-Bremen nadir instrument operated onboard the Cessna on 31 August 2015 (morning flight), together with the time-coincident MPIC Mobile-DOAS measurements. The H_2CO VCDs range between 1$\pm$0.25 x 10^{16} molec cm^{-2} and 7.5$\pm$2 x 10^{16} molec cm^{-2}, a maximum observed inside the city. We estimated the H_2CO reference column for the airborne data using the Mobile-DOAS measurements. Both NO_2 and H_2CO are in good agreement when comparing their distributions as seen from the airborne and ground-based instruments. However, if the highest H_2CO VCDs are found above the Bucharest city center, they are not coincident with the NO_2 maximum, as can be seen comparing the upper and lower panels of Fig. 7, for instance on the second Cessna flight line from the north.

The H_2CO hotspot observed above Bucharest is mainly anthropogenic. Indeed, biogenic emissions typically account for 1 to 2 x 10^{16} molec cm^{-2} (J.-F. Müller, personal communication), in agreement with the background VCDs measured by the Mobile-DOAS along the Bucharest ring. During the measurements, the wind was blowing from south and west. The difference

between NO_2 and H_2CO spatial patterns may be explained by the different origins of NO_x compared to H_2CO or by the formation time of H_2CO through the oxidation of VOCs.

Anthropogenic hotspots of H_2CO have already been observed, e.g. above Houston (Texas), an urban area which includes significant emissions from transport and petrochemical industry (Parrish et al., 2012; Nowlan et al., 2018). Nowlan et al. also deployed an airborne DOAS nadir instrument, they reported H_2CO VCDs up to 5 x 10^{16} molec cm^{-2} in September 2013.

3.2 The Jiu Valley

3.2.1 Spatial distribution of NO_2

Figure 8 presents the horizontal distribution of the NO_2 VCDs in the Jiu Valley measured with the MPIC Mobile-DOAS on 23 August 2015. The figure shows elevated NO_2 VCDs close to the four power plants listed in Table S1 of the Supplement, with up to 8x10^{16} molec cm^{-2} downwind of Turceni and Rovinari. In comparison, the area East of Craiova is very clean, with typical NO_2 VCDs under 1x10^{15} molec cm^{-2}.

The situation of Fig. 8 is characteristic of the conditions encountered in the Jiu Valley, with high NO_2 VCDs observed north and west of the plants due to the prevailing wind directions. During both campaigns, we observed maximum NO_2 VCDs reaching up to 1.3x10^{17} molec cm^{-2} close to the plants with Mobile-DOAS instruments.

Figure 10 (upper panels) shows the AirMAP and SWING NO_2 VCDs measured around the Turceni power plant on 28 August 2015. The two airborne instruments largely agree, detecting NO_2 VCDs up to 8x10^{16} molec cm^{-2} in the exhaust plume of the power plant. Figure S5 in the Supplement (upper panel) extracts the AirMAP and SWING NO_2 VCDs along the path of the simultaneous ground-based zenith-only Mobile-DOAS measurements and compares the three datasets. This comparison confirms the good agreement for the airborne instruments but indicates that comparing airborne nadir-looking DOAS with ground-based zenith Mobile-DOAS instruments is not straightforward in these conditions. Table S2 in the Supplement gives the typical AMFs used in this analysis for airborne and zenith-only Mobile-DOAS. When observed with the Mobile-DOAS, the plume shows higher NO_2 VCDs and appears narrower than with the airborne instruments. This is partly related to air mass factor uncertainties, but they can not explain alone such a discrepancy. Close to the power plant, the plume is very thin and heterogeneous which leads to 3-D effects in the radiative transfer, as suggested in a previous AROMAT study (Merlaud et al., 2018). In these conditions, the 1-D atmosphere of the radiative transfer models used to calculate the airborne AMFs may not be realistic enough and bias the VCDs measured from the aircraft.

Figure 9 shows those AROMAT-1 NO_2 sonde measurements above Turceni which detected the plume. The NO_2 is not well-mixed in the boundary layer, with maxima aloft and lower VMRs close to the surface. This is understandable so close to the source, as high-temperature NO_x is emitted from the 280 m high stack. In these balloon-borne datasets, the observed maximum NO_2 VMR is about 60 ppb inside the plume, and the NO_2 VMR vanishes above 1200 m a.s.l.. These results suggest that airborne measurements with the ULM-DOAS, which can fly safely at 1500 m a.s.l., can provide reliable measurements of the integrated column amount inside the plume. Note that we measured NO_2 VMRs of up to 95 ppb on the ground at the soccer field (see Fig. S11 in the Supplement) when the wind was blowing from the power plant.

3.2.2 Horizontal distribution of SO_2

Figure 10 (lower panels) presents the SO_2 horizontal distributions measured around Turceni with AirMAP (lower left panel) and SWING (lower right panel) on 28 August 2015. The maps show the plume from the Turceni plant transported in the northwest direction, and other areas with elevated SO_2 VCDs in the east and south of Turceni. Meier (2018) presents in detail these AirMAP SO_2 observations and compares them with SWING results. Figure S4 in the Supplement shows the corresponding time series of SWING and AirMAP SO_2 DSCDs. It is found that the AirMAP-derived SO_2 columns inside the plume SO_2 reach 6x10^{17} molec cm^{-2} and that the AirMAP and SWING SO_2 VCDs agree within 10%. Moreover, for these airborne data, the SO_2 horizontal distribution broadly follows that of NO_2. The discrepancies can be explained by the different lifetimes of the two species.

We have measured higher SO_2 levels during AROMAT-2 than during AROMAT-1, both in terms of VCDs and VMRs, as shown in Fig. S12 of the Supplement. This corresponds to a shutdown of the desulfurization unit of the power plant, which local workers reported during the campaign. On 26 August 2015 in particular, the SO_2 VMR went up to 250 ppb, above the WMO guidelines of 191 ppb for the 10 minutes mean, while it never exceeded 50 ppb in 2014.

As for NO_2, it appears difficult to quantitatively relate the airborne and Mobile-DOAS SO_2 VCDs observations in the close vicinity of the power plant. As shown in Fig. S5 of the Supplement (lower panel), the maximum SO_2 VCD measured from the ground on the road close to the factory amounts to 1.3 x 10^{18} molec cm^{-2} while from the aircraft, the SO_2 VCD reached 8 x 10^{17} molec cm^{-2}. Part of this difference can be explained by 3-D effects on the radiative transfer, as for NO_2. As discussed below, it seems easier to compare the SO_2 flux.

4 Discussion

This section addresses the lessons learned from our study for the validation of satellite observations of the three investigated tropospheric trace gases, namely NO_2, SO_2, and H_2CO. For each molecule, we discuss the added value of conducting such an airborne campaign as well as the choice of Romania as a campaign site. The last part of the section estimates the NO_x and SO_2 emissions from Bucharest and from the power plants of the Jiu Valley, using the different datasets of the campaigns.

4.1 Lessons learned for the validation of space-borne NO_2 VCDs

4.1.1 Number of possible pixels and dynamic range at the TROPOMI resolution

Regarding Bucharest, the mapped area of Fig. 5 (right panel) virtually covers 43 TROPOMI near-nadir pixels. Averaging the high spatial resolution AirMAP NO_2 VCDs within these 43 hypothetical TROPOMI measurements reduces the dynamic range of the observed NO_2 field. The latter decreases from 3.5x10^{16} to 2.6x10^{16} molec cm^{-2} (37 σ where σ is the required precision on the tropospheric NO_2 VCD). Nevertheless, 33 of the 43 hypothetical TROPOMI pixels exhibits a NO_2 VCD above the required 2-σ random error for TROPOMI (1.4x10^{15} molec cm^{-2}).

Regarding the Jiu Valley, a similar exercise based on our measurments on 28 August 2012 (Fig. 10, upper panel) leads to 48 near-nadir TROPOMI pixels, out of which 35 would have a NO_2 VCD above the 2-σ TROPOMI error. The largest NO_2 tropospheric VCD seen by TROPOMI would be around 2x10^{16} molec cm^{-2} (29 σ for TROPOMI).

4.1.2 Characterization of the reference measurements

Table 3 summarizes the NO_2 observations during the AROMAT campaigns. For each instrument, the table indicates the measured range of NO_2 VCDs (or VMRs), the ground sampling distance and a typical detection limit and bias. Regarding DOAS instruments, we estimated the detection limits on the NO_2 VCDs from typical 1-σ DOAS fit uncertainties divided by typical air mass factors (AMF). Table S2 in the Supplement presents these typical AMFs and detection limits. The 1-σ DOAS fit uncertainty is instrument specific and an output of the DOAS fitting algorithms. The AMF depends on the observation's geometry, atmospheric and surface optical properties. Uncertainties on the AMF usually dominate the systematic part of the error for the DOAS measurements. Therefore, for these instruments, the bias given in Table 3 corresponds to the uncertainty in their associated AMF.

Combined with the ground sampling distance, the detection limit enables one to quantify the random uncertainty of a reference observation at the satellite horizontal resolution. Indeed, considering reference measurements averaged within a satellite pixel, the random error associated with the averaged reference measurements decreases with the square root of the number of measurements, following Poisson statistics. For instance, a continuous mapping performed with SWING at a spatial resolution of 300 x 300 m^2 inside a TROPOMI pixel of 3.5 x 5.5 km^2 would lead to 214 SWING pixels. Averaging the NO_2 VCDs of these SWING pixels would divide the SWING original uncertainty (1.2x10^{15} molec.cm^{-2}) by $\sqrt{214}$, leading to 8.2x10^{13} molec.cm^{-2}, about one tenth of the random error of TROPOMI (7x10^{14} molec.cm^{-2}) given in table 2.

However, the temporal variation of the NO_2 VCDs further adds uncertainty to the reference measurements when comparing them with satellite data. The validation areas typically extend over a few tens of kilometers. At this scale, satellite observations are a snapshot in time of the atmospheric state, while an airborne mapping typically takes one or two hours.

Figure 11 illustrates our estimation of the temporal variation of the NO_2 VCDs comparing consecutive AirMAP overpasses above Bucharest from the morning flight of 31 August 2015. During this flight, the Cessna covered the same area three times in a row between 07:06 and 08:52 UTC. Figure S3 in the Supplement presents the corresponding AirMAP and SWING NO_2 DSCDs. For each AirMAP overpass, we averaged the NO_2 VCDs at the horizontal resolution of TROPOMI (see previous section). The standard deviation of the differences between two averaged overpasses then indicates the random part of the NO_2 VCDs temporal variation during an aircraft overpass. This standard deviation is 3.7x10^{15} and 4.2x10^{15} molec cm^{-2}, respectively between the first and second, and second and third overpass. Hereafter, we used 4x10^{15} molec cm^{-2} as random error due to the temporal variation.

Clearly, the NO_2 VCD temporal variation depends on characteristics of a given validation experiments, such as the source locations and the wind conditions during the measurements. The temporal variation also depends on the time of the day and we base our estimate here on measurements around 11:00 LT while TROPOMI overpass is at 13:30 LT. In the studied case however, this error source is larger for the reference measurements than the TROPOMI precision (7x10^{14} molec cm^{-2}). This is

quite different from using static MAX-DOAS as reference. The latter are usually averaged within one hour around the satellite overpass. Compernolle et al. (2020) quantify the temporal error for MAX-DOAS NO_2 VCDs, typically ranging between 1 to 5x10^{14} molec cm^{-2}. In the next section, we investigate the effect of underestimating the temporal random error.

4.1.3 Simulations of validation exercises in different scenarios

We simulated TROPOMI Cal/Val exercises with the spatially averaged AirMAP observations described in Sect. 4.1.1. We considered these averaged AirMAP NO_2 VCDs as the ground truth in simulated TROPOMI pixels, on which we added Gaussian noise to build synthetic satellite and reference NO_2 VCDs datasets. For the synthetic satellite observations, the noise standard deviation corresponded to the TROPOMI random error (the precision in Table 2). For the synthetic airborne observations, we added in quadrature the aforementioned averaged airborne shot noise (e.g. 7x10^{13} molec cm^{-2} for SWING) and temporal error (4x10^{15} molec cm^{-2}, which we assumed to be also realistic around Turceni). We then applied weighted orthogonal distance regressions to a series of such simulations to estimate the uncertainty on the regression slope. This led to slope uncertainties of about 6% and 10% in Bucharest and Turceni, respectively.

In a real-world validation experiment, this regression slope would quantify the combined biases of the two NO_2 VCDs datasets (satellite and reference). These biases mainly originate from errors in the AMFs, resulting in particular from uncertainties on the NO_2 and aerosol profiles, and on the surface albedo. To some extent, these quantities can be measured from an aircraft with the type of instrumentation deployed in the AROMAT activity. The ground albedo can be retrieved with the DOAS instruments by normalizing uncalibrated airborne radiances to a reference area with known albedo (Meier et al., 2017) or by using a radiometrically calibrated DOAS sensor (Tack et al., 2019). The NO_2 and aerosol profiles can be measured with in-situ instruments such as a CAPS NO_2 monitor and a nephelometer. For legal reasons, vertical soundings are difficult above cities. One can measure the NO_2 and aerosol profile further down in the exhaust plume, once the latter is above rural areas. The conditions inside the city can be different and this motivates the deployment of ground-based instruments, e.g. sunphotometers and MAX-DOAS, inside the city.

Regarding uncertainties on the references AMFs, the added value of knowing the aerosol and NO_2 profile appears when comparing the AMF error budget for airborne measurements above Bucharest (26%, Meier et al. (2017)) and above the Turceni power plant (10%, Merlaud et al. (2018)). In the latter case, there was accurate information on the local NO_2 and aerosol profiles thanks to the lidar and the balloon-borne NO_2 sonde, respectively. We used these two AMF uncertainties to estimate a total possible bias between reference and satellite observations.

Table 6 presents total error budgets for different scenarios of validation exercises using reference airborne mapping to validate spaceborne tropospheric NO_2 VCDs. We estimated the random and systematic uncertainties between satellite and reference measurements with SWING and AirMAP, including (or not) profile information on the aerosols and NO_2 VMR, and for measurements over Bucharest or Turceni. Note that we considered 25% for the satellite accuracy. The temporal error of the airborne measurements clearly dominates the total random error, making the differences in detection limit between AirMAP and SWING irrelevant for this application. Adding the profile information on the other hand reduces the total multiplicative

bias from 37% to 28% or 29% in Bucharest and Turceni. This quantifies the capabilities of such airborne measurements for the validation of the imaging capabilities of TROPOMI regarding the NO_2 VCDs above Bucharest and the Jiu Valley.

Finally, it should be noted that these regression simulations assume a correct estimation of the temporal random error. Underestimating this error propagates in the fit of the regression slope. Figure 12 presents the possible effect of such an underestimation when the a priori random error of the reference measurements is set at 1x10^{15} molec cm^{-2}, using again the AirMAP observations of Fig. 5 (right panel) as input data. As the dynamic range of the reference measurements increases with the applied error, the fitted slope decreases. For a true error of 4x10^{15}, this leads for instance to an underestimation of the slope of about 5%. This effect is small but other sources of random error (e.g undersampling the satellite pixels) would add up in a real-world experiment. Wang et al. (2017) observed such a systematic decrease of the regression slope when averaging MAX-DOAS measurements within larger time windows around the satellite overpass.

4.2 Lessons learned for the validation of space-borne H_2CO VCDs

Table 4 is similar to Table 3 but for H_2CO, which we only measured in significant amounts in and around Bucharest.

The background level of the H_2CO VCD around the city is around 1x10^{16} molec cm^{-2} and the anthropogenic increase in the city center is up to 7x10^{16} molec cm^{-2} (Fig. 7). The background falls within the TROPOMI H_2CO spread (1.2x10^{16} molec cm^{-2}), and Fig. 7 indicates that the extent of the urban hotspot only corresponds to a few TROPOMI pixels, with a maximum at 6 σ. This limits the relevance of individual mapping flights for the validation of H_2CO, yet systematic airborne measurements would improve the statistics. The information on the H_2CO horizontal variability is nevertheless useful, as it justifies the installation of a second MAX-DOAS in the city center, in addition to background measurements outside the city. Indeed, long-term ground-based measurements at two sites would be useful to investigate seasonal variations of H_2CO, as already demonstrated in other sites (De Smedt et al., 2015). Averaging the H_2CO over a season would reduce the random errors of the satellite measurements and it could reveal the horizontal variability of H_2CO from space. The H_2CO hotspot around Bucharest seems to be visible in the TROPOMI data of summer 2018 (I. De Smedt, personnal communication).

Getting information on the profile of H_2CO during an airborne campaign may also help to understand the differences between ground-based and space-borne observations. This could be done by adding to the BN-2 instrumental set-up an in-situ H_2CO sensor such as the In Situ Airborne Formaldehyde instrument (ISAF, Cazorla et al. (2015)) or the COmpact Formaldehyde FluorescencE Experiment (COFFEE, St. Clair et al. (2017)).

4.3 Lessons learned for the validation of space-borne SO_2 VCDs

Table 5 is similar to Table 3 but for SO_2, which we only measured in significant amounts in the Jiu Valley. The higher bias of the airborne measurements for SO_2 compared to NO_2 is due to the albedo. The latter is lower in the UV where we retrieve SO_2, which leads, for the same albedo error, to a larger AMF uncertainty (e.g. Merlaud et al., 2018, Fig.10).

Averaging the SO_2 VCDs from the airborne mapping of Fig. 10 at the TROPOMI resolution leads to 30 near nadir TROPOMI pixels above a 2-σ error of 5.4x10^{16} molec cm^{-2}. The maximum SO_2 tropospheric VCD seen by TROPOMI would be 2.4x10^{17} molec cm^{-2} (7 σ). This tends to indicate that airborne mappings of SO_2 VCDs above large power plants could help to validate

the horizontal variability of the SO_2 VCDs measured from space, to a limited extent in the AROMAT conditions due to the small dynamic range (7 σ). As for H_2CO, systematic airborne measurements would improve the statistics.

However, it would be difficult to quantify the bias of the satellite SO_2 VCD with AROMAT-type of airborne measurements. Adding in quadrature the biases of the SO_2 VCDs for airborne measurements (40%, Table 5) and for TROPOMI (30%, Table 2) already leads to a combined uncertainty of 50%, without considering any temporal variation or regression error. This best-case scenario is already at the upper limit of the TROPOMI requirements for tropospheric SO_2 VCDs (Table 2).

Similar to H_2CO, the validation of the satellite-based SO_2 measurements should thus rely on ground-based measurements, enabling to improve the signal-to-noise ratio of the satellite and reference measurements by averaging their time series. An additional difficulty for validating SO_2 VCDs emitted by a power plant arise from the spatial heterogeneity of the SO_2 field around the point source, which renders ground-based VCDs measurements complicated.

On the other hand, Fioletov et al. (2017) presented a method to derive the SO_2 emissions from OMI data and validated it against reported emissions. The SO_2 fluxes can be measured locally in several ways and we tested some of them during AROMAT-2 (see Sect. 4.4.2 below). To validate satellite-derived SO_2 products in Europe, it thus seems possible to compare satellite and ground-based reference SO_2 fluxes. Theys et al. (2019) already validated TROPOMI-derived volcanic SO_2 fluxes against ground-based measurements. In this context, a SO_2 camera pointing to the plant stack would be a valuable tool since it could be permanently installed and automated. One advantage of such a camera compared to the other tested remote-sensing instruments, beside its low operating cost, is that it derives the extraction speed from the measurements, avoiding dependence on low-resolution wind information. The next section presents the SO_2 fluxes derived with such a camera during the 2015 campaign.

Note that since the desulfurization unit of the Turceni power plant was not fully operational during AROMAT-2, the SO_2 VCDs detected above Turceni on 28 August 2015 are expectedly higher than for standard conditions, all the more so as the SO_2 VCDs in the area seem to have further decreased (D. Constantin, personnal communication). The first reported TROPOMI SO_2 measurements above the area pinpoint other power plants in Serbia, Bosnia–Herzegovina, and Bulgaria (Fioletov et al., 2020). For validation studies, it would be worth to install automatic SO_2 cameras around these plants, until they are equipped with FGD units.

4.4 Emissions of NO_x and SO_2 from Bucharest and the Jiu Valley

This section presents our estimates of the NO_x and SO_2 fluxes from Bucharest and the power plants in the Jiu Valley, combining our different 2014 and 2015 measurements and comparing them with available reported emissions. Campaign-based estimates of NO_x emissions from large sources are relevant in a context of satellite validation since the high resolution of TROPOMI enables to derive such emissions on a daily basis (Lorente et al., 2019). Regarding SO_2, as discussed in the previous section, the low signal-to-noise ratio of the satellite measurements implies averaging for several months to derive a SO_2 flux (Fioletov et al., 2020), yet campaign measurements are useful to select an interesting site and test the ground-based apparatus and algorithms.

The comparisons with reported emissions should not be overintrepreted since we compare campaign-based flux measurements performed during a few days in daytime with reported emissions which represent yearly averages. Nevertheless, they give interesting indications about the operations of the FGD units of the power plants and possible biases in emission inventories.

Our flux estimates are all based on optical remote sensing measurements. They involve integrating a transect of the plume along its spatial extent and multiplying the outcome by the plume speed, which may correspond to the stack exit velocity (camera pointing to the stack) or to the wind speed (Mobile-DOAS and imaging-DOAS). We refer the reader to previous studies for the practical implementations. Ibrahim et al. (2010) presented the method we used for Bucharest, where we encircled the city with the Mobile-DOAS. Meier et al. (2017) presented the AirMAP-derived flux estimations, while Johansson et al. (2014) derived industrial emissions from a car-based Mobile-DOAS instrument as we did for the Turceni power plant. Constantin et al. (2017) presented the fluxes based on the ULM-DOAS measurements. Regarding the SO_2 cameras, they are now commonly used to monitor SO_2 emissions from volcanoes (see McGonigle et al. (2017) and references therein), but their capacity to measure SO_2 fluxes from power plants have been demonstrated as well (e.g., Smekens et al., 2014).

4.4.1 NO_x flux from Bucharest

We estimated NO_x fluxes from the Bucharest urban area using the NO_2 VCDs measured with the Mobile-DOAS systems along the external ring and the wind data on 8 September 2014 and 31 August 2015. We derived the wind direction from the maxima of the NO_2 VCDs in the DOAS observations. For the wind speed, we took 1.1 m s^{-1} on 8 September 2014, the value Meier (2018) used for the AirMAP-derived flux, which originates from meteorological measurements at Baneasa airport. On 31 August 2015, we used the ERA5 wind data (C3S, 2017) at the time when the Mobile-DOAS crossed the NO_2 plume (15:00 UTC). The ERA5 database indicates a constant windspeed between 1000 and 900 hPA of 1.2 m s^{-1}. Finally and similarly to Meier (2018), we took a ratio of 1.32 for the NO_x to NO_2 ratio and estimated the chemical loss of NO_x with a lifetime of 3.8h and an effective source location in the center of Bucharest.

Table 7 presents the AirMAP and Mobile-DOAS derived NO_x fluxes from Bucharest, ranging between 12.5 and 17.5 mol.s^{-1}. On 8 September 2014, the Mobile and airborne observations were coincident. Their estimated NO_x fluxes agree within 20%. This gives confidence in the flux estimation yet one should keep in mind that the same wind data was used for both estimations. Meier (2018) estimated the uncertainties on the AirMAP-derived NO_x flux to be around 63%, while the uncertainty of Mobile-DOAS derived NO_x flux typically range between 30% and 50% (Shaiganfar et al., 2017).

We compared our measured NO_x fluxes with the European Monitoring and Evaluation Programme inventory (EMEP, https://www.ceip.at/). In practice, we summed the EMEP gridded yearly NO_x emissions between 44.2°and 44.6°N and between 25.9 °E and 26.3 °E and we assumed the emissions are constant during one year. This led to NO_x emissions of 6.14 and 6.33 mol s^{-1} for 2014 and 2015. Studying the reported emissions from several European cities including Bucharest, Trombetti et al. (2018) mentions that the EMEP emissions are well below other inventories for all the pollutants. We thus also compared our flux with the Emissions Database for Global Atmospheric Research (EDGAR v4.3.2, Crippa et al. (2018)), which is only available until 2012. The same method led to a NO_x flux of 18.4 mol s^{-1}, to compared with the 2012 EMEP NO_x emissions of 7.1 mol s^{-1}. Based on summer measurements, the AROMAT-derived NO_x emissions do not include residential heating. The

latter ranges between 10 and 40% of the total NO_x according to Trombetti et al. (2018). This tends to confirm that the EMEP inventory underestimates the NO_x emissions for Bucharest.

4.4.2 NO_x and SO_2 fluxes from the power plants in the Jiu Valley

Figure 13 presents a scatter plot of the slant columns of NO_2 and SO_2 for the ultralight flight of 26 August 2015, which detected the four exhaust plumes of the Valley. Two regimes are visible in the SO_2 to NO_2 ratio. When considering the longitude, the low SO_2 to NO_2 ratio (1.33) appears to correspond to the Rovinari exhaust plume, while the other power plants exhibit a higher ratio (13.55). The low ratio observed at Rovinari corresponds to the FGD units operating at this power plant.

We estimated the NO_x and SO_2 flux from the power plants using several instruments: a Mobile-DOAS, the ULM-DOAS, and the SO_2 camera. For the DOAS instruments, we inferred the wind direction from the plume position and we retrieved the wind speed from the ERA5 database. Considering the observed vertical extent of the plume downwind of Turceni (Fig. 9), we took the wind speed at 950 hPa (ca. 500 m a.s.l.).

Figure 14 presents the ULM-DOAS-estimated fluxes of NO_x and SO_2 from the power plants in Turceni, Rovinari, and Craiova for the flight on 26 August 2015. The figure also shows the reported emissions from the European Environment Agency (EEA) large combustion plants database (EEA, 2018), assuming constant emissions throughout the year. Turceni appears to be the largest SO_2 source (78 mol s^{-1}), while Rovinari is the largest NO_x source (8 mol s^{-1}).

It is difficult to interpret the discrepancies between those measured fluxes and the yearly reported emissions since we observed large variations in the instantaneous emissions with the SO_2 camera (see below and Fig. 15). However, the ratio of the two fluxes appears interesting since we can assume its relative stability. This ratio for a given power plant depends on whether or not a desulfurization unit is operational at the plant. On Fig. 14, Turceni appears to have both the largest measured ratio and the largest discrepancy between the measured and reported ratios. This is consistent with a temporary shutdown of the desulfurization unit of the Turceni power plant, as was reported by the plant workers during the campaign. The ULM-DOAS measurements on 25 August 2015 (shown in Fig. S14 the Supplement), which also sampled the Isalnita plume, are consistent with those of 26 August 2015. These measurements enable to estimate total NO_x and SO_2 fluxes to be about 22 and 147 mol s^{-1}, respectively.

Table 8 focuses on the Turceni power plant and lists all estimates of the NO_x and SO_2 emissions from this source. Meier (2018) estimated the NO_x flux from the Turceni power plant using the AirMAP measurements of 2014 and 2015. This leads to similar values for the two flights on 11 September 2014 and 28 August 2015, of about 8 mol.s^{-1}. On this second day, the UGAL Mobile-DOAS crossed the plume along the road in front of the power plant. These ground-based measurements lead to a NO_2 flux of 2.2 mol.s^{-1}, much lower than the aforementioned AirMAP-derived value. However, Meier (2018) calculated the latter based on AirMAP measurements at 3.5 km from the source. At shorter distances, the AirMAP estimated NO_2 flux is smaller and close to the Mobile-DOAS observations. This is probably related to the fact that the NO/NO_2 ratio has not yet reached its steady state value above the road where we performed the Mobile-DOAS observations, which is only around 1 km from the stack. The agreement is better for SO_2 (25 and 32 mol.s^{-1}). On 25 August 2015, we had a coincidence of ULM-DOAS and Mobile-DOAS observations and we observed a similar range of values. This gives us confidence in our estimate of

the NO_x flux from the aircraft but confirms that the nearby road is too close to the plant to estimate a meaningful NO_x flux from Mobile-DOAS NO_2 observations. Note that the conversion of NO into NO_2 is also visible right above the Turceni stack in the NO_2 imager data of 24 August 2015, as appears in Fig.6 of Dekemper et al. (2016).

Figure 15 presents a time series of the SO_2 emissions from the Turceni power plant between 9:00 and 10:50 UTC on 28 August 2015. We derived SO_2 fluxes at different altitudes above the stack using a UV SO_2 camera which is an updated version of the Envicam2 system, used during the SO_2 camera intercomparison described by Kern et al. (2015). We converted the measured optical densities to SO_2 column densities using simultaneous measurements with an integrated USB spectrometer (Lübcke et al., 2013). We estimated the stack exit velocity from the SO_2 images, recorded with a time resolution of about 15 seconds, by tracking the spatial features of the plume. Dekemper et al. (2016) used a similar approach to derive the NO_2 flux from NO_2 camera imagery.

The SO_2 fluxes retrieved for transverses at 400 to 700 m vertical distances above the stack agree on average with each other within 20%. Emissions estimated 100 m above the stack are underestimated due to saturation (SO_2 column densities above 2 x 10^{18} molec.cm^{-2}) and high aerosol concentration close to the exhaust.

The SO_2 emissions show large fluctuations. During the time of our observations they increased from 1 kg.s^{-1} (15.6 mol.s^{-1}) to around 4 $\pm$ 1 kg^{-1} (62.4 mol.s^{-1}). The images (Fig.S13 in the Supplement) also show a second and weaker source that emits SO_2. This is probably the desulfurization unit, which was reported to be turned on again on this day, after the temporary shutdown. Indeed, as appears in Table 8, the SO_2/NO_2 ratio measured from AirMAP is lower than the ones measured from the ULM-DOAS during the previous days, and the same holds true for the Mobile-DOAS measurements.

5 Conclusions

The two AROMAT campaigns took place in Romania in September 2014 and August 2015. These campaigns combined airborne and ground-based atmospheric measurements and focused on air quality-related species (NO_2, SO_2, H_2CO, and aerosols). The AROMAT activity targeted the urban area of Bucharest and the power plants of the Jiu Valley. The campaigns aimed at testing new instruments, measuring the concentrations and emissions of key pollutants in the two areas, and investigating the concept of such campaigns for the validation of air quality satellite-derived products.

We have shown that the airborne mapping of tropospheric NO_2 VCDs above Bucharest is potentially valuable for the validation of current and future nadir-looking satellite instruments. These measurements agree within 7% with ground-based measurements and cover a significant part of the dynamic range of the NO_2 tropospheric VCDs at an appropriate signal to noise ratio. Our simulations, which are based on our measurements and TROPOMI characteristics, indicate that we can constrain the accuracy of the satellite NO_2 VCDs within 37 or 28%, with and without information on the aerosol and NO_2 profile, respectively. This points out the importance of the profile information to approach the TROPOMI optimal target accuracy for tropospheric NO_2 VCDs (25%).

A unique advantage of airborne mapping is its ability to validate the imaging capabilities of nadir-looking satellites. This feature becomes more important as the satellite horizontal resolutions reaches the suburban scale. Judd et al. (2019) pointed

out the difficulty for static ground-based measurements to represent the NO_2 VCDs measured from space in polluted areas, due to the horizontal representativeness error. This error cancels out by mapping the full extent of satellite pixels. The caveat is the temporal error, which can be larger than with static ground-based measurements. We have estimated the temporal error to be about 4 x 10^{15} molec cm^{-2} in our observations above Bucharest, but it varies with local conditions for a given experiment. This indicates the usefulness of simultaneous ground-based measurements, which may also be useful to estimate the reference NO_2 VCDs in the airborne observations. These conclusions for NO_2 above Bucharest apply to other large polluted urban areas.

We also detected a clear signal of H_2CO in and around Bucharest, with an anthropogenic hotspot in the city center. Due to the lower signal to noise ratio of the spaceborne H_2CO observations, this structure is not visible in daily satellite measurements. We thus propose considering long-term ground-based MAX-DOAS measurements in the city for the validation of H_2CO.

In the Jiu Valley, NO_2 is clearly visible from both satellite and aircraft, and the VCDs are comparable in magnitude with the signal detected above Bucharest. However, it appears more complicated to quantitatively compare the NO_2 VCDs datasets in the thick exhaust plumes of the power plants. These plants also emit SO_2 but, as for H_2CO, the low signal to noise ratio of satellite measurements reduces the validation relevance of individual airborne measurements. As the SO_2 emissions have been drastically reduced with the installation of flue-gas desulfurization units in the Jiu Valley, we propose targeting SO_2 emissions from other coal-fired power plants having higher emissions, e.g. in Serbia.

Considering the optimal validation study mentioned in the introduction, the validation relevance of an international airborne campaign is usually limited by its timespan of typically a couple of weeks, imposed in practice by cost considerations. To overcome this limitation, one might consider routine airborne mapping of NO_2 VCDs by local aircraft operators, close to a well-equipped ground-based observatory. Such a set-up would reduce the fixed costs of the observations, which could be allocated to flight hours in different seasons. This would combine the advantages of long-term ground-based and airborne measurements. In the longer term, high altitude pseudo-satellites (HAPS) could help to achieve such routine measurements above selected supersites, which would be particularly valuable to validate the observations from geostationary satellites.

Competing interests. The authors declare that they have no conflict of interest.

Author contributions. AM, LB, D-EC, MDH, ACM, LG, DN, and MVR planned and organised the campaign. All coauthors contributed to the campaign either as participants or during campaign preparation and/or follow up data analysis, including the writing of this manuscript, which was coordinated by AM and MVR with feedback and contributions from all the coauthors.

Acknowledgements. The AROMAT activity was supported by ESA (contract $4000113511/15/NL/FF/gp$) and by the Belgian Science Policy (contract $BR/121/PI/UAVReunion$). Regarding the AirMAP instrument, financial support through the University of Bremen Institutional Strategy Measure M8 in the framework of the DFG Excellence Initiative is gratefully acknowledged. Part of the work performed for this study was funded by the Romanian Ministry of Research and Innovation through Program I - Development of the national research-

development system, Subprogram 1.2 - Institutional Performance - Projects of Excellence Financing in RDI, Contract No.19PFE / 17.10.2018 and by Romanian National Core Program Contract No.18N/2019. Katharina Riffel supported the MPIC mobile DOAS measurements. We thank Klaus Pfeilsticker, Isabelle De Smedt, Nicolas Theys, Ermioni Dimitropoulou, and Lori Neary for useful discussions. We also thank the people of Turceni and the Air Traffic Control of Romania for their support and cooperation.

References

Alpopi, C. and Colesca, S. E.: Urban air quality. A comparative study of major European capitals, Theoretical and Empirical Researches in Urban Management, 5, 92–107, 2010.

Bauwens, M., Stavrakou, T., Müller, J.-F., De Smedt, I., Van Roozendael, M., van der Werf, G. R., Wiedinmyer, C., Kaiser, J. W., Sindelarova, K., and Guenther, A.: Nine years of global hydrocarbon emissions based on source inversion of OMI formaldehyde observations, Atmos. Chem. Phys., 16, https://doi.org/10.5194/acp-16-10133-2016, 2016.

Boersma, K. F., Eskes, H. J., Dirksen, R. J., van der A, R. J., Veefkind, J. P., Stammes, P., Huijnen, V., Kleipool, Q. L., Sneep, M., Claas, J., Leitão, J., Richter, A., Zhou, Y., and Brunner, D.: An improved tropospheric NO_2 column retrieval algorithm for the Ozone Monitoring Instrument, Atmos. Meas. Tech., 4, 1905–1928, https://doi.org/10.5194/amt-4-1905-2011, 2011.

Boersma, K. F., Vinken, G. C. M., and Tournadre, J.: Ships going slow in reducing their NOx emissions: changes in 2005–2012 ship exhaust inferred from satellite measurements over Europe, Environmental Research Letters, 10, 074 007, https://doi.org/10.1088/1748-9326/10/7/074007, 2015.

Boersma, K. F., Eskes, H. J., Richter, A., De Smedt, I., Lorente, A., Beirle, S., van Geffen, J. H. G. M., Zara, M., Peters, E., Van Roozendael, M., Wagner, T., Maasakkers, J. D., van der A, R. J., Nightingale, J., De Rudder, A., Irie, H., Pinardi, G., Lambert, J.-C., and Compernolle, S. C.: Improving algorithms and uncertainty estimates for satellite NO_2 retrievals: results from the quality assurance for the essential climate variables (QA4ECV) project, Atmospheric Measurement Techniques, 11, 6651–6678, https://doi.org/10.5194/amt-11-6651-2018, https://www.atmos-meas-tech.net/11/6651/2018/, 2018.

Bösch, T., Meier, A., Schönhardt, A., Peters, E., Richter, A., Ruhtz, T., and Burrows, J.: Airborne measurements of different trace gases during the AROMAT-2 campaign with an Avantes spectrometer, in: EGU General Assembly, Vienna, Austria, 17–22 April 2016, pp. EGU2016–7394, 2016.

Brenot, H., Theys, N., Clarisse, L., Geffen, J. V., Gent, J. V., Roozendael, M. V., and Hurtmans, D.: Support to Aviation Control Service (SACS): an online service for near-real-time satellite monitoring of volcanic plumes, pp. 1099–1123, https://doi.org/10.5194/nhess-14-1099-2014, 2014.

Brinksma, E. J., Pinardi, G., Volten, H., Braak, R., Richter, A., Schönhardt, A., van Roozendael, M., Fayt, C., Hermans, C., Dirksen, R. J., Vlemmix, T., Berkhout, A. J. C., Swart, D. P. J., Oetjen, H., Wittrock, F., Wagner, T., Ibrahim, O. W., de Leeuw, G., Moerman, M., Curier, R. L., Celarier, E. A., Cede, A., Knap, W. H., Veefkind, J. P., Eskes, H. J., Allaart, M., Rothe, R., Piters, A. J. M., and Levelt, P. F.: The 2005 and 2006 DANDELIONS NO2 and aerosol intercomparison campaigns, J. Geophys. Res., 113, https://doi.org/10.1029/2007JD008808, 2008.

Burrows, J. P., Weber, M., Buchwitz, M., Rozanov, V., Ladstätter-Weißenmayer, A., Richter, A., DeBeek, R., Hoogen, R., Bramstedt, K., Eichmann, K.-U., Eisinger, M., Perner, D., Burrows, J. P., Weber, M., Buchwitz, M., Rozanov, V., Ladstätter-Weißenmayer, A., Richter, A., DeBeek, R., Hoogen, R., Bramstedt, K., Eichmann, K.-U., Eisinger, M., and Perner, D.: The Global Ozone Monitoring Experiment (GOME): Mission Concept and First Scientific Results, J. Atmospheric Sci., 56, https://doi.org/10.1175/1520-0469(1999)056<0151:TGOMEG>2.0.CO;2, 1999.

C3S: ERA5: Fifth generation of ECMWF atmospheric reanalyses of the global climate. Copernicus Climate Change Service Climate Data Store (CDS), accessed 24 September 2019, 2017.

Cazorla, M., Wolfe, G. M., Bailey, S. A., Swanson, A. K., Arkinson, H. L., and Hanisco, T. F.: A new airborne laser-induced fluorescence instrument for in situ detection of formaldehyde throughout the troposphere and lower stratosphere, Atmos. Meas. Tech., 8, 541–552, https://doi.org/10.5194/amt-8-541-2015, 2015.

Chance, K., Liu, X., Suleiman, R. M., Flittner, D. E., Al-Saadi, J., and Janz, S. J.: Tropospheric emissions: monitoring of pollution (TEMPO), p. 88660D, International Society for Optics and Photonics, https://doi.org/10.1117/12.2024479, 2013.

Compernolle, S., Verhoelst, T., Pinardi, G., Granville, J., Hubert, D., Keppens, A., Niemeijer, S., Rino, B., Bais, A., Beirle, S., Boersma, F., Burrows, J. P., De Smedt, I., Eskes, H., Goutail, F., Hendrick, F., Lorente, A., Pazmino, A., Piters, A., Peters, E., Pommereau, J.-P., Remmers, J., Richter, A., van Geffen, J., Van Roozendael, M., Wagner, T., and Lambert, J.-C.: Validation of Aura-OMI QA4ECV NO_2 Climate Data Records with ground-based DOAS networks: role of measurement and comparison uncertainties, Atmos. Chem. Phys. Discuss., 2020, 1–44, https://doi.org/10.5194/acp-2019-877, 2020.

Constantin, D., Merlaud, A., Van Roozendael, M., Voiculescu, M., Fayt, C., Hendrick, F., Pinardi, G., and Georgescu, L.: Measurements of Tropospheric NO2 in Romania Using a Zenith-Sky Mobile DOAS System and Comparisons with Satellite Observations, Sensors, 13, 3922–3940, https://doi.org/10.3390/s130303922, 2013.

Constantin, D., Voiculescu, M., Dragomir, C., Georgescu, L., Merlaud, A., and Van Roozendael, M.: Measurements of NO2 using a Mobile DOAS system in Gorj county, Romania, The 18th International Conference TEHNOMUS, 2015.

Constantin, D.-E., Merlaud, A., Voiculescu, M., Dragomir, C., Georgescu, L., Hendrick, F., Pinardi, G., and Van Roozendael, M.: Mobile DOAS Observations of Tropospheric NO2 Using an UltraLight Trike and Flux Calculation, Atmosphere, 8, 78, https://doi.org/10.3390/atmos8040078, 2017.

Crippa, M., Guizzardi, D., Muntean, M., Schaaf, E., Dentener, F., van Aardenne, J. A., Monni, S., Doering, U., Olivier, J. G. J., Pagliari, V., and Janssens-Maenhout, G.: Gridded emissions of air pollutants for the period 1970–2012 within EDGAR v4.3.2, Earth Syst. Sci. Data, 10, 1987–2013, https://doi.org/10.5194/essd-10-1987-2018, 2018.

De Smedt, I., Müller, J.-F., Stavrakou, T., van der A, R., Eskes, H., and Van Roozendael, M.: Twelve years of global observations of formaldehyde in the troposphere using GOME and SCIAMACHY sensors, Atmos. Chem. Phys., 8, 4947–4963, https://doi.org/10.5194/acp-8-4947-2008, 2008.

De Smedt, I., Stavrakou, T., Hendrick, F., Danckaert, T., Vlemmix, T., Pinardi, G., Theys, N., Lerot, C., Gielen, C., Vigouroux, C., Hermans, C., Fayt, C., Veefkind, P., Müller, J.-F., and Van Roozendael, M.: Diurnal, seasonal and long-term variations of global formaldehyde columns inferred from combined OMI and GOME-2 observations, Atmos. Chem. Phys., 15, 12 519–12 545, https://doi.org/10.5194/acp-15-12519-2015, 2015.

Dekemper, E., Vanhamel, J., Van Opstal, B., and Fussen, D.: The AOTF-based NO2 camera, Atmos. Meas. Tech., 9, 6025–6034, https://doi.org/10.5194/amt-9-6025-2016, 2016.

Donner, S., Lampel, J., Shaiganfar, R., Gu, M., and T, W.: Construction and characterisation of a new compact MAX-DOAS instrument—Correction of detector non-linearity, in: 7th international DOAS workshop, Brussels, Belgium, 2015.

Drosoglou, T., Koukouli, M. E., Kouremeti, N., Bais, A. F., Zyrichidou, I., Balis, D., van der A, R. J., Xu, J., and Li, A.: MAX-DOAS NO_2 observations over Guangzhou, China; ground-based and satellite comparisons, Atmos. Meas. Tech., 11, 2239–2255, https://doi.org/10.5194/amt-11-2239-2018, 2018.

EEA: Reported information on large combustion plants, Tech. Rep. 4.2, European Environment Agency, Copenhagen, Denmark, 2018.

EEA: Air quality in Europe -2019 report, Tech. Rep. 10.2019, European Environment Agency, Copenhagen, Denmark, 2019.

Eisinger, M. and Burrows, J. P.: Tropospheric sulfur dioxide observed by the ERS-2 GOME instrument, Geophys. Res. Lett., 25, 4177–4180, https://doi.org/10.1029/1998GL900128, 1998.

ESA: Requirements for the Geophysical Validation of Sentinel-5 Precursor Products, Tech. Rep. S5P-RS-ESA-SY-164, European Space Agency, Noordwijk, The Netherlands, 2014.

Fioletov, V., McLinden, C. A., Kharol, S. K., Krotkov, N. A., Li, C., Joiner, J., Moran, M. D., Vet, R., Visschedijk, A. J. H., and Denier van der Gon, H. A. C.: Multi-source SO_2 emission retrievals and consistency of satellite and surface measurements with reported emissions, Atmos. Chem. Phys., 17, 12 597–12 616, https://doi.org/10.5194/acp-17-12597-2017, 2017.

Fioletov, V., McLinden, C. A., Griffin, D., Theys, N., Loyola, D. G., Hedelt, P., Krotkov, N. A., and Li, C.: Anthropogenic and volcanic point source SO_2 emissions derived from TROPOMI onboard Sentinel 5 Precursor: first results, Atmos. Chem. Phys. Discuss., 2020, 1–30, https://doi.org/10.5194/acp-2019-1095, 2020.

Griffin, D., Zhao, X., McLinden, C. A., Boersma, F., Bourassa, A., Dammers, E., Degenstein, D., Eskes, H., Fehr, L., Fioletov, V., Hayden, K., Kharol, S. K., Li, S.-M., Makar, P., Martin, R. V., Mihele, C., Mittermeier, R. L., Krotkov, N., Sneep, M., Lamsal, L. N., Linden, M. t., Geffen, J. v., Veefkind, P., and Wolde, M.: High-Resolution Mapping of Nitrogen Dioxide With TROPOMI: First Results and Validation Over the Canadian Oil Sands, Geophys. Res. Lett., 46, 1049–1060, https://doi.org/10.1029/2018GL081095, 2019.

Grigoraş, G., Ştefan, S., Rada, C., and Grigoraş, C.: Assessing of surface-ozone concentration in Bucharest, Romania, using OML and satellite data, Atmos. Pollut. Res., 7, 567–576, https://doi.org/10.1016/j.apr.2016.02.001, 2016.

Heland, J., Schlager, H., Richter, A., and Burrows, J. P.: First comparison of tropospheric NO2 column densities retrieved from GOME measurements and in situ aircraft profile measurements, Geophys. Res. Lett., 29, https://doi.org/200210.1029/2002GL015528, 2002.

Heue, K. P., Richter, A., Bruns, M., Burrows, J. P., v. Friedeburg, C., Platt, U., Pundt, I., Wang, P., and Wagner, T.: Validation of SCIAMACHY tropospheric NO2 columns with AMAXDOAS measurements, Atmos. Chem. Phys., 5, 1039–1051, https://doi.org/10.5194/acp-5-1039-2005, 2005.

Hönninger, G., von Friedeburg, C., and Platt, U.: Multi axis differential optical absorption spectroscopy (MAX-DOAS), Atmos. Chem. Phys., 4, 231–254, https://doi.org/10.5194/acp-4-231-2004, 2004.

Ibrahim, O., Shaiganfar, R., Sinreich, R., Stein, T., Platt, U., and Wagner, T.: Car MAX-DOAS measurements around entire cities: quantification of NO_x emissions from the cities of Mannheim and Ludwigshafen (Germany), Atmos. Meas. Tech., 3, 709–721, https://doi.org/10.5194/amt-3-709-2010, 2010.

Ingmann, P., Veihelmann, B., Langen, J., Lamarre, D., Stark, H., and Courrèges-Lacoste, G. B.: Requirements for the GMES Atmosphere Service and ESA's implementation concept: Sentinels-4/-5 and -5p, Remote Sensing of Environment, 120, 58–69, https://doi.org/10.1016/j.rse.2012.01.023, 2012.

Irie, H., Kanaya, Y., Akimoto, H., Tanimoto, H., Wang, Z., Gleason, J. F., and Bucsela, E. J.: Validation of OMI tropospheric NO2 column data using MAX-DOAS measurements deep inside the North China Plain in June 2006: Mount Tai Experiment 2006, Atmos. Chem. Phys., 8, https://doi.org/10.5194/acp-8-6577-2008, 2008.

Johansson, J. K. E., Mellqvist, J., Samuelsson, J., Offerle, B., Moldanova, J., Rappenglück, B., Lefer, B., and Flynn, J.: Quantitative measurements and modeling of industrial formaldehyde emissions in the Greater Houston area during campaigns in 2009 and 2011, J. Geophys. Res. Atmos., 119, 4303–4322, https://doi.org/10.1002/2013JD020159, 2014.

Judd, L. M., Al-Saadi, J. A., Valin, L. C., Pierce, R. B., Yang, K., Janz, S. J., Kowalewski, M. G., Szykman, J. J., Tiefengraber, M., and Mueller, M.: The Dawn of Geostationary Air Quality Monitoring: Case Studies From Seoul and Los Angeles, Frontiers in Environmental Science, 6, 85, https://doi.org/10.3389/fenvs.2018.00085, 2018.

Judd, L. M., Al-Saadi, J. A., Janz, S. J., Kowalewski, M. G., Pierce, R. B., Szykman, J. J., Valin, L. C., Swap, R., Cede, A., Mueller, M., Tiefengraber, M., Abuhassan, N., and Williams, D.: Evaluating the impact of spatial resolution on tropospheric NO_2 column comparisons within urban areas using high-resolution airborne data, Atmos. Meas. Tech. Discuss., 2019, 1–25, https://doi.org/10.5194/amt-2019-161, 2019.

Kanaya, Y., Irie, H., Takashima, H., Iwabuchi, H., Akimoto, H., Sudo, K., Gu, M., Chong, J., Kim, Y. J., Lee, H., Li, A., Si, F., Xu, J., Xie, P.-H., Liu, W.-Q., Dzhola, A., Postylyakov, O., Ivanov, V., Grechko, E., Terpugova, S., and Panchenko, M.: Long-term MAX-DOAS network observations of NO2 in Russia and Asia (MADRAS) during the period 2007-2012: instrumentation, elucidation of climatology, and comparisons with OMI satellite observations and global model simulations, Atmos. Chem. Phys., 14, https://doi.org/10.5194/acp-14-7909-2014, 2014.

Kebabian, P. L., Herndon, S. C., and Freedman, A.: Detection of nitrogen dioxide by cavity attenuated phase shift spectroscopy, Anal. Chem., 77, 724–728, https://doi.org/10.1021/ac048715y, 2005.

Kern, C., Lübcke, P., Bobrowski, N., Campion, R., Mori, T., Smekens, J.-F., Stebel, K., Tamburello, G., Burton, M., Platt, U., and Prata, F.: Intercomparison of SO2 camera systems for imaging volcanic gas plumes, J. Volcanol. Geotherm. Res., 300, 22 – 36, https://doi.org/https://doi.org/10.1016/j.jvolgeores.2014.08.026, 2015.

Kim, J.: GEMS(Geostationary Environment Monitoring Spectrometer) onboard the GeoKOMPSAT to Monitor Air Quality in high Temporal and Spatial Resolution over Asia-Pacific Region, in: EGU2012-4051, EGU General Assembly, 2012.

Kim, S.-W., Heckel, A., Frost, G. J., Richter, A., Gleason, J., Burrows, J. P., McKeen, S., Hsie, E.-Y., Granier, C., and Trainer, M.: NO2 columns in the western United States observed from space and simulated by a regional chemistry model and their implications for NOx emissions, Journal of Geophysical Research: Atmospheres, 114, https://doi.org/10.1029/2008JD011343, 2009.

Kowalewski, M. G. and Janz, S. J.: Remote sensing capabilities of the GEO-CAPE airborne simulator, 9218, 92 181I, https://doi.org/10.1117/12.2062058, 2014.

Krotkov, N. A., McLinden, C. A., Li, C., Lamsal, L. N., Celarier, E. A., Marchenko, S. V., Swartz, W. H., Bucsela, E. J., Joiner, J., Duncan, B. N., Boersma, K. F., Veefkind, J. P., Levelt, P. F., Fioletov, V. E., Dickerson, R. R., He, H., Lu, Z., and Streets, D. G.: Aura OMI observations of regional SO2 and NO2 pollution changes from 2005 to 2015, Atmos. Chem. Phys., 16, 4605–4629, https://doi.org/10.5194/acp-16-4605-2016, 2016.

Leitch, J. W., Delker, T., Good, W., Ruppert, L., Murcray, F., Chance, K., Liu, X., Nowlan, C., Janz, S., Krotkov, N., Pickering, E., Kowalewski, M., and J., W.: The GeoTASO airborne spectrometer project, Proc.SPIE, 9218, https://doi.org/10.1117/12.2063763, 2014.

Levelt, P., van den Oord, G., Dobber, M., Malkki, A., Visser, H., de Vries, J., Stammes, P., Lundell, J., and Saari, H.: The ozone monitoring instrument, IEEE T. Geosci. Remote., 44, https://doi.org/10.1109/TGRS.2006.872333, 2006.

Lorente, A., Boersma, K. F., Eskes, H. J., Veefkind, J. P., van Geffen, J. H., de Zeeuw, M. B., Denier van der Gon, H. A., Beirle, S., and Krol, M. C.: Quantification of nitrogen oxides emissions from build-up of pollution over Paris with TROPOMI, Sci. Rep., https://doi.org/10.1038/s41598-019-56428-5, 2019.

lorga, G., Raicu, C. B., and Stefan, S.: Annual air pollution level of major primary pollutants in Greater Area of Bucharest, Atmospheric Pollution Research, 6, 824–834, https://doi.org/10.5094/APR.2015.091, 2015.

Lübcke, P., Bobrowski, N., Illing, S., Kern, C., Alvarez Nieves, J. M., Vogel, L., Zielcke, J., Delgado Granados, H., and Platt, U.: On the absolute calibration of SO_2 cameras, Atmospheric Measurement Techniques, 6, 677–696, https://doi.org/10.5194/amt-6-677-2013, 2013.

Ma, J. Z., Beirle, S., Jin, J. L., Shaiganfar, R., Yan, P., and Wagner, T.: Tropospheric NO_2 vertical column densities over Beijing: results of the first three years of ground-based MAX-DOAS measurements (2008-2011) and satellite validation, Atmos. Chem. Phys., 13, 1547–1567, https://doi.org/10.5194/acp-13-1547-2013, 2013.

Marmureanu, L., Deaconu, L., Vasilescu, J., Ajtai, N., and Talianu, C.: Combined optoelectronic methods used in the monitoring of SO_2 emissions and imissions, Environ. Eng. Manag. J., 12, 277–282, 2013.

Martin, R. V., Parrish, D. D., Ryerson, T. B., Nicks, J. K., Chance, K., Kurosu, T. P., Jacob, D. J., Sturges, E. D., Fried, A., and Wert, B. P.: Evaluation of GOME satellite measurements of tropospheric NO2 and HCHO using regional data from aircraft campaigns in the southeastern United States, Journal of Geophysical Research D: Atmospheres, https://doi.org/10.1029/2004JD004869, 2004.

McGonigle, A. J. S., Pering, T. D., Wilkes, T. C., Tamburello, G., D'Aleo, R., Bitetto, M., Aiuppa, A., and Willmott, J. R.: Ultraviolet Imaging of Volcanic Plumes: A New Paradigm in Volcanology, Geosciences, 7, https://doi.org/10.3390/geosciences7030068, 2017.

Meier, A. C.: Measurements of horizontal trace gas distributions using airborne imaging differential optical absorption spectroscopy, Ph.D. thesis, University of Bremen, 2018.

Meier, A. C., Schönhardt, A., Bösch, T., Richter, A., Seyler, A., Ruhtz, T., Constantin, D.-E., Shaiganfar, R., Wagner, T., Merlaud, A., Van Roozendael, M., Belegante, L., Nicolae, D., Georgescu, L., and Burrows, J. P.: High-resolution airborne imaging DOAS measurements of NO_2 above Bucharest during AROMAT, Atmos. Meas. Tech., 10, 1831–1857, https://doi.org/10.5194/amt-10-1831-2017, 2017.

Merlaud, A.: Development and use of compact instruments for tropospheric investigations based on optical spectroscopy from mobile platforms, Presses univ. de Louvain, 2013.

Merlaud, A., Tack, F., Constantin, D., Georgescu, L., Maes, J., Fayt, C., Mingireanu, F., Schuettemeyer, D., Meier, A. C., Schönardt, A., Ruhtz, T., Bellegante, L., Nicolae, D., Den Hoed, M., Allaart, M., and Van Roozendael, M.: The Small Whiskbroom Imager for atmospheric compositioN monitorinG (SWING) and its operations from an unmanned aerial vehicle (UAV) during the AROMAT campaign, Atmos. Meas. Tech., 11, 551–567, https://doi.org/10.5194/amt-11-551-2018, 2018.

MPC, S.: S5P MPC Product Readme Nitrogen Dioxide, Tech. Rep. S5P-MPC-KNMI-PRF-NO2, S5P Mission Performance Center, 2019.

Nicolae, D., Vasilescu, J., Carstea, E., Stebel, K., and Prata, F.: Romanian Atmospheric research 3D Observatory: Synergy of instruments, Rom. Rep. Phys., 62, 2010.

Nisulescu, C., Calinoiu, D., Timofte, A., Boscornea, A., and Talianu, C.: Diurnal Variation of Particulate Matter in the Proximity of Rovinari Fossil-Fuel Powerplant, Environ. Eng. Manag. J., 10, 99–105, 2011.

Nowlan, C. R., Liu, X., Leitch, J. W., Chance, K., González Abad, G., Liu, C., Zoogman, P., Cole, J., Delker, T., Good, W., Murcray, F., Ruppert, L., Soo, D., Follette-Cook, M. B., Janz, S. J., Kowalewski, M. G., Loughner, C. P., Pickering, K. E., Herman, J. R., Beaver, M. R., Long, R. W., Szykman, J. J., Judd, L. M., Kelley, P., Luke, W. T., Ren, X., and Al-Saadi, J. A.: Nitrogen dioxide observations from the Geostationary Trace gas and Aerosol Sensor Optimization (GeoTASO) airborne instrument: Retrieval algorithm and measurements during DISCOVER-AQ Texas 2013, Atmos. Meas. Tech., 9, 2647–2668, https://doi.org/10.5194/amt-9-2647-2016, 2016.

Nowlan, C. R., Liu, X., Janz, S. J., Kowalewski, M. G., Chance, K., Follette-Cook, M. B., Fried, A., González Abad, G., Herman, J. R., Judd, L. M., Kwon, H.-A., Loughner, C. P., Pickering, K. E., Richter, D., Spinei, E., Walega, J., Weibring, P., and Weinheimer, A. J.: Nitrogen dioxide and formaldehyde measurements from the GEOstationary Coastal and Air Pollution Events (GEO-CAPE) Airborne Simulator over Houston, Texas, Atmos. Meas. Tech., 11, 5941–5964, https://doi.org/10.5194/amt-11-5941-2018, 2018.

Parrish, D. D., Ryerson, T. B., Mellqvist, J., Johansson, J., Fried, A., Richter, D., Walega, J. G., Washenfelder, R. A., De Gouw, J. A., Peischl, J., Aikin, K. C., McKeen, S. A., Frost, G. J., Fehsenfeld, F. C., and Herndon, S. C.: Primary and secondary sources of formaldehyde in urban atmospheres: Houston Texas region, Atmos. Chem. Phys., 12, 3273–3288, https://doi.org/10.5194/acp-12-3273-2012, 2012.

Platt, U. and Stutz, J.: Differential Optical Absorption Spectroscopy: Principles and Applications, Physics of Earth and Space Environments, Springer, Berlin, 2008.

Richter, A., Richter, A., Weber, M., Burrows, J. P., Lambert, J.-C., and van Gijsel, A.: Validation strategy for satellite observations of tropospheric reactive gases, Annals of Geophysics, 56, https://doi.org/10.4401/ag-6335, 2014.

Schaub, D., Boersma, K. F., Kaiser, J. W., Weiss, A. K., Folini, D., Eskes, H. J., and Buchmann, B.: Comparison of GOME tropospheric NO2 columns with NO2 profiles deduced from ground-based in situ measurements, Atmos. Chem. Phys., 6, https://doi.org/10.5194/acp-6-3211-2006, 2006.

Schönhardt, A., Altube, P., Gerilowski, K., Krautwurst, S., Hartmann, J., Meier, A. C., Richter, A., and Burrows, J. P.: A wide field-of-view imaging DOAS instrument for two-dimensional trace gas mapping from aircraft, Atmos. Meas. Tech., 8, 5113–5131, https://doi.org/10.5194/amt-8-5113-2015, 2015.

Shaiganfar, R., Beirle, S., Denier van der Gon, H., Jonkers, S., Kuenen, J., Petetin, H., Zhang, Q., Beekmann, M., and Wagner, T.: Estimation of the Paris NO_x emissions from mobile MAX-DOAS observations and CHIMERE model simulations during the MEGAPOLI campaign using the closed integral method, Atmos. Chem. Phys., 17, 7853–7890, https://doi.org/10.5194/acp-17-7853-2017, 2017.

Sluis, W. W., Allaart, M. A. F., Piters, A. J. M., and Gast, L. F. L.: The development of a nitrogen dioxide sonde, Atmos. Meas. Tech., 3, 1753–1762, https://doi.org/10.5194/amt-3-1753-2010, 2010.

Smekens, J. F., Burton, M. R., and Clarke, A. B.: Validation of the SO2 camera for high temporal and spatial resolution monitoring of SO2 emissions, J. Volcanol. Geoth. Res., 300, 37–47, https://doi.org/10.1016/j.jvolgeores.2014.10.014, 2014.

St. Clair, J. M., Swanson, A. K., Bailey, S. A., Wolfe, G. M., Marrero, J. E., Iraci, L. T., Hagopian, J. G., and Hanisco, T. F.: A new non-resonant laser-induced fluorescence instrument for the airborne in situ measurement of formaldehyde, Atmos. Meas. Tech., 10, 4833–4844, https://doi.org/10.5194/amt-10-4833-2017, 2017.

Stebel, K., Amigo, A., Thomas, H., and Prata, A.: First estimates of fumarolic SO2 fluxes from Putana volcano, Chile, using an ultraviolet imaging camera, J. Volcanol. Geotherm. Res., 300, 112 – 120, https://doi.org/https://doi.org/10.1016/j.jvolgeores.2014.12.021, 2015.

Stefan, S., Radu, C., and Belegante, L.: Analysis of air quality in two sites with different local conditions, Environ. Eng. Manag. J., 12, 371–379, 2013.

Tack, F., Merlaud, A., Meier, A. C., Vlemmix, T., Ruhtz, T., Iordache, M.-D., Ge, X., van der Wal, L., Schuettemeyer, D., Ardelean, M., Calcan, A., Constantin, D., Schönhardt, A., Meuleman, K., Richter, A., and Van Roozendael, M.: Intercomparison of four airborne imaging DOAS systems for tropospheric NO_2 mapping – the AROMAPEX campaign, Atmos. Meas. Tech., 12, 211–236, https://doi.org/10.5194/amt-12-211-2019, 2019.

Theys, N., Hedelt, P., De Smedt, I., Lerot, C., Yu, H., Vlietinck, J., Pedergnana, M., Arellano, S., Galle, B., Fernandez, D., Carlito, C. J., Barrington, C., Taisne, B., Delgado-Granados, H., Loyola, D., and Van Roozendael, M.: Global monitoring of volcanic SO 2 degassing with unprecedented resolution from TROPOMI onboard Sentinel-5 Precursor, Sci. Rep., 9, https://doi.org/10.1038/s41598-019-39279-y, 2019.

Trombetti, M., Thunis, P., Bessagnet, B., Clappier, A., Couvidat, F., Guevara, M., Kuenen, J., and López-Aparicio, S.: Spatial inter-comparison of Top-down emission inventories in European urban areas, Atmos. Env., 173, 142–156, https://doi.org/10.1016/J.ATMOSENV.2017.10.032, 2018.

Veefkind, J., Aben, I., McMullan, K., Förster, H., de Vries, J., Otter, G., Claas, J., Eskes, H., de Haan, J., Kleipool, Q., van Weele, M., Hasekamp, O., Hoogeveen, R., Landgraf, J., Snel, R., Tol, P., Ingmann, P., Voors, R., Kruizinga, B., Vink, R., Visser, H., and Levelt, P.:

TROPOMI on the ESA Sentinel-5 Precursor: A GMES mission for global observations of the atmospheric composition for climate, air quality and ozone layer applications, Remote Sens. Environ., 120, 70 – 83, https://doi.org/https://doi.org/10.1016/j.rse.2011.09.027, 2012.

von Clarmann, T.: Validation of remotely sensed profiles of atmospheric state variables: strategies and terminology, Atmos. Chem. Phys., 6, 4311–4320, https://doi.org/10.5194/acp-6-4311-2006, 2006.

Wagner, T., Ibrahim, O., Shaiganfar, R., and Platt, U.: Mobile MAX-DOAS observations of tropospheric trace gases, Atmos. Meas. Tech., 3, 129–140, 2010.

Wang, Y., Beirle, S., Lampel, J., Koukouli, M., De Smedt, I., Theys, N., Li, A., Wu, D., Xie, P., Liu, C., Van Roozendael, M., Stavrakou, T., Müller, J.-F., and Wagner, T.: Validation of OMI, GOME-2A and GOME-2B tropospheric NO2, SO2 and HCHO products using MAX-DOAS observations from 2011 to 2014 in Wuxi, China: investigation of the effects of priori profiles and aerosols on the satellite products, Atmos. Chem. Phys., 17, 5007–5033, https://doi.org/10.5194/acp-17-5007-2017, 2017.

Zieger, P., Ruhtz, T., Preusker, R., and Fischer, J.: Dual-aureole and sun spectrometer system for airborne measurements of aerosol optical properties., Applied Optics, 46, 8542–8552, 2007.

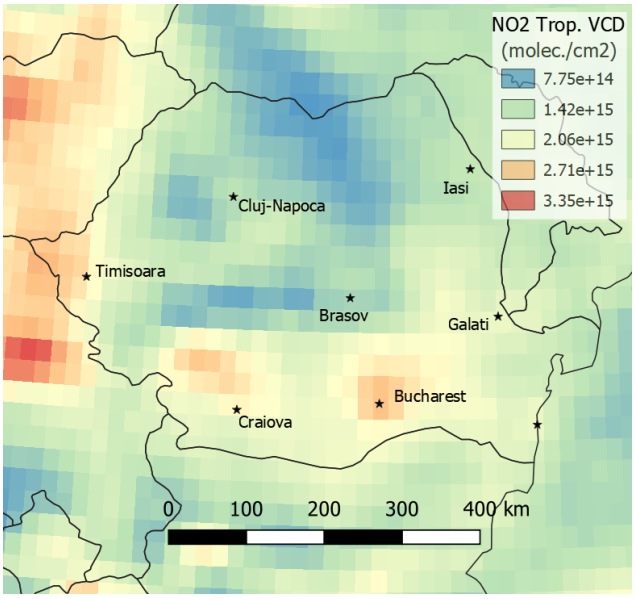

Figure 1. The tropospheric NO_2 VCD field seen from space with the OMI/AURA instrument above Romania (OMNO2d product, averaged for 2012-2016 with Giovanni, NASA GES DISC). The black stars pinpoint the largest cities of Romania.

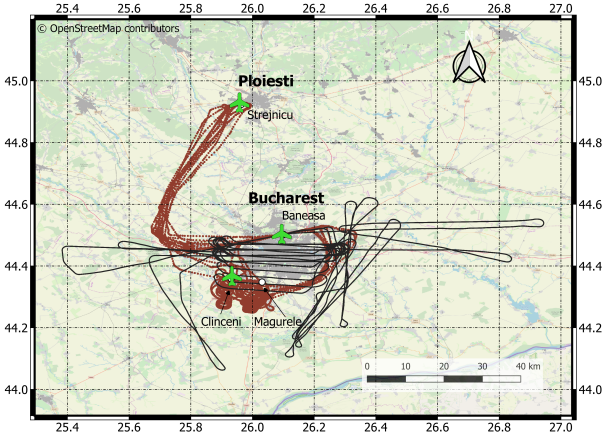

Figure 2. The Bucharest area with important locations for the AROMAT campaigns: the INOE atmospheric observatory in Magurele, the Baneasa airport, and the Clinceni airfield. Buit-up areas appear in grey. The red and black lines, respectively, show the BN-2 and Cessna flight tracks during AROMAT-2.

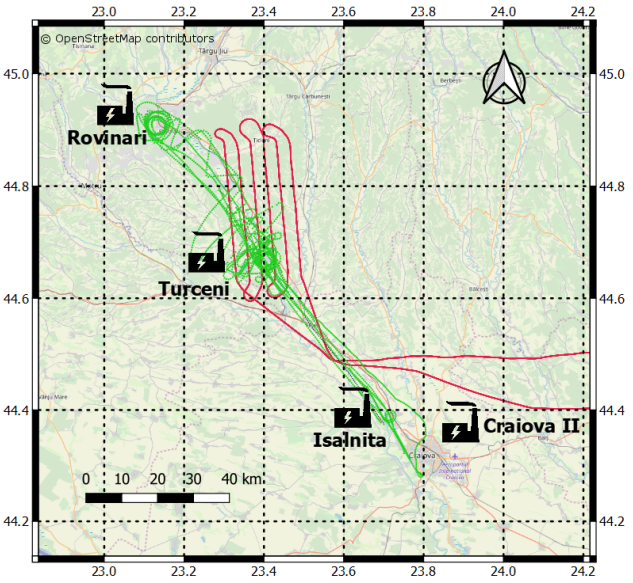

Figure 3. The Jiu Valley and its four power plants between Targu Jiu and Craiova. The scientific crew was based in Turceni during the AROMAT campaigns. The green and red lines, respectively, show the ultralight and Cessna flight tracks during AROMAT-2.

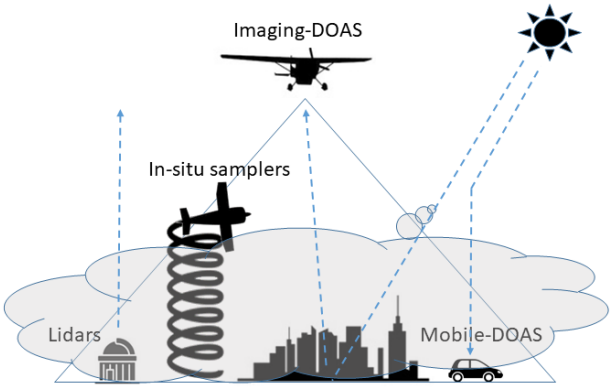

Figure 4. Geometry of the main measurements performed during the AROMAT campaigns. The Imaging-DOAS instruments map the NO_2 and SO_2 VCDs at 3 km altitude above the target area while the in-situ samplers measure profiles of trace gases and aerosols. Ancillary ground measurements include Mobile-DOAS to quantify trace gases VCDs and lidars to measure the aerosol optical properties.

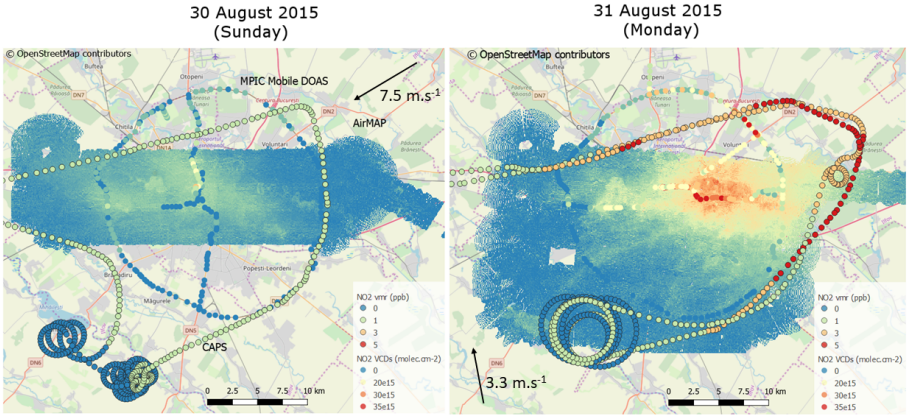

Figure 5. Measurements of NO_2 VCDs and volume mixing ratios in Bucharest on 30 (Sunday) and 31 (Monday) August 2015 with AirMAP (continuous map), the CAPS (black-rimmed circles), and the MPIC Mobile-DOAS (plain colour circles).

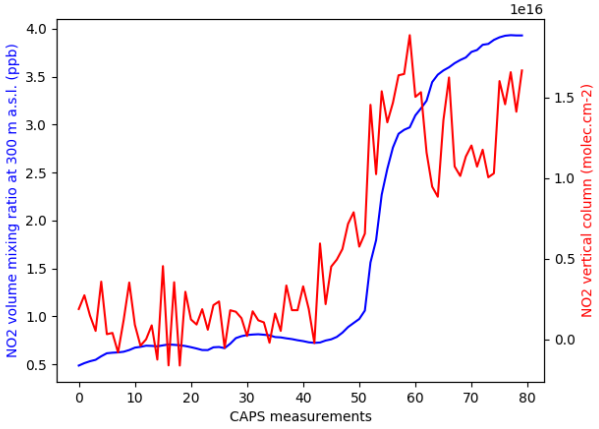

Figure 6. Volume mixing ratio and VCDs of NO_2 in and out of the pollution plume of Bucharest, as measured with the CAPS (on the BN-2) and AirMAP (on the Cessna) during the afternoon flights on 31 August 2015. Note that the two measurements are not exactly time coincident and that the plot shows the VCDs extracted at the position of the CAPS measurements.

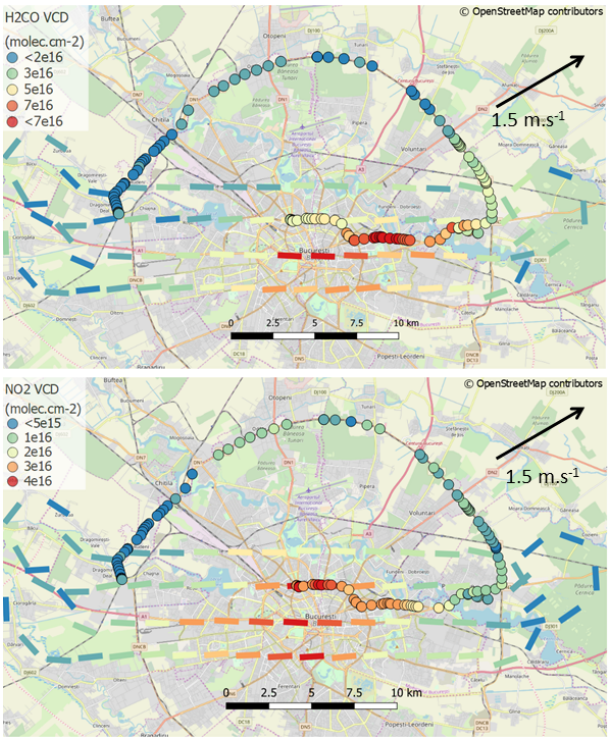

Figure 7. Horizontal distribution of tropospheric H_2CO and NO_2 VCDs measured on 31 August 2015 with the IUP-UB nadir-only compact spectrometer from the Cessna (flight tracks) and with the MPIC Mobile-DOAS (coloured circles).

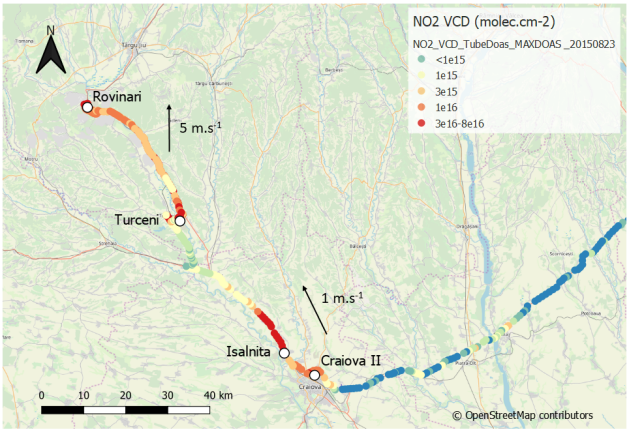

Figure 8. Tropopsheric vertical column densities of NO_2 measured with the MPIC Mobile-DOAS instruments in the Jiu Valley on 23 August 2015.

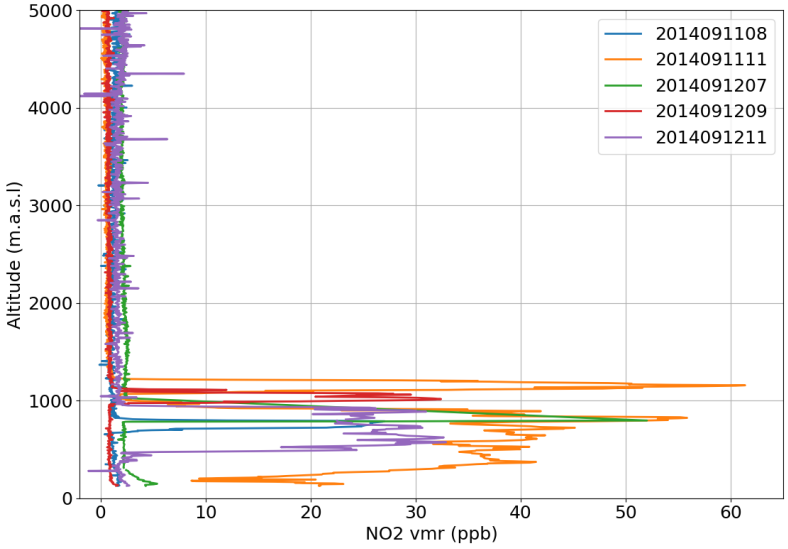

Figure 9. Examples of NO_2 sondes data from Turceni during AROMAT-1 (11 and 12 September 2014).

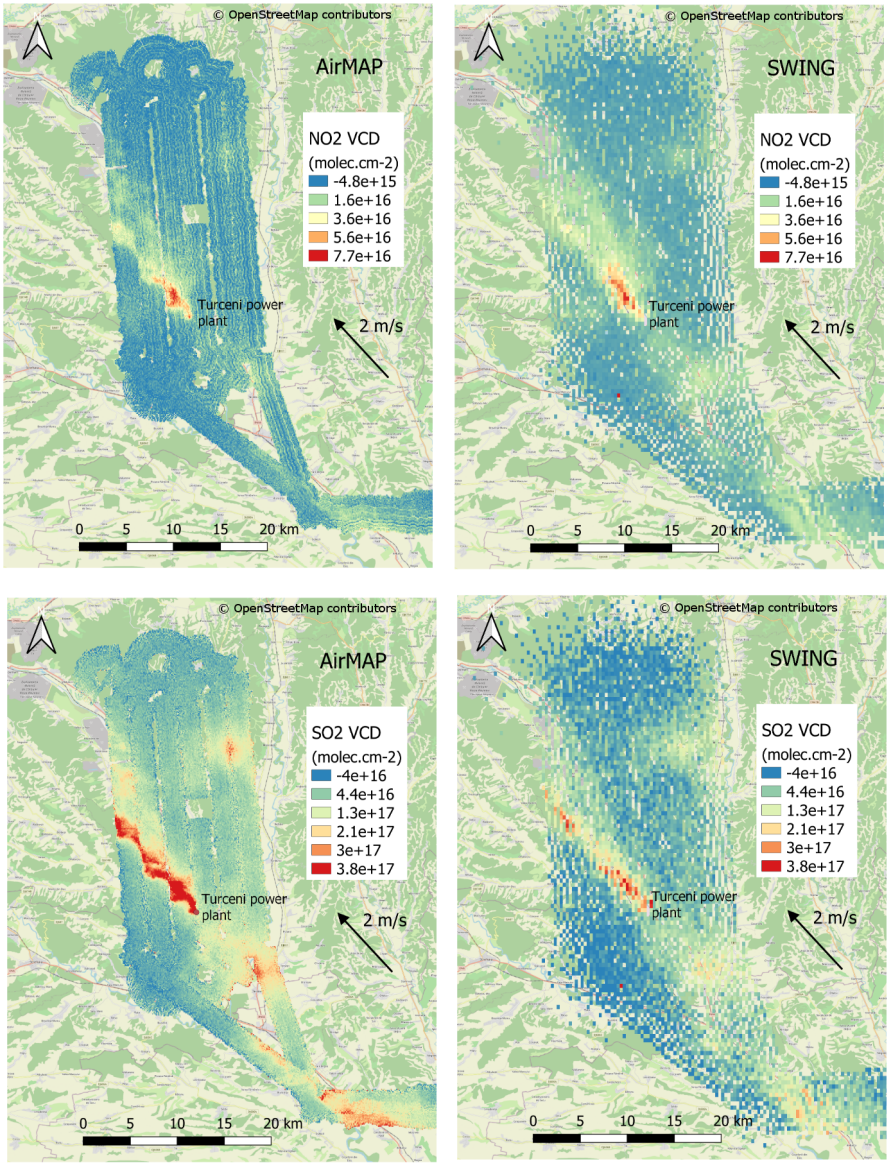

Figure 10. AirMAP (left panels) and SWING (right panels) NO_2 (upper panels) and SO_2 (lower panels) VCDs above Turceni (28 August 2015).

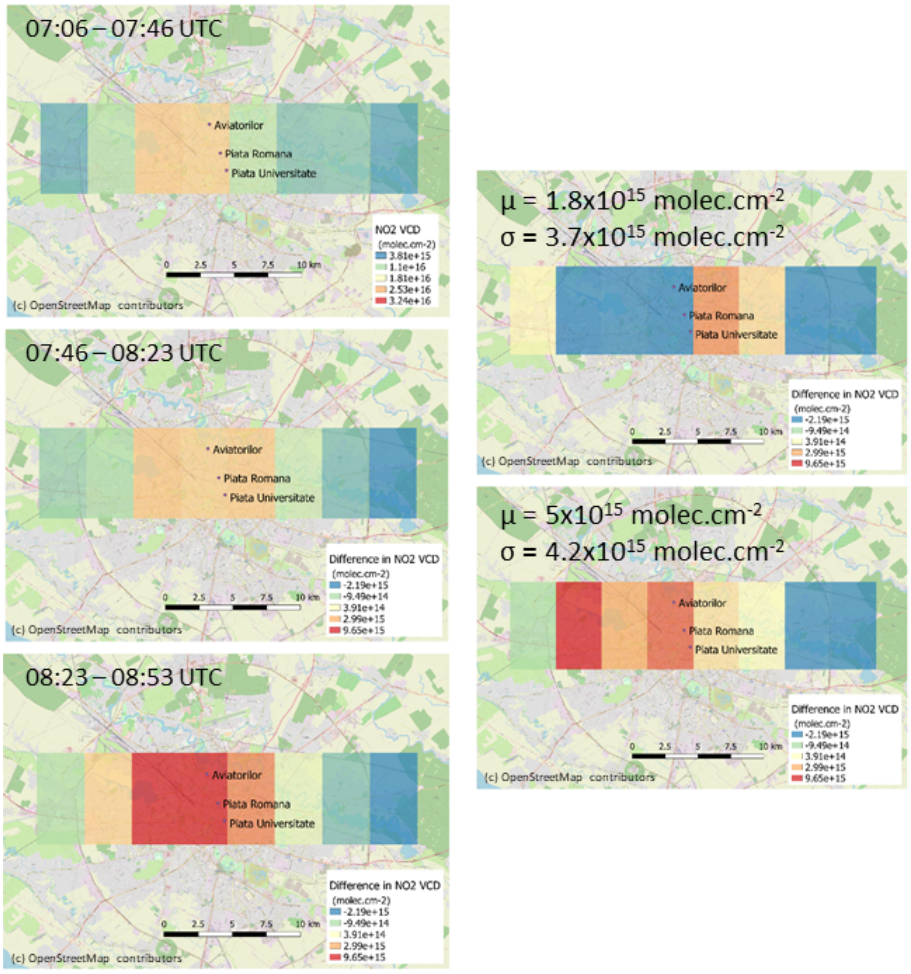

Figure 11. AirMAP measurements of NO_2 VCDs degraded at the TROPOMI resolution during three overpasses of the morning flight of 31 August 2015 (left panels), together with the differences of these degraded NO_2 VCDs for consecutive overpasses (right panels). The right panels also indicate the means (μ) and standard deviations (σ) of the two differences. The maps pinpoint the positions of the three mobile-DOAS sites of Fig.S9.

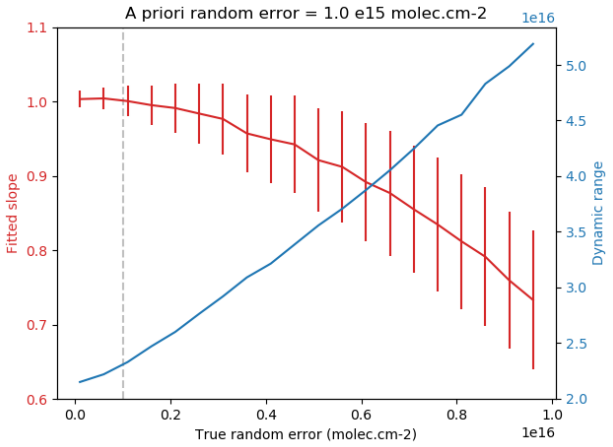

Figure 12. Effect of an underestimation of the random error in a regression analysis simulating TROPOMI validation using airborne mapping as reference measurements of NO_2 VCDs. The dynamic range (blue line) of the reference measurements increases with the applied random error. For the considered a priori random error (dashed vertical line, 1x10^{15} molec.cm^{-2}), this leads to an underestimation of the regression slope (red line). These simulations use the AirMAP data of 31 August 2015 (afternoon flight).

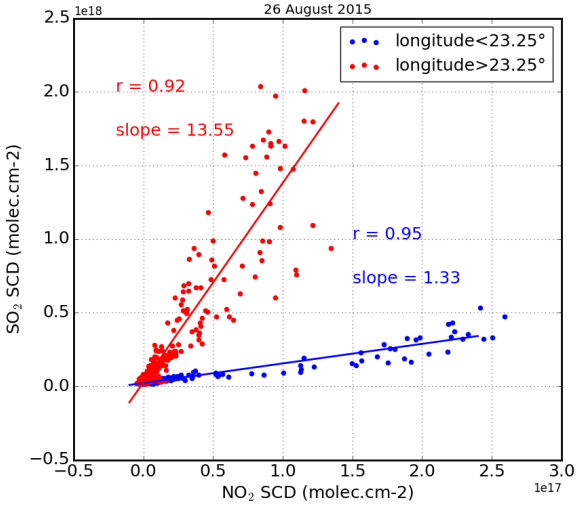

Figure 13. SO_2 and NO_2 SCDs SCDs measured from the ULM-DOAS above the Jiu Valley on 26 August 2015. Blue dots indicate the measurements above Rovinari, whereas the red ones are for all the other plants.

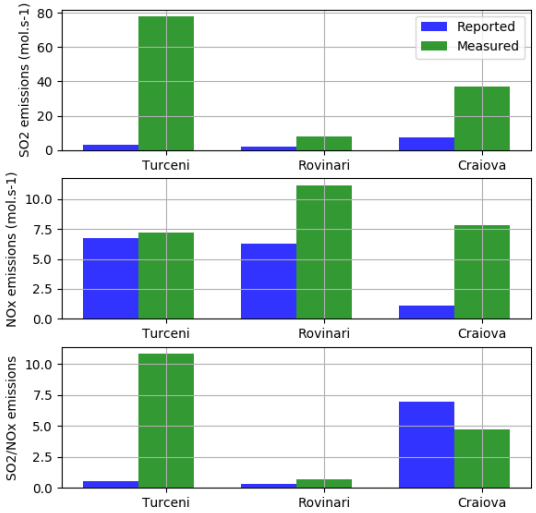

Figure 14. SO_2 and NO_x fluxes from three power plants of the Jiu Valley as (1) measured with the ULM-DOAS on 26 August 2015 (green bars) and (2) estimated from the reported emissions of 2015 assuming constant emissions throughout the year (blue bars). Uncertainties on the ULM-DOAS-derived fluxes are around 60%.

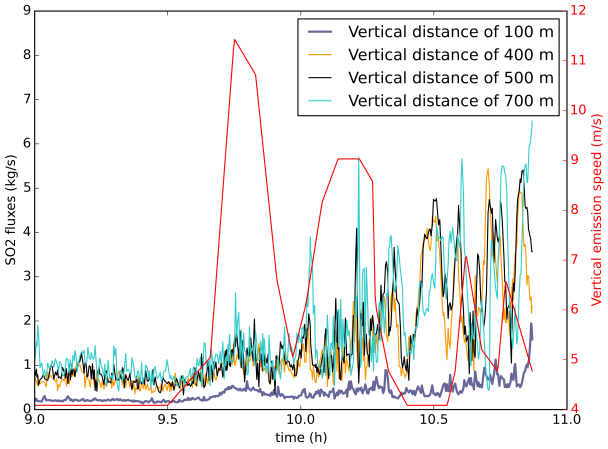

Figure 15. SO_2 fluxes from the Turceni power plant on 28 August 2015. They were estimated with the Envicam2 SO_2 camera for 4 transverses at vertical altitudes above the stack of 100, 400, 500 and 700 m. The red line shows the estimated plume speed ($m.s^{-1}$).

Table 1. Past and near-future space missions focused on air quality: coverage, pixel size, and temporal sampling.

Launch year	Instrument	Pixel size at nadir (km^2)	Coverage	Revisit time
1995	GOME	320 x 40	Global	3 days
2002	SCIAMACHY	60 x 30	Global	6 days
2004	OMI	13 x 24	Global	1 day
2006	GOME-2	80 x 40	Global	1 day
2011	OMPS	50 x 50	Global	1 day
2017	TROPOMI	3.5 x 5.5	Global	1 day
2023 (planned)	Sentinel-5	7 x 7	Global	1 day
2020	GEMS	7 x 8	East Asia	1 hour
2022 (planned)	TEMPO	2 x 4.5	North America	1 hour
2023 (planned)	Sentinel-4	8 x 8	Europe	1 hour

Table 2. Data quality targets for the S5P TROPOMI data products relevant in the AROMAT context (extracted from ESA (2014)).

Product	Accuracy	Precision
Tropospheric NO_2	25-50%	7x10^{14} molec cm^{-2}
Tropospheric SO_2	30-50%	2.7-8.1x10^{16} molec cm^{-2}
Total H_2CO	40-80%	0.4-1.2x10^{16} molec cm^{-2}

Table 3. Summary of the AROMAT measurements of NO_2.

Instrument	Type	Ground Sampling Distance (m)	Observed range (molec cm^{-2} / ppb)	Detection limit (molec cm^{-2} / ppb)	Bias (%)	Reference
AirMAP	Imager	100	0-8 x 10^{16}	1.5 x 10^{15}	25%	Meier et al. (2017)
SWING	Imager	300	0-8 x 10^{16}	1.2 x 10^{15}	25%	Merlaud et al. (2018)
ULM-DOAS	Nadir	400	0-1.7 x 10^{17}	5 x 10^{14}	25%	Constantin et al. (2017)
Tube MAX-DOAS	car-based	500	0-1.3 x 10^{17}	1.3 x 10^{14}	20%	Donner et al. (2015)
Mini Max-DOAS	car-based	500	0-1.3 x 10^{17}	6 x 10^{14}	20%	Wagner et al. (2010)
UGAL Mobile	car-based	500	0-2.5 x 10^{17}	4 x 10^{14}	25%	Constantin et al. (2013)
BIRA Mobile	car-based	500	0-1.3 x 10^{17}	8 x 10^{14}	20%	Merlaud (2013)
KNMI sonde	in-situ	n.a.	0-60	1	40%	Sluis et al. (2010)
CAPS	in-situ	n.a.	0-20	0.1	40%	Kebabian et al. (2005)

Table 4. Summary of the AROMAT measurements of H_2CO.

Instrument	Type	Ground Sampling Distance (m)	Observed range (molec cm^{-2})	Detection limit (molec cm^{-2})	Bias (%)	Reference
IUP-Bremen nadir	Airborne nadir	1800	1-7 x 10^{16}	6 x 10^{15}	25%	Bösch et al. (2016)
Tube MAX-DOAS	car-based	500	1-7.5 x 10^{16}	8 x 10^{14}	20%	Donner et al. (2015)

Table 5. Summary of the AROMAT measurements of SO_2.

Instrument	Type	Ground Sampling Distance (m)	Observed range (molec cm^{-2})	Detection limit (molec cm^{-2})	Bias (%)	Reference
AirMAP	Imager	100	0-6 x 10^{17}	1.7 x 10^{16}	40%	Meier et al. (2017)
SWING	Imager	300	0-4 x 10^{17}	2 x 10^{16}	40%	Merlaud et al. (2018)
ULM-DOAS	Nadir	400	0-2.5x 10^{18}	3 x 10^{15}	40%	Constantin et al. (2017)
Tube MAX-DOAS	car-based	500	0-1x10^{18}	5 x 10^{15}	20%	Donner et al. (2015)
Mini Max-DOAS	car-based	500	0-2.2x10^{18}	1 x 10^{16}	20%	Wagner et al. (2010)
UGAL Mobile	car-based	500	0-4x 10^{18}	4 x 10^{15}	25%	Constantin et al. (2013)

Table 6. Total simulated error budget for the validation of spaceborne NO_2 VCDs validation using airborne mapping at different resolution, with or without profile informations.

		Precision (molec cm^{-2})			Accuracy		
	Place	Shot noise	Time error	Tot.	Ref.	Fit	Tot.
AirMAP	B	3x10^{13}	4x10^{15}	4.1x10^{15}	26%	6%	37%
SWING	B	7x10^{13}	4x10^{15}	4.1x10^{15}	26%	6%	37%
AirMAP + profile	B	3x10^{13}	4x10^{15}	4.1x10^{15}	10%	6%	28%
AirMAP	T	3x10^{13}	4x10^{15}	4.1x10^{15}	26%	10%	37%
AirMAP + profile	T	3x10^{13}	4x10^{15}	4.1x10^{15}	10%	10%	29%

Table 7. NO_x emissions from Bucharest estimated from the AROMAT measurements.

	AirMAP	Mobile-DOAS
8 September 2014	14.6 mol.s^{-1}	12.5 mol.s^{-1}
9 September 2014	13.1 mol.s^{-1}	n.a.
31 August 2015	n.a.	17.5 mol.s^{-1}

Table 8. NO_x and SO_2 emissions from the Turceni power plant estimated from the AROMAT measurements.

	Instrument	Distance	SO_2 flux	NO_x flux	$\frac{SO_2}{NO_2}$
11 September 2014 - 09:00 UTC	AirMAP	7 km	n.a.	8 mol.s^{-1}	n.a.
25 August 2015 - 07:45 UTC	Mobile-DOAS	1 km	105 mol.s^{-1}	4 mol.s^{-1}	15.4
25 August 2015 - 08:30 UTC	Mobile-DOAS	1 km	52 mol.s^{-1}	2 mol.s^{-1}	26
25 August 2015 - 08:30 UTC	ULM-DOAS	10 km	85 mol.s^{-1}	10 mol.s^{-1}	8.5
26 August 2015 - 10:00 UTC	ULM-DOAS	5 km	78 mol.s^{-1}	6 mol.s^{-1}	13
27 August 2015 - 07:45 UTC	ULM-DOAS	8.5 km	145 mol.s^{-1}	17 mol.s^{-1}	8.5
27 August 2015 - 07:55 UTC	Mobile-DOAS	1 km	77 mol.s^{-1}	5 mol.s^{-1}	16
28 August 2015 - 07:00 UTC	Mobile-DOAS	1 km	24.8 mol.s^{-1}	1.7 mol.s^{-1}	14.7
28 August 2015 - 10:00 UTC	AirMAP	7 km	25 mol.s^{-1}	8 mol.s^{-1}	3.1
28 August 2015 - 10:15 UTC	Mobile-DOAS	1 km	32 mol.s^{-1}	4 mol.s^{-1}	8
28 August 2015 - 09:00-11:00 UTC	SO_2 camera	Above stack	15.6-62.4 mol.s^{-1}	n.a	n.a.

Supplement of The Airborne ROmanian Measurements of Aerosols and Trace gases (AROMAT) campaigns

Alexis Merlaud[1], Livio Belegante[2], Daniel-Eduard Constantin[3], Mirjam Den Hoed[4], Andreas Carlos Meier[5], Marc Allaart[4], Magdalena Ardelean[6], Maxim Arseni[3], Tim Bösch[5], Hugues Brenot[1], Andreea Calcan[6], Emmanuel Dekemper[1], Sebastian Donner[8], Steffen Dörner[8], Mariana Carmelia Balanica Dragomir[3], Lucian Georgescu[3], Anca Nemuc[2], Doina Nicolae[2], Gaia Pinardi[1], Andreas Richter[5], Adrian Rosu[3], Thomas Ruhtz[7], Anja Schönhardt[5], Dirk Schuettemeyer[10], Reza Shaiganfar[8], Kerstin Stebel[9], Frederik Tack[1], Sorin Nicolae Vâjâiac[6], Jeni Vasilescu[2], Jurgen Vanhamel[1], Thomas Wagner[8], and Michel Van Roozendael[1]

[1]Royal Belgian Institute for Space Aeronomie (BIRA-IASB), Avenue Circulaire 3, 1180 Brussels, Belgium
[2]National Institute of R&D for Optoelectronics (INOE), Magurele, Street Atomistilor 409, Magurele 77125, Romania
[3]"Dunarea de Jos" University of Galati, Faculty of Sciences and Environment, Str. Domneasca, Nr. 111, Galati 800008, Romania
[4]Royal Netherlands Meteorological Institute (KNMI), De Bilt, The Netherlands
[5]Institute of Environmental Physics, University of Bremen, Otto-Hahn-Allee 1, 28359 Bremen, Germany
[6]National Institute for Aerospace Research "Elie Carafoli" (INCAS), Bd. Iuliu Maniu no. 220, Bucharest, Romania
[7]Institute for Space Sciences, Free University of Berlin, Carl-Heinrich-Becker-Weg 6-10, 12165 Berlin, Germany
[8]Max-Planck-Institute for Chemistry (MPIC), Hahn-Meitner-Weg 1, 55128 Mainz, Germany
[9]Norwegian Institute for Air Research (NILU), Instituttveien 18, 2007 Kjeller, Norway
[10]European Space Agency (ESA-ESTEC), Keplerlaan 1, 2201 AZ Noordwijk, The Netherlands

Correspondence: A.Merlaud (alexism@oma.be)

1 Site characteristics

Table S1. Main characteristics of the power plants of the Jiu Valley.

	Craiova II	Islanita	Turceni	Rovinari
Latitude (°N)	44.343	44.39	44.67	44.91
Longitude (°E)	23.81	23.72	23.41	23.135
Nominal capacity (MW)	300	630	1650	1320
Smokestack height (m)	149	200	280	280

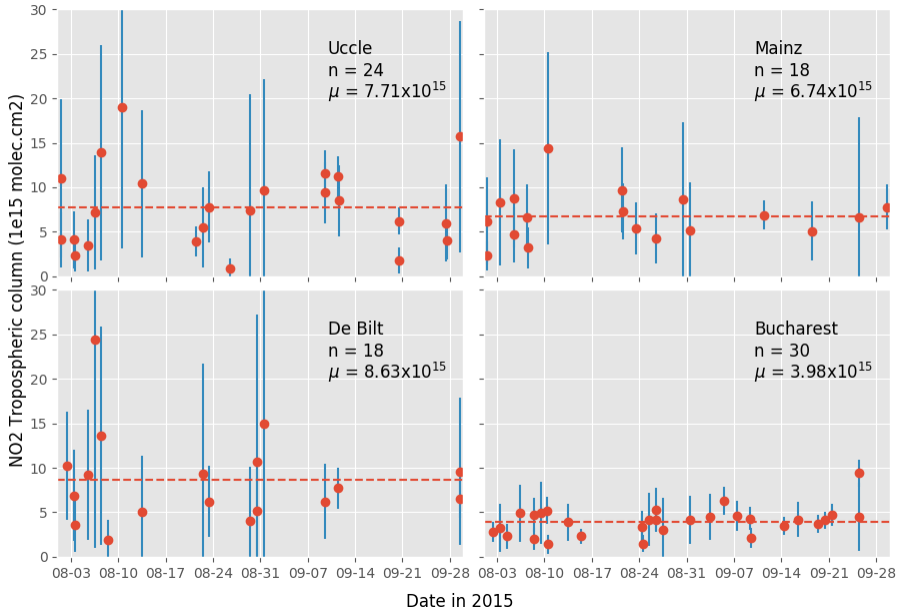

Figure S1. Tropospheric NO_2 VCDs for OMI overpasses around four European sites including Bucharest, filtered to remove cloudy scenes and row anomalies (TEMIS NO_2 overpass data). The red dashed line indicates the mean NO_2 VCD in the time window. The NO_2 column is smaller above Bucharest. This site is less affected by clouds.

2 Main instruments operated during the AROMAT campaigns

2.1 Airborne remote sensing

2.1.1 AirMAP

The AirMAP (Schönhardt et al., 2015; Meier et al., 2017) has been developed at IUP-Bremen. A PhD thesis (Meier, 2018) describes the AirMAP operations and data analysis during the AROMAT campaigns. AirMAP is a pushbroom UV/vis imager with a field-of-view of around 51°, leading to a swath width of about the flight altitude. Light is collected by optical fibers from 35 individual viewing directions. The spectrometer is an Acton 300i imaging spectrograph with a focal length of 300 mm, and a f-number of f/3.9. When measuring primarily NO_2, AirMAP records spectra in the range 420-461 nm (AROMAT-1 settings) or 429-493 nm (AROMAT-2 settings). For the SO_2 measurements, the spectral range was set to 303-367 nm. For this UV configuration, the field-of-view decreases to 44°. The spectrometer is temperature stabilized at 35 °C. AirMAP was installed in the FUB Cessna during the AROMAT campaigns.

2.1.2 SWING

The SWING payload has been developed at BIRA-IASB. It is a compact whiskbroom UV/vis imager. SWING was upgraded between AROMAT-1 and AROMAT-2. Merlaud et al. (2018) describes the instrument used in AROMAT-1. For AROMAT-2, the instrument capabilities in the UV were improved, which enabled to simultaneously measure SO_2 and NO_2. Light is collected by a scanning mirror driven by a micocontroller. The spectrometer is an Avantes spectrometer (ULS-2048XL) with a focal length of 75 mm, which covers the spectral range of 280-550 nm. The field-of-view of the instrument is tunable but can reach 100°. The instantaneous field-of-view is 5°. The SWING instrument is 12 cm x 8 cm x 33 cm large and weight 1.2 kg. SWING was operated from the UGAL UAV during AROMAT-1 and from the FUB Cessna during AROMAT-2.

2.1.3 ULM-DOAS

The ULM-DOAS payload Constantin et al. (2017) is based on an ULS-2048XL Avantes spectrometer with a focal length of 75 mm, which covers the spectral range of 280-550 nm. A piece of wood under the aircraft wing holds the telescope, which has a 1.2 °field-of-view in the nadir direction. Light is sent from this input optics to the spectrometer by an optical fiber of 400 μ m. A laptop controls the acquisition and stores the spectra as well as the georeferencing data of a GPS antenna. The entire set-up is powered by the 12 V of the aircraft through an inverter. The ULM-DOAS measured NO_2 and SO_2 from the UGAL ultralight aircraft above the Jiu Valley during the AROMAT-2 campaign.

2.1.4 IUP-Bremen nadir-only DOAS

A nadir-only DOAS system was operated alongside AirMAP during AROMAT-2. The spectrometer is an Avantes ULS 2048x64, it has a focal length of 75 mm and covers the spectral range 287-551 nm at a spectral resolution of 0.8 nm (FWHM). A round-to-linear bundle of 14 100 µm thick fibers collects the light, achieving an effective field of view of 8.1°. This leads to an across track footprint of 425 m at 3 km a.g.l. During the Bucharest flight for H_2CO, the integration time was set to 30 s which leads to a pixel length of 1.8 km.

2.1.5 FUBISS-ASA2

The airborne spectrometer system FUBISS-ASA2 (Zieger et al., 2007) has been developed at the Institute for Space Sciences at the Free University of Berlin. It simultaneously measures the direct solar irradiance and the aureole radiance in two different solid angles. Light is collected by a sun tracker. Ring shaped apertures shield the direct sunlight and only allow radiation between 4°and 6°. The spectrometers used for the sun as well as the aureole photometers provide 256 evenly spaced channels from 300 to 1000 nm. During the AROMAT campaigns, the FUBISS-ASA2 was operated from the FUB Cessna and provided aerosol optical depth profiles in the vicinity of Bucharest.

2.2 Airborne in-situ

2.2.1 KNMI NO_2 sonde

The measurement principle of the KNMI NO_2-sonde(Sluis et al., 2010) is based upon the chemical reaction between NO_2 and luminol, a chemiluminescent reaction that produces a faint blue light. Ambient air is pumped through a teflon pump, and bubbled through the sensing solution. The light that is produced by the reaction is detected by an array of photodiodes that is glued to the reaction chamber. The electric current from the photodiodes is converted into a voltage with a highly sensitive operational amplifier, and passed through a filter that removes high frequency fluctuations. During AROMAT-1, the NO_2-sonde was mounted on the UGAL UAV and attached to meteorological balloons. During AROMAT-2, the NO_2-sonde was installed onboard the INCAS BN-2.

2.2.2 AS32M CAPS

The AS32M NO_2 monitor is a commercial instrument manufactured by Environnement S.A. It follows the Cavity Attenuated Phase Shift (CAPS) principle(Kebabian et al., 2005). It measures the NO_2 volume mixing ratio using a blue light-emitting diode (LED) as a light source, a near-co focal arrangement of two high reflectivity mirrors in tandem with an enclosed sample cell of 26 centimeter in length and a vacuum phototube detector. The wavelength and spectral band pass of the measurement are defined by the use of an interference filter centered at 450 ± 10 nanometer. The monitor is enclosed within a standard 19 inch rack-mounted instrumentation box, weighs 12.5 kilogram, and uses 225 Watts of electrical power including the vacuum pump. The NO_2 CAPS was mounted onboard the BN-2 during AROMAT-2.

2.2.3 TSI Aerodynamic particle sizer

The TSI Aerodynamic Particle Sizer 3321 (Pfeifer et al., 2016) provides the diameter of particles in the range 0.5-20 μm. Particles are accelerated on an air flow through a nozzle and their times of flight measured between two lasers provide proxies for their sizes. During AROMAT-1, this instrument was mounted on the INCAS UAV. During AROMAT-2 it was installed in the INCAS BN-2.

2.2.4 PICARRO G2401-mc

The Picarro G2401-mc is a commercial instrument that simultaneously quantifies the concentrations of water vapor, carbon monoxide, carbon dioxide and methane(Chen et al., 2013). The instrument uses a tunable laser and applies the cavity ring down spectroscopy technique to measure spectral absorption of molecules in an optical cavity. The model G2401-mc is designed for airborne operations and also provides the dry gas mole fractions. The PICARRO G2401-mc was operated from the BN-2 during AROMAT-2.

2.3 Car-based Mobile-DOAS systems

2.3.1 BIRA Double channel Mobile-DOAS

The BIRA double channel Mobile-DOAS instrument(Merlaud, 2013) is based on a double channel Avantes spectrometer installed on a car. The entry slit is 50 μm, the focal length 75 mm and the grating is a 600 l.mm^{-1}, blazed at 300 nm. The spectral range is 200-750 nm with a 1.3 nm resolution (FWHM). The CCD detector is a Sony2048 linear array with a Deep-UV coating for signal enhancement below 350 nm. An optical head, mounted on the car window, holds the two telescopes achieving a 2.5 °field-of-view with fused silica collimating lenses. One telescope points zenith while the other is directed 30°above the horizon. Two 400 μm chrome plated brass optical fibers connects the telescopes to the spectrometer. The integration time is around 5ms. Each measurement is an average of (typically) 10 seconds of 10 scans accumulations. A GPS antenna is used for georeferencing the measurement, the whole set-up is powered by the car 12V through an inverter. While measuring, the instrument is recording spectra continuously and simultaneously from the two directions.

2.3.2 UGAL and BIRA zenith-only Mobile-DOAS

The zenith only Mobile DOAS systems used by UGAL and BIRA(Constantin et al., 2013) are based on Avantes spectrometers installed on a car. They have only one zenith channel, the entry slit is 50 μm, the focal length 75 mm and the grating is a 1200 l.mm^{-1}, blazed at 250 nm. The spectral range is 290-550 nm with a 0.7 nm resolution (FWHM). The CCD detector is a 2048 linear array Hamamatsu S11155 with pixels of 14 μm x 500 μm. The fiber is attached to the car and points to the zenith through a fused silica collimating lens resulting in a field of view of 2.5 °. The integration time is around 150ms. Each measurement is an average of (typically) 10 seconds of 10 scans accumulations. The system also uses a GPS antenna for georeferencing the measurements and is also powered by an inverter plugged on the car 12V.

2.3.3 MPIC Scanning Mobile-DOAS

Two mobile Max-DOAS instruments were used by MPIC during the AROMAT campaigns: a Mini-MAX-DOAS and a newly developed instrument, the so-called Tube MAX-DOAS.

The Mini-MAX-DOAS instrument is a commercial instrument produced by Hoffman GMBH, it is described in detail by (Wagner et al., 2010) which also presents its car-based operation. This instrument uses a thermoelectrically cooled USB2000+ Ocean Optics spectrometer. The latter covers the spectral range 320-460 nm at a spectral resolution of 0.7 nm. Light is collected within a field of view of 1.2°through a lens of focal length 40 mm. The optics, spectrometer, and controlling electronics is mounted in a sealed-box enclosure. The whole set-up is rotated by a stepper motor.

The Tube MAX-DOAS has been developed at MPIC and is based on an ULS 2048x64 Avantes spectrometer which covers the spectral range 315-474 nm at a spectral resolution of 0.7 nm FWHM. This spectrometer uses a 100 μm entry slit, a 1800 l.mm^{-1} grating, and a Schott BG3 filter to reduce the visible straylight. The spectrometer is installed inside the car and stabilized at 15°C. It is connected to the telescope unit through a round-to-linear fibre bundle based on 4 monofibers of

diameter 200 µm. The telescope unit consists of a stepper motor inside a plastic tube which rotates the fiber and a 50 mm lens outside the tube, leading to a field of view of about 0.7°.

2.4 Ground-based remote sensing

2.4.1 INOE RALI lidar

The Multiwavelength depolarization Raman Lidar RALI (Nicolae et al., 2010; Belegante et al., 2011) measures the Raman backscattering radiation from atmospheric water vapor, nitrogen, and Mie/Rayleigh backscattering radiation from atmospheric molecules and aerosol particles. It emits and receives light at 1064, 532, and 355 nm. The output parameters are the backscatter coefficient, the extinction coefficient, water vapor mixing ratio, and particle depolarization ratio. The altitude of full overlap is around 800 m. Advanced products have been dedicated to aerosol typing (Nicolae et al., 2018), microphysical inversion and aerosol mass concentration retrievals. The system is part of the European Aerosol Research Lidar Network (EARLINET) as an advanced Lidar station. This instrument performed measurements during both of the campaigns only in Magurele at RADO observatory.

2.4.2 INOE MILI lidar

The UV depolarization eye-safe Lidar MILI detects Mie/Rayleigh backscattering from atmospheric molecules and aerosol particles. It emits laser pulses at 355 nm (20mJ) and measures the backscattered light in two orthogonal polarization states. The laser pulse duration is 8 ns (at 355 nm), the repetition rate is 20Hz, and the beam diameter lies between 3 and 5 mm (FWHM). The dynamic range covers 1-5 km, depending on the atmosphere transmission, with a spatial resolution of 7.5 m. The reception uses a 200 mm Cassegrain telescope, and the system acquisition is analog and photon counting, with 20 MS.s^{-1} analog sampling rate and 250 MHz photon counting count rate. The altitude of full overlap was around 500 m during the AROMAT campaigns, it can be aligned to 300 m.

2.4.3 SO_2 camera

The SO_2 camera is an updated version of the Envicam-2 system described in Kern et al. (2015). It uses a Hamamatsu C8484 fast-sampling camera (1344x1024 pixels), a four-position filter wheel, and a UV spectrometer. The filter wheel holds two 10 nm filters centered at 310 and 325 nm, respectively corresponding to a strong and weak absorption of SO_2, a UV broadband view, and a blackened plate for dark-current measurements. A co-aligned spectrometer receives light within a field-of-view of 0.33°through a 100 mm diameter lens. During AROMAT-2, we used a 25 mm lens for the camera, leading to a field of view of 14.3°x 10.9°.

2.5 ALTIUS NO_2 camera

The NO_2 camera is a hyperspectral imager that can take spectral images of a scene with a spectral resolution better than 1 nm (Dekemper et al., 2016). The tuning of the acquisition wavelength is sequential, but takes place in a few milliseconds.

The passband selection is made by an acousto-optical tunable filter (AOTF). The AOTF principle relies on the acousto-optic interaction in a birefringent crystal: the passband central wavelength is determined by the frequency of an acoustic wave propagating in the crystal. Its main advantages are: a small and lightweight packaging, a low power consumption, a fast response, and a high diffraction efficiency. This instrument is composed of a telecentric optical system which images a scene with a 6°x 6°square field of view (FOV) onto a CCD camera (512x512 pixels). In typical light conditions, a frame rate of 1 Hz is achieved. Thanks to its imaging capabilities, and its frame rate, this instrument is capable of tracking the signature of NO_2 in dynamic targets, such as smokestacks exhausts.

2.6 Ground-based in-situ

2.6.1 Aerosol mass spectrometer

The compact time-of-flight aerosol mass spectrometer (AMS) measures the chemical composition and size resolved mass concentration of non-refractory PM1 aerosols, using mass spectrum or particle time-of-flight mode of operation (Jayne et al., 2000). The AMS samples continuously aerosols near to the ground through a 100 μm critical orifice. The particles are thermal vaporized, followed by the electron impact ionization of the vaporized species and detection by mass spectrometry. The output parameters are mass concentration time series for organics, nitrate, sulfate, ammonium, chloride aerosols species and vacuum aerodynamic size distribution of submicronic aerosols.

2.6.2 Aerosol Chemical Speciation Monitor

Aerosol Chemical Speciation Monitor (ACSM) is a simplified version of the AMS, using a quadrupole mass spectrometer (Petit et al., 2015). An automated zeroing system is implemented, which measure alternatively particle-free sample or ambient particles using the filter and sample mode of operation. Also a naphthalene filter is used as an internal calibration standard. The output parameters are average mass concentrations of particulate organics, sulfate, nitrate, ammonium and chloride.

Table S2. Typical air mass factors (AMF), 1-σ DOAS fitting errors (σ_S), and integration times (Tint) for the NO_2 DOAS instruments. See the references in Sect. 2 for details on the AMF calculations of the airborne instruments. We used geometric approximations for the ground-based DOAS instruments, pointing to zenith (AMF = 1) and 22°above the horizon (AMF = 2.7).

	AMF	σ_S (molec cm^{-2})	Tint
AirMAP	1.5	2.2x10^{15}	0.5 s
SWING	1.5	1.8x10^{15}	0.5 s
ULM-DOAS	1.5	8x10^{14}	10 s
Tube MAX-DOAS	2.7	2.5x10^{14}	30 s
Mini MAX-DOAS	2.7	1.2x10^{15}	30 s
UGAL Mobile-DOAS	1	4x10^{14}	30 s
BIRA Mobile-DOAS	1	8x10^{14}	30 s

Table S3. Typical air mass factors (AMF), 1-σ DOAS fitting errors (σ_S), and integration times (Tint) for the SO_2 DOAS instruments. See the references in Sect. 2 for details on the AMF calculations of the airborne instruments. We used geometric approximations for the ground-based DOAS instruments, pointing to zenith (AMF = 1) and 22°above the horizon (AMF = 2.7).

	AMF	σ_S (molec cm^{-2})	Tint
AirMAP	1	1.7x10^{16}	0.5 s
SWING	1	2x10^{16}	0.5 s
ULM-DOAS	1	5x10^{15}	10 s
Tube MAX-DOAS	2.7	1x10^{16}	30 s
Mini MAX-DOAS	2.7	2x10^{16}	30 s
UGAL Mobile-DOAS	1	4x10^{15}	30 s

Table S4. Typical air mass factors (AMF), 1-σ DOAS fitting errors (σ_S), and integration times (Tint) for the H_2CO DOAS instruments. See the reference in Sect. 2 for details on the AMF calculations of the airborne instrument. We used geometric approximation for the ground-based DOAS instrument pointing to 22°above the horizon (AMF = 2.7).

	AMF	σ_S (molec cm^{-2})	Tint
IUP-Bremen nadir	1	6x10^{15}	30 s
Tube MAX-DOAS	2.7	1.6x10^{15}	30 s

3 Practical implementations of the campaigns

Table S5. Measurements table during the AROMAT 2O14 campaign. B stands for Bucharest, J for the Jiu Valley.

	1-9-14	2-9-14	3-9-14	7-9-14	8-9-14	9-9-14	11-9-14	12-9-14
AirMAP	B	B	-	-	B	B	J	J
SWING	-	-	-	-	-	J	J	-
NO_2 sonde	-	-	-	-	J	J	J	J
APSR	B	B	-	-	-	-	-	-
BIRA Mobile-DOAS	B	B	B	J	J	J	J	J
UGAL Mobile-DOAS	B	B	B	B	B	J	J	J
MPIC Mobile-DOAS	-	B	B	B	B	J	J	J
RALI	B	B	-	B	B	B	B	B
MILI	B	B	-	-	-	J	J	-
ACSM	B	B	B	-	J	J	J	-
AMS	B	B	B	B	B	B	B	B
Trace gas monitors	B	B	B	-	J	J	J	-

Table S6. Measurements during the AROMAT 2O15 campaign. B stands for Bucharest, J for the Jiu Valley.

	24-8-15	25-8-15	26-8-15	27-8-15	28-8-15	29-8-15	30-8-15	31-8-15
AirMAP	-	-	-	-	J	-	B	B
SWING	-	-	-	-	J	-	B	B
FUBISS	-	-	-	-	-	-	B	B
ULM-DOAS	J	J	J	J	-	-	-	-
NO_2 camera	J	J	-	-	-	-	-	-
SO_2 camera	J	J	J	J	J	J	-	-
NO_2Sonde	-	B	-	B	B	-	-	-
CAPS	-	B	-	B	B	-	B	B
Nephelometer	-	B	-	B	B	-	B	B
PICARRO	-	B	-	B	B	-	B	B
APSR	-	B	-	B	B	-	B	B
BIRA Mobile-DOAS	J	J	J	J	J	B	B	B
MPIC Mobile-DOAS	J	J	J	J	J	B	B	B
UGAL Mobile-DOAS	-	-	-	J	J	B	B	B
RALI	B	B	B	B	B	B	B	B
MILI	J	J	J	J	J	J	-	-
ACSM	B	B	B	-	J	J	J	-
AMS	B	B	B	B	B	B	B	B
Trace gas monitors	J	J	J	J	J	J	-	-

4 Intercomparison results

This section presents the intercomparisons performed during the AROMAT-2 campaign which are the most relevant for the findings of this study. Meier et al. (2017) and Merlaud et al. (2018) presented other comparisons based on the AROMAT-1 data.

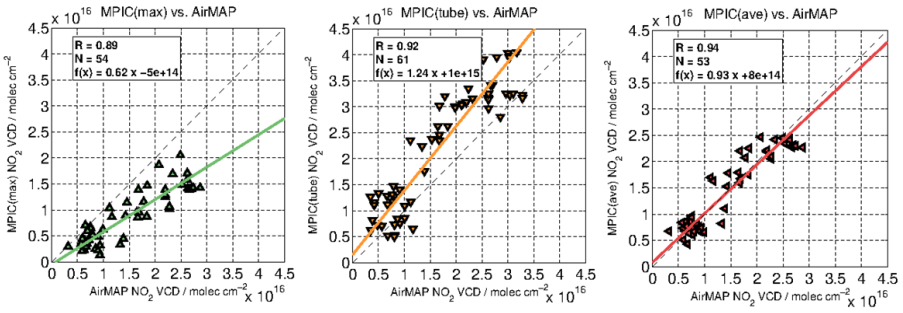

Figure S2. Comparison of AirMAP and MPIC Mobile DOAS NO_2 VCDs measurements during the morning flight on 31 August 2015. The left panel compares AirMAP with the Mini-MAX-DOAS which pointed forward, 22°above the horizon. The middle panel compares AirMAP with the Tube MAX-DOAS which pointed backward, 22°above the horizon. The right panel compares AirMAP with the average of the Mini-MAX-DOAS and Tube MAX-DOAS.

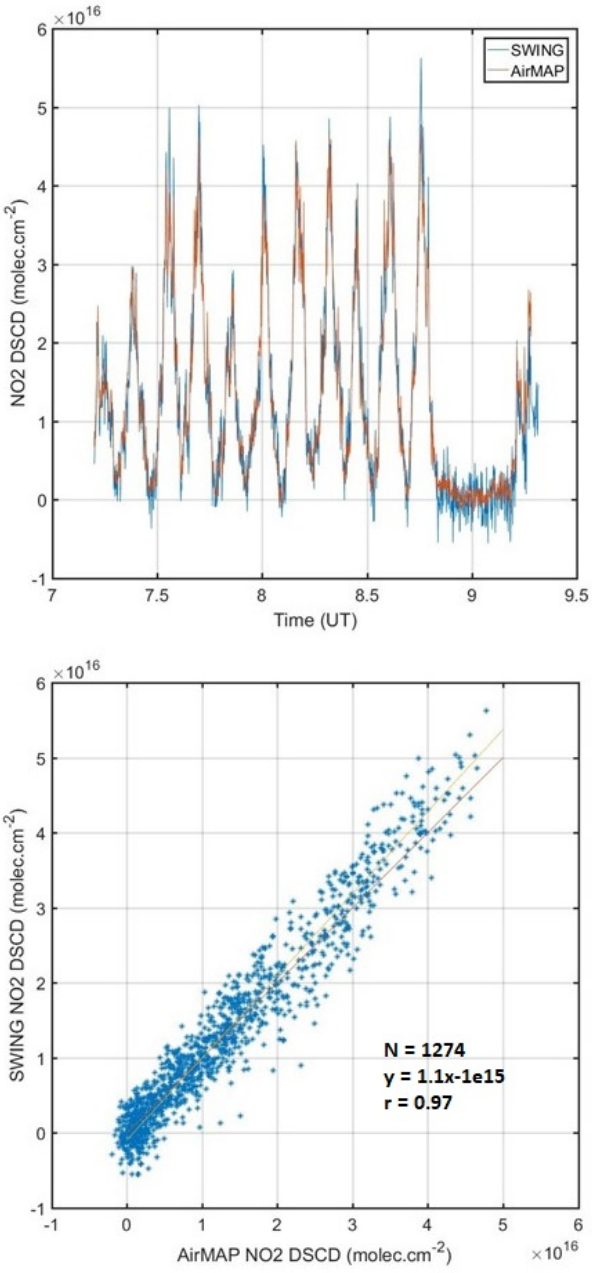

Figure S3. Comparison of the AirMAP and SWING NO_2 DSCDs above Bucharest (31 August 2015). The lower panel also shows the orthogonal regression (blue) and 1:1 (red) lines.

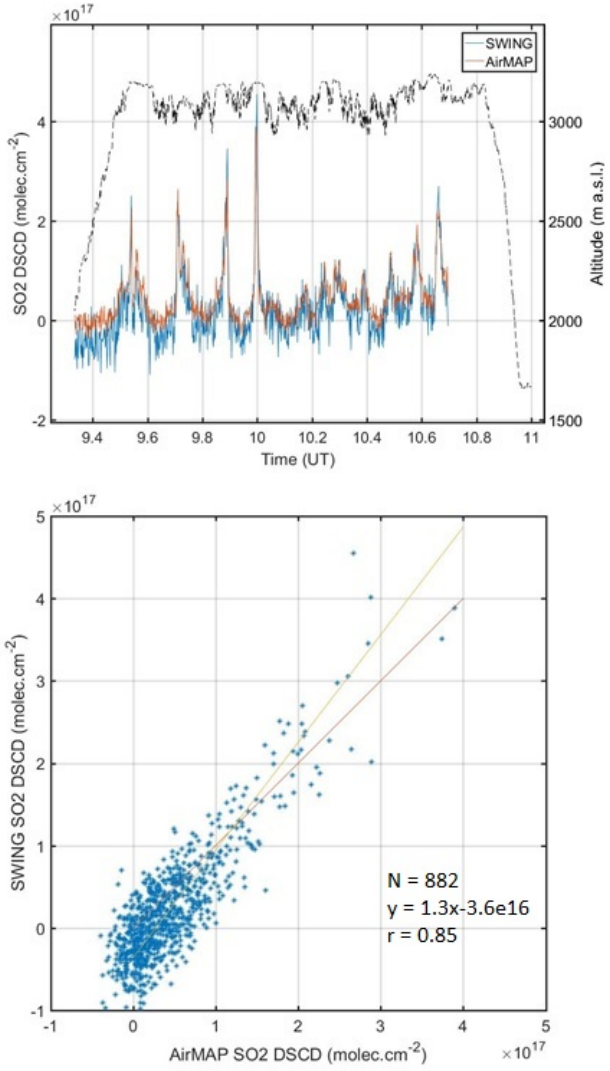

Figure S4. Comparison of the AirMAP and SWING SO_2 DSCDs above the Jiu Valley (28 August 2015). The upper panel also shows the flight altitude. The lower panel shows the orthogonal regression (blue) and 1:1 (red) lines.

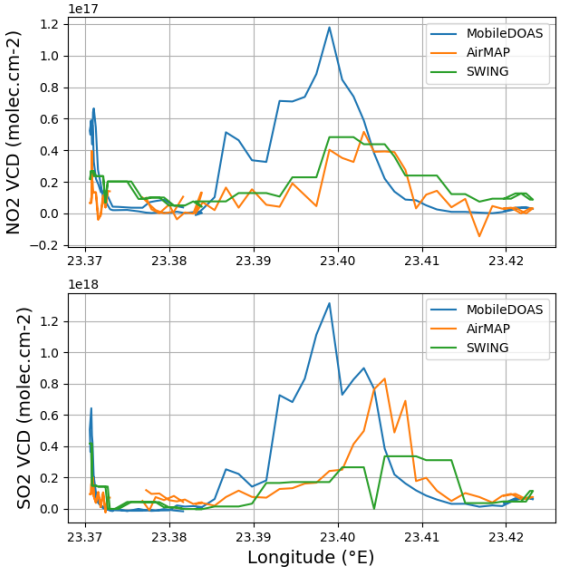

Figure S5. Comparison of the AirMAP, SWING, and zenith-only Mobile-DOAS SO_2 and NO_2 VCDs around Turceni Jiu (28 August 2015)

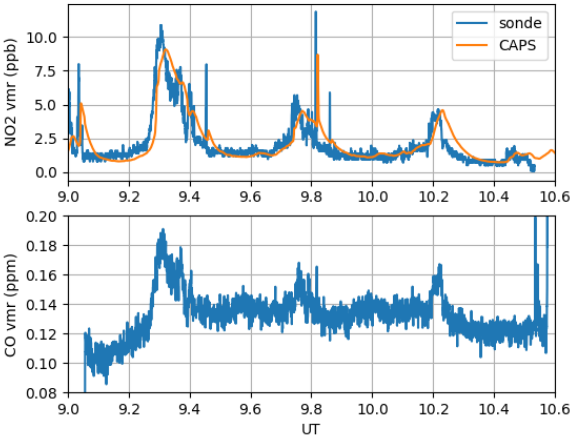

Figure S6. CAPS (orange) and NO_2 sonde (blue) measurements (upper panel) with CO measurements from the PICARRO (lower panel) onboard the BN-2 around Bucharest (25 August 2015). Note that the longer response time of the CAPS explains its time shift compared to the sonde.

5 Geophysical findings

5.1 Aerosol optical properties and boundary layer height in Bucharest

Figure S7 shows the lidar extinction profiles at 532 nm measured at INOE in Margurele (44.35° N, 26.03° E) during two days of AROMAT-2: 30 (red), and 31 (blue) August 2015. We retrieved these daytime extinction profiles from the backscatter profiles using a column-averaged lidar ratio constrained with the AOD from collocated sunphotometer measurements. The extinction was larger on 30 August 2015. It reached 0.21 km^{-1} in the boundary layer and up to 0.32 km^{-1} in an elevated layer at 2 km altitude. A similar elevated layer also appeared in the FUBISS data (Meier et al., 2017, Fig.7).

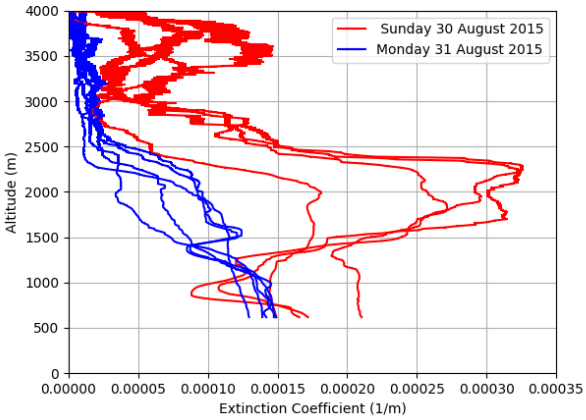

Figure S7. RALI extinction profiles at 532 nm above Magurele during two days of AROMAT-2. The different lines correspond to the different lidar measurements between 07:33 and 12:32 UTC (30 August 2015) and 07:29 and 15:01 UTC (31 August 2015).

During AROMAT-2, the AOD at 532 nm was around 0.2 most of the days, except on 30 August 2015 (0.35) and 1 September 2015 (0.05). Interestingly, the maximum AOD was seen on a Sunday, when the anthropogenic emissions of NO_x from Bucharest were minimal.

We estimated the boundary layer height (BLH) using a gradient method applied to the lidar range corrected signal (Belegante et al., 2014; Timofte et al., 2015). Figure S8 presents such BLH estimates using the RALI lidar observations during AROMAT-2 in Bucharest. The BLH varied between 700 m (morning of the 30 August 2015) and 2500 m (afternoon of the 24, 26, and 31 August 2015). During AROMAT-1, similar estimates resulted in BLH ranging between 1300 m (2 September 2014) and 2200 m (11 September 2014).

Figure S9 presents the PICARRO measurements of CO, CH_4, H_2O, and CO_2 volume mixing ratios (vmr) during two soundings of the BN-2: (i) between 11:24 and 11:41 UTC on 30 August 2015 (ii) between 12:20 and 12:39 UTC on 31 August 2015. All the species exhibit clear discontinuities in their vertical distribution at the altitude of the lidar-derived BLH: 800 m on 30 August 2015 and 1200 m a.s.l on 31 August 2015.

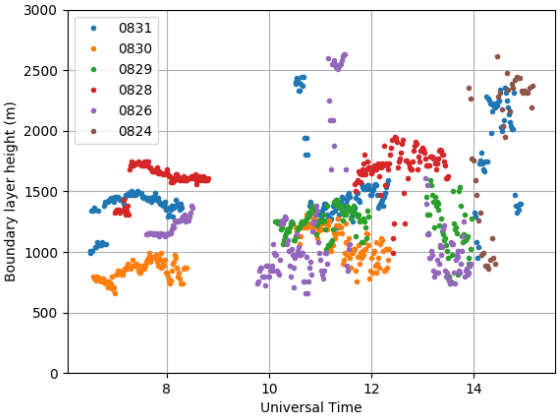

Figure S8. Lidar-derived boundary layer heights above Magurele in August 2015 during AROMAT-2.

Except for CH_4 on 31 August 2015, the vmrs were relatively stable in the boundary layer, and rapidly decreased above. Both soundings exhibit more polluted layers aloft, probably linked with long-range transport. These vertical distributions give confidence in the lidar-derived BLH, under which convection and turbulences homogenize the distribution of aerosols and trace gases.

Unfortunately, the BN-2 did not vertically sample the exhaust plume of Bucharest due to flight restrictions. We thus have little access to the vertical distributions of the aerosols and NO_2 in the Bucharest plume.

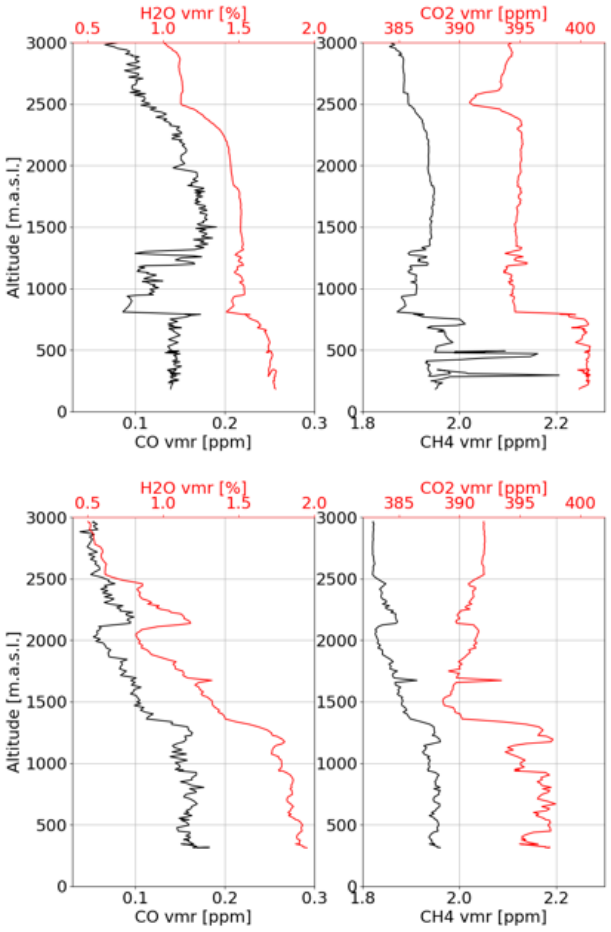

Figure S9. Vertical distributions of gases measured from the BN-2 during AROMAT-2 with the PICARRO. The upper panels shows the sounding at 08:30 UTC on 30 August 2015, the lower panel shows the sounding at 12:30 UTC on 31 August 2015.

5.2 Power plant plume measurements in Turceni

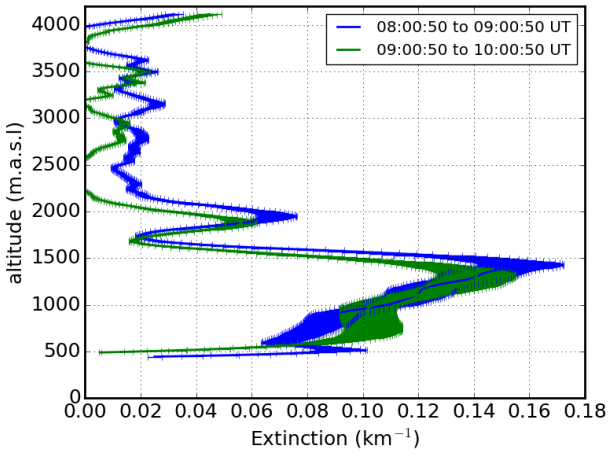

Figure S10. Extinction profiles measured in Turceni by the MILI lidar during the Cessna overpass on 28 August 2015. Note that the low values around 500 m are caused by the lidar partial overlap.

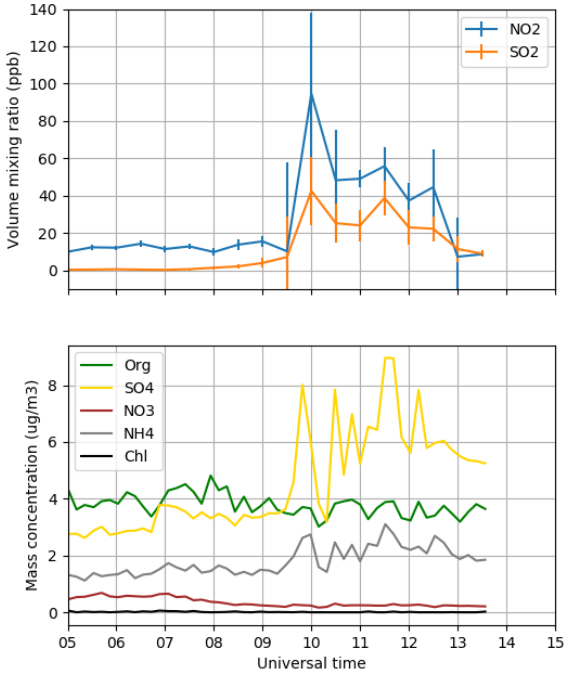

Figure S11. NO_2 and SO_2 in-situ and aerosol chemical speciation monitor measurements during AROMAT-1 (11 September 2014).

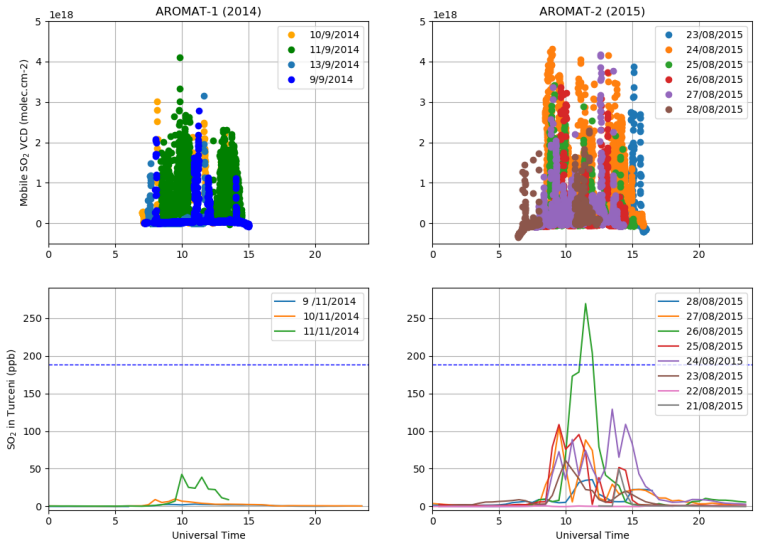

Figure S12. Zenith-only Mobile DOAS in the Jiu Valley and in-situ measurements in Turceni during AROMAT-1 (left panels) and AROMAT-2 (right panels). The blue dashed line indicates the 10 minutes mean threshold recommended by the World Health Organization.

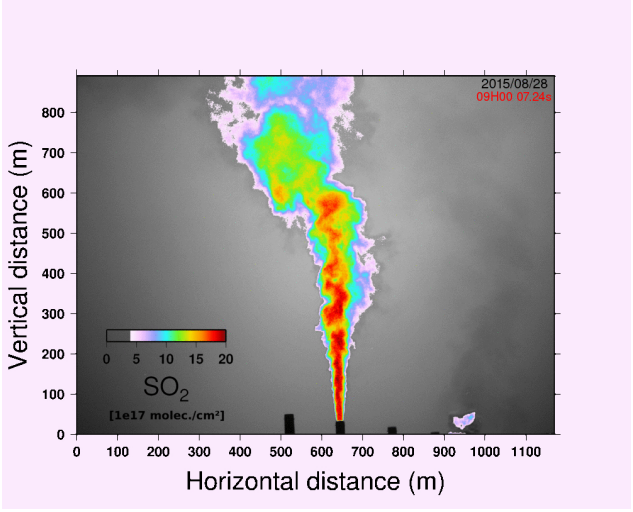

Figure S13. Image of the SO_2 plume above the Turceni power plant, recorded with the Envicam2 SO_2 camera (28 August 2015).

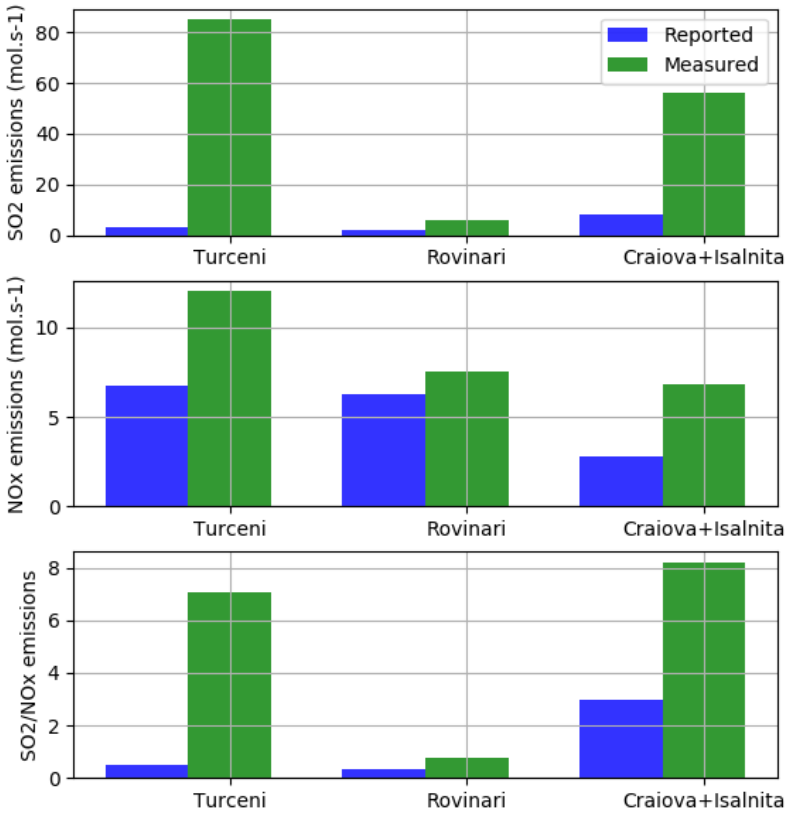

Figure S14. SO_2 and NO_x fluxes from the power plants of the Jiu Valley as (1) measured with the ULM-DOAS measurements on 25 August 2015 (green bars) and (2) estimated from the reported emissions of 2015 assuming constant emissions (blue bars). Uncertainties on the ULM-DOAS fluxes are around 60%.

Table S7. Range of measurements during the AROMAT 2014 campaign.

	Bucharest (min-max)	Jiu Valley (min-max)
NO vmr (ppb)	0-4	0-92
NO_2 vmr (ppb)	1-26	1-95
SO_2 vmr (ppb)	0-2	0-43
SO_2 column (molec.cm^{-2})	0-1e^{16}	0-4e^{18}
NO_2 column (molec.cm^{-2})	0-4e^{16}	0-1.3e^{17}
AOD (500 nm)	0.1-0.4	n.a
Aerosol extinction in BL (m^{-1})	6e^{-5} - 3.5e^{-4}	1e^{-4} - 2.8e^{-3}
Maximum boundary layer height (m)	2200	1500

Table S8. Range of measurements during the AROMAT 2015 campaign.

	Bucharest (min-max)	Jiu Valley (min-max)
CO vmr (ppm)	n/a	0.01-0.18
CH_4 vmr (ppm)	n/a	2.3-2.7
NO vmr (ppb)	n/a	0-18
NO_2 vmr (ppb)	n/a	1-34
O_3 vmr (ppb)	n/a	5-82
SO_2 vmr (ppb)	n/a	0-280
AOD (500 nm)	0.05-0.38	n/a
Aerosol extinction in BL (m^{-1})	1e^{-4} - 3e^{-4}	1e^{-4} - 4e^{-4}
Maximum boundary layer height (m)	3000	2300
SO_2 column (molec.cm^{-2})	n/a	0-4e^{18}
NO_2 column (molec.cm^{-2})	0-4e16	0-1.3e^{17}
H_2CO column (molec.cm^{-2})	1-7e^{16}	n/a

References

Belegante, L., Talianu, C., Nemuc, C., and Nicolae, D.: Detection of local weather events from multiwavelength lidar measurements during the EARLI09 campaign, Rom. J. Phys., 56, 484–494, 2011.

Belegante, L., Nicolae, D., Nemuc, A., Talianu, C., and Derognat, C.: Retrieval of the boundary layer height from active and passive remote sensors. Comparison with a NWP model, Acta Geophysica, 62, 276–289, https://doi.org/10.2478/s11600-013-0167-4, 2014.

Chen, H., Karion, A., Rella, C. W., Winderlich, J., Gerbig, C., Filges, A., Newberger, T., Sweeney, C., and Tans, P. P.: Accurate measurements of carbon monoxide in humid air using the cavity ring-down spectroscopy (CRDS) technique, Atmos. Meas. Tech., 6, 1031–1040, https://doi.org/10.5194/amt-6-1031-2013, 2013.

Constantin, D., Merlaud, A., Van Roozendael, M., Voiculescu, M., Fayt, C., Hendrick, F., Pinardi, G., and Georgescu, L.: Measurements of Tropospheric NO2 in Romania Using a Zenith-Sky Mobile DOAS System and Comparisons with Satellite Observations, Sensors, 13, 3922–3940, https://doi.org/10.3390/s130303922, 2013.

Constantin, D.-E., Merlaud, A., Voiculescu, M., Dragomir, C., Georgescu, L., Hendrick, F., Pinardi, G., and Van Roozendael, M.: Mobile DOAS Observations of Tropospheric NO2 Using an UltraLight Trike and Flux Calculation, Atmosphere, 8, 78, https://doi.org/10.3390/atmos8040078, 2017.

Dekemper, E., Vanhamel, J., Van Opstal, B., and Fussen, D.: The AOTF-based NO2 camera, Atmos. Meas. Tech., 9, 6025–6034, https://doi.org/10.5194/amt-9-6025-2016, 2016.

Jayne, J. T., Leard, D. C., Zhang, X., Davidovits, P., Smith, K. A., Kolb, C. E., and Worsnop, D. R.: Development of an Aerosol Mass Spectrometer for Size and Composition Analysis of Submicron Particles, Aerosol Sci. Tech., 33, 49–70, https://doi.org/10.1080/027868200410840, 2000.

Kebabian, P. L., Herndon, S. C., and Freedman, A.: Detection of nitrogen dioxide by cavity attenuated phase shift spectroscopy, Anal. Chem., 77, 724–728, https://doi.org/10.1021/ac048715y, 2005.

Kern, C., Lübcke, P., Bobrowski, N., Campion, R., Mori, T., Smekens, J.-F., Stebel, K., Tamburello, G., Burton, M., Platt, U., and Prata, F.: Intercomparison of SO2 camera systems for imaging volcanic gas plumes, J. Volcanol. Geotherm. Res., 300, 22 – 36, https://doi.org/https://doi.org/10.1016/j.jvolgeores.2014.08.026, 2015.

Meier, A. C.: Measurements of horizontal trace gas distributions using airborne imaging differential optical absorption spectroscopy, Ph.D. thesis, University of Bremen, 2018.

Meier, A. C., Schönhardt, A., Bösch, T., Richter, A., Seyler, A., Ruhtz, T., Constantin, D.-E., Shaiganfar, R., Wagner, T., Merlaud, A., Van Roozendael, M., Belegante, L., Nicolae, D., Georgescu, L., and Burrows, J. P.: High-resolution airborne imaging DOAS measurements of NO_2 above Bucharest during AROMAT, Atmos. Meas. Tech., 10, 1831–1857, https://doi.org/10.5194/amt-10-1831-2017, 2017.

Merlaud, A.: Development and use of compact instruments for tropospheric investigations based on optical spectroscopy from mobile platforms, Presses univ. de Louvain, 2013.

Merlaud, A., Tack, F., Constantin, D., Georgescu, L., Maes, J., Fayt, C., Mingireanu, F., Schuettemeyer, D., Meier, A. C., Schönardt, A., Ruhtz, T., Bellegante, L., Nicolae, D., Den Hoed, M., Allaart, M., and Van Roozendael, M.: The Small Whiskbroom Imager for atmospheric compositioN monitorinG (SWING) and its operations from an unmanned aerial vehicle (UAV) during the AROMAT campaign, Atmos. Meas. Tech., 11, 551–567, https://doi.org/10.5194/amt-11-551-2018, 2018.

Nicolae, D., Vasilescu, J., Carstea, E., Stebel, K., and Prata, F.: Romanian Atmospheric research 3D Observatory: Synergy of instruments, Rom. Rep. Phys., 62, 2010.

Nicolae, D., Vasilescu, J., Talianu, C., Binietoglou, I., Nicolae, V., Andrei, S., and Antonescu, B.: A neural network aerosol-typing algorithm based on lidar data, Atmos. Chem. Phys., 18, 14 511–14 537, https://doi.org/10.5194/acp-18-14511-2018, 2018.

Petit, J.-E., Favez, O., Sciare, J., Crenn, V., Sarda-Estève, R., Bonnaire, N., Močnik, G., Dupont, J.-C., Haeffelin, M., and Leoz-Garziandia, E.: Two years of near real-time chemical composition of submicron aerosols in the region of Paris using an Aerosol Chemical Speciation Monitor (ACSM) and a multi-wavelength Aethalometer, Atmos. Chem. Phys., 15, 2985–3005, https://doi.org/10.5194/acp-15-2985-2015, 2015.

Pfeifer, S., Müller, T., Weinhold, K., Zikova, N., Martins dos Santos, S., Marinoni, A., Bischof, O. F., Kykal, C., Ries, L., Meinhardt, F., Aalto, P., Mihalopoulos, N., and Wiedensohler, A.: Intercomparison of 15 aerodynamic particle size spectrometers (APS 3321): uncertainties in particle sizing and number size distribution, Atmos. Meas. Tech., 9, 1545–1551, https://doi.org/10.5194/amt-9-1545-2016, 2016.

Schönhardt, A., Altube, P., Gerilowski, K., Krautwurst, S., Hartmann, J., Meier, A. C., Richter, A., and Burrows, J. P.: A wide field-of-view imaging DOAS instrument for two-dimensional trace gas mapping from aircraft, Atmos. Meas. Tech., 8, 5113–5131, https://doi.org/10.5194/amt-8-5113-2015, 2015.

Sluis, W. W., Allaart, M. A. F., Piters, A. J. M., and Gast, L. F. L.: The development of a nitrogen dioxide sonde, Atmos. Meas. Tech., 3, 1753–1762, https://doi.org/10.5194/amt-3-1753-2010, 2010.

Timofte, A., Belegante, L., Cazacu, M. M., B., A., C., T., and S., G.: Study of planetary boundary layer height from LIDAR measurements and ALARO model, J. Optoelectron. Adv. M., 17, 2015.

Wagner, T., Ibrahim, O., Shaiganfar, R., and Platt, U.: Mobile MAX-DOAS observations of tropospheric trace gases, Atmos. Meas. Tech., 3, 129–140, 2010.

Zieger, P., Ruhtz, T., Preusker, R., and Fischer, J.: Dual-aureole and sun spectrometer system for airborne measurements of aerosol optical properties., Applied Optics, 46, 8542–8552, 2007.

List of relevant changes

- We have merged the SO2 and NO2 maps (the latter was previously in the supplement)
- We have moved the section describing the deployment from the supplement to the main article
- We have added a schematic for the general set-up during the campaign
- We have moved the lidar an picarro measurements to the supplement
- We have moved the figure with the temporal error estimation to the main manuscript
- We haved added an introduction to the flux section
- We have added a figure to show the effect of an underestimation of the random error on the reference measurements in our conditions
- We haved added a figure showing the two so2/no2 regimes in the jiu valley